

ACCOMPLISHMENT OF VACSY EXPERIMENTAL SET-UP
AND ITS APPLICATION TO INVESTIGATE MOLECULAR
ORIENTATION DISTRIBUTION OF SOLID-STATE
POLYMERS

Dissertation



zur Erlangung des akademischen Grades doktor rerum naturalium

(Dr. rer. nat.)

vorgelegt der

Mathematisch-Naturwissenschaftlich-Technischen Fakultät

der Martin-Luther-Universität Halle-Wittenberg

von Herrn Zhanjun Fang

geb. am: 20. 03. 1965 in Beijing, China

Gutachter:

1. Prof. Dr. H. Schneider (FB Physik/Universität Halle)
2. Prof. Dr. Ch. Jäger (IOQ/HF/Universität Jena)
3. Doz. Dr. S. Grande (Inst. F. Exp. Physik/Universität Leipzig)

Halle (Saale), den 30.11.1999

Abstract

Accomplishment of VACSYS experimental set-up and Its Application to Investigate Molecular Orientation Distribution of Solid-State Polymers

by Zhanjun Fang

The macroscopic characteristics of polymer materials, especially liquid crystalline polymer materials, depend significantly on their molecular orientation distribution. Mainly three methods, X-ray diffraction, neutron scattering and NMR, are used to investigate molecular orientation distribution in polymer materials. While X-ray diffraction is suitable for studying the orientation distribution of samples in crystalline state, neutron scattering and NMR are two widely adopted methods for samples in amorphous state. NMR's unprecedented selectivity makes it the unique experimental tool to investigate the orientation distribution of individual segments in a long molecular chain. Along with the advancements of solid-state NMR technology during the last twenty years, a number of NMR approaches become available to study molecular orientation distribution of solid-state polymers. ^2H NMR with line-shape analysis is the most popularly used method, this is mainly due to its good S/N ratio and its simplicity of data analysis. However, this method requires very expensive and time consuming isotope labelling. ^1H wide-line NMR and moment analysis approach has also been widely used for studying orientation distribution of weakly order polymer samples, but this method can hardly provide us the orientation information of a specific segment in a long molecular chain. Several ^{13}C NMR approaches, which utilise the orientation dependent chemical shift anisotropy and correlate them with their structural related chemical shift isotropy, have the greatest advantage to investigate the orientation distribution of individual segments in a long molecular chain of un-labelled polymer materials.

VACSYS as a promising method to re-introduce the Chemical Shift Anisotropy (CSA) under the condition of fast variable angle sample spinning and separate them by their corresponding Chemical Shift Isotropy (CSI) in the second dimension of a 2D NMR correlation spectrum has been selected by us to study the orientation distribution of liquid crystal polymers (LCPs). In this work, a probehead specially designed for the implementation of VACSYS experiment is constructed from scratches. On top of other functionalities of a normal CPMAS double resonance probe, the VACSYS probe adds the capability for the accurate controlling of the angle between the sample spinning axis and the external magnetic field \mathbf{B}_0 direction. Much effort has been paid to optimise the double resonance RF circuit for maximum efficiency and the angle control system to achieve an accuracy better than 0.25° . A computer program for VACSYS spectra simulation in the case of slow sample spinning is created and successfully applied to simulate the influences on the final CSA line-shape due to insufficient sample spinning speed, the angle mis-setting (between the sample spinning axis and the external

magnetic field \mathbf{B}_0 direction), the number of angle sampling steps, etc. The VACSYS simulation result proves to be very useful in selecting the correct experimental parameters. To reduce the phase artefacts due to an incomplete time domain data sampling which are inherent to VACSYS experiment, two new VACSYS data processing approaches are proposed and successfully applied to process our VACSYS experimental data. Comparing with the normal interpolation approach published by Frydman et al, these two new proposals allow the final VACSYS spectra to be displayed in phase sensitive mode and the interpolation noise is also reduced to some degree.

The VACSYS experimental set-up and its corresponding processing software are firstly applied to measure the values of chemical shift tensor elements for well known samples such as Glycine, DMS, HMB and Durene, the measurement results are in good agreement with published values. Then, this VACSYS experimental set-up is applied to investigate the orientation distribution behaviour of two polymer liquid crystalline samples: hexa-hydroxytriphenylene and polyacrylates. The procedure for creating certain orientation distribution in LC samples is: heat the sample over its clearing temperature (T_c) while it is put inside a strong magnetic field (9.4T), wait for equilibrium and then slowly cool it down below its glass transition temperature (T_g) to freeze the orientation distribution within the sample. From ^{13}C VACSYS spectra of the LC samples in both isotropic state and oriented state, the orientation distribution is analysed by the method of CSA line-shape fitting approach. For a reliable extraction of orientation distribution through an accurate line-shape analysis approach, fast sample spinning relative to the chemical shift anisotropy is highly desirable. For the hexa-hydroxytriphenylene sample, the result is compared with the result of ^2H NMR line splitting measurements published by D. Goldfarb and Z. Luz. Suggestions for further improvements of VACSYS as a method for the study of orientation distribution of solid-state polymers are also given.

Zusammenfassung

Aufbau eines VACSY-NMR Experiments und seine Anwendung zur Untersuchung der molekularen Orientierungsverteilung in festen Polymeren

von Zhanjun Fang

Die makroskopischen Eigenschaften von polymeren Materialien, besonders von flüssigkristallinen Polymeren, hängen stark von der molekularen Orientierung ab. Im wesentlichen existieren drei Methoden (Röntgen-Beugung, Neutronenstreuung und NMR), um die molekulare Orientierung und deren Verteilung in polymeren Materialien zu untersuchen. Während die Röntgen-Beugung für das Studium der Orientierungsverteilung im kristallinen Zustand geeignet ist, sind Neutronenstreuung und NMR weit verbreitete Methoden für Proben im amorphen Zustand. Die unübertroffene Selektivität der NMR macht sie zu einem einmaligen Werkzeug für die Untersuchung der Orientierungsverteilung von verschiedenen molekularen Einheiten in einer langen Molekülkette. In Verbindung mit den Fortschritten der Festkörper-NMR-Technologie der letzten 20 Jahre wurden eine Reihe von NMR-Zugängen für die Untersuchung der molekularen Orientierungsverteilung in festen Polymeren möglich. Dabei ist die ^2H -NMR-Linienformanalyse die am häufigsten verwendete Methode, vor allem durch das gute Signal-Rausch-Verhältnis und die einfache Analyse der Daten. Allerdings erfordert diese Methode die teure und zeitaufwendige Isotopenmarkierung. Die ^1H -Breitlinien-NMR und Momentenanalyse wird ebenfalls häufig zum Studium der Orientierungsverteilung in schwach geordneten Polymeren angewendet, allerdings kann diese Methode die Orientierungsinformation über ein spezielles Segment einer langen Molekülkette nicht liefern. Verschiedene ^{13}C -NMR-Zugänge, welche die orientierungsabhängige anisotrope Chemische Verschiebung (ACV) ausnutzt und sie mit der strukturabhängigen isotropen Chemischen Verschiebung (ICV) korreliert, sind für die Untersuchung der Orientierungsverteilung von individuellen Segmenten in einer langen Molekülkette in nicht-isotopenmarkierten Polymeren am erfolgversprechendsten.

VACSY ist eine erfolgversprechende Methode zur Wiedereinführung der Anisotropie der Chemischen Verschiebung unter den Bedingungen des schnellen Variable-Angle Spinning und ihrer Trennung durch die entsprechend Isotrope Chemische Verschiebung in der zweiten Dimension eines 2D-NMR-Korellationspektrums. Diese Methode wurde von uns zur Untersuchung der Orientierungsverteilung von flüssigkristallinen Polymeren ausgewählt. In der vorliegenden Arbeit wurde ein NMR-Probenkopf für die speziellen Anforderungen des VACSY-Experiments gebaut. Außer den NMR-Funktionen eines gewöhnlichen CPMAS-Doppelresonanz-Probenkopfes mußte die

Fähigkeit für die exakte Einstellung und Änderung des Winkel zwischen der MAS-Rotorachse und dem externe Magnetfeld geschaffen werden. Großer Wert wurde auf die Optimierung des Doppelresonanz-HF-Kreises auf maximale Effizienz und auf eine Genauigkeit von besser als 0.25° für die Winkeleinstellung gelegt. Ein Computerprogramm für die Simulation von VACSY-Spektren bei endlicher Rotationsfrequenz und deren Einfluß auf die 2D-VACSY-Spektren, des Einflusses von nicht-exakten Winkeleinstellungen, die Abhängigkeit der Spektren von der Anzahl der Winkelinkremente usw. wurde erstellt. Die Simulationsrechnungen haben sich als sehr wertvoll für die Auswahl optimaler experimenteller Parameter erwiesen. Zur Verminderung von Phasen-Artefakten, bedingt durch den eingeschränkten experimentell zugänglichen Wertebereich im VACSY-Experiment, wurden zwei neuartige Verarbeitungsroutinen für VACSY-Datensätze vorgeschlagen. Verglichen mit der originalen Verarbeitungsprozedur verbessert sich die Qualität der 2D-VACSY-Spektren durch die Möglichkeit der Darstellung in phase-sensitive mode und durch den Wegfall der Dateninterpolation.

Das VACSY-NMR-Experiment und seine Verarbeitungs-Software wurden angewendet zur Bestimmung der Parameter der ACV für wohl bekannte Modellsubstanzen wie Glyzin, Dimethylsulfon (DMS), Hexamethylbenzen (HMB) und 1,2,4,5-Tetramethylbenzen (Durene). Die Ergebnisse stimmen mit den bekannten Werten überein und bestätigen die korrekte Arbeitsweise der VACSY-hard- und Software. Im weiterem wurden VACSY-Experimente an zwei flüssigkriattlinien Substanzen durchgeführt: Hexahexyloxytriphennylen (HHOTP) und einen flüssigkristallinen Polymer auf Polyakrylatbasis. Zur Schaffung eines orientierten Zustandes wurde folgende Prozedur angewendet: Aufheizen der Probe in einem starken Magnetfeld (9,4T) bis über die Klärtemperatur (T_C), abwarten bis zur Einstellung eines Gleichgewichtszustandes und anschließende langsame Abkühlung bis unterhalb der Glastemperatur (T_g) zum Einfrieren des orientierten Zustandes. Die VACSY-Spektren des flüssigkristallinen Proben wurden sowohl im isotropen als auch im orientierten Zustand mittels NMR-Linienformanalyse der ACV analysiert. Für HHOTP wurden die Ergebnisse mit früheren Experimenten anderer Autoren verglichen. Vorschläge für die weitere Verbesserung der Methode werden gegeben.

TABLE OF CONTENTS

Chapter 1. Introduction	1
1.1 Motivation	1
1.2 Scope of thesis	3
Chapter 2. NMR and molecular orientation distribution	5
2.1 Important NMR interactions in solid materials	5
2.2 Co-ordinates system	7
2.3 Dependence of NMR frequency on molecular segmental orientation	9
2.3.1 Chemical shift interaction - static case	9
2.3.2 Chemical shift interaction - macroscopic sample rotation	12
2.4 Study of orientation distribution from anisotropic NMR interactions	15
2.4.1 The anisotropy of dipole-dipole interaction	15
2.4.2 The anisotropy of quadrupolar interaction	16
2.4.3 The anisotropy of chemical shift interaction	17
2.5 Procedures to extract orientation distribution from CSA line-shape	18
2.5.1 Direct reconstruction procedure	18
2.5.2 Moment analysis procedure	20
Chapter 3. NMR methods to measure chemical shift anisotropy	25
3.1 Introduction	25
3.2 Methods to retrieve anisotropic CSA patterns	26
3.2.1 Stop-and-go	26
3.2.2 Magic-Angle-Hopping, Magic-Angle-Turning (MAT)	27
3.2.3 Fast flipping between MAS and OMAS	28
3.2.4 Tycko's 4- π -pulses method	29
3.2.5 RF field modulation	30
3.2.6 VACSY	31
Chapter 4. VACSY and interpolation of experimental data	32
4.1 Introduction	32
4.2 Theory of VACSY	33
4.3 Methods to implement interpolation or extrapolation	35
4.3.1 Normal interpolation - Frydman procedure	35
4.3.2 Normal interpolation and Linear Prediction	37

4.3.3 Non-orthogonal interpolation	43
4.3.4 VACSY transformation with eigen-coordinates	48
Chapter 5. Simulation	51
5.1 Introduction	51
5.2 Simulation program	52
5.2.1 Stepwise procedure	53
5.2.2 Conroy procedure	53
5.3 Simulation results	55
5.3.1 Influence of sample spinning speed on CSA line-shape	56
5.3.2 Influence of angle β mis-setting on CSA line-shape	59
5.3.3 Influence of angle β sampling range on CSA line-shape	61
5.3.4 Influence of angle β sampling numbers on CSA line-shape	63
5.3.5 Influence of fluctuation in sample spinning speed on CSA line-shape	64
Chapter 6. Construction of a VACSY probe	67
6.1 Introduction	67
6.2 Basics of radio frequency engineering	68
6.2.1 Capacitance	68
6.2.2 Inductance	69
6.2.3 $\lambda/4$ wavelength cable	70
6.2.4 Single resonance circuit	71
6.2.5 Matching	72
6.2.6 Double resonance circuit	73
6.3 RF design in VACSY probe	75
6.4 VACSY RF circuit optimisation	76
6.5 Angle control	77
Chapter 7. Experimental results and discussion	80
7.1 Introduction	80
7.2 VACSY to measure CS tensor elements	80
7.2.1 1D VAS experiment to measure CS tensor elements of glycine	80
7.2.2 VACSY experiment to measure CS tensor elements of HMB and DMS	82
7.2.3 VACSY experiment to measure CS tensor elements of Durene	84
7.3 Liquid crystal phase and polymer liquid crystal materials	85
7.3.1 Liquid crystal phase	85

7.3.2 Polymer liquid crystal materials	88
7.4 VACSY to study orientation distribution of hexa-hexyloxytriphenylene	88
7.5 VACSY to study orientation distribution of polyacrylates (LCSPs)	93
7.6 Summary	102

References

Acknowledgements

Erklärung

Curriculum Vitae

INTRODUCTION

1.1 Motivation

In material science, the relationship between macroscopic properties and microscopic structures is crucial for scientists to improve known and design new materials. This is particularly important for the case of synthetic polymers, where material properties depend strongly on both the molecular structure and the organisation of macromolecules in solid state: their phase structure, morphology, molecular order, molecular dynamics, etc. [Flory 1953; Kroschwitz 1990]. Different methods have been developed to study these aspects respectively. In general, information about structure and order are frequently studied through X-ray scattering, neutron scattering and various kinds of microscopy methods. Information about dynamics are mainly obtained from relaxation experiments [McCrum et al., 1967].

Nuclear Magnetic Resonance (NMR) [Abragam, 1961; Slichter, 1980] is well established in structural characterisation of liquids or compounds in solution, but much less in solids [Fyfe, 1983; Bovey, 1988]. However, in solid state, due to the presence of angular dependent NMR anisotropic interactions and its unprecedented selectivity, NMR serves as a unique method for studying molecular orientation distribution of weakly ordered solid state polymers.

It is well known that: in both natural and synthetic materials, the orientation distribution of the molecular chains directly influence their properties, some examples of these materials are:

- High modulus polymer fibres, such as KELVAR, they consist of strongly elongated macromolecules which lead to extremely high strength. The higher the molecular order, the bigger the modulus of the fiber.
- Natural materials, like wood and human bones, they also show up a high degree of molecular orientation.
- Liquid Crystal materials. Their main applications as electrically driven optical devices are based on the ability of the molecules to orient themselves with respect to neighbouring molecules or with respect to external magnetic/electric field.

Preferred orientation can arise, either accidentally or purposely, when polymers are subjected to particular fabrication procedures [Ward, 1982, 1985]. The complete description of the orientation order of polymer materials requires a specification of the orientation distribution function of every relevant molecular moiety, which is usually given in terms of three angles that describe the segment orientation with respect to the macroscopic sample direction. Where the macroscopic sample direction often means the drawn direction or the direction of plane normal for thin film samples. However, in many practical cases the characterisation of orientation distribution can be simplified. For example, in the case of the sample has macroscopic uniaxial symmetry, the number of relevant angles is reduced to one, the theoretical calculation is then greatly simplified. Additionally, in many polymers some or all segments are fixed relative to one another by intra- or intermolecular forces, so that the whole sample can be characterised by the orientation distribution of chain axes in amorphous materials or by unit cell in crystalline materials. In the case of very broad orientation, it is often enough to describe the orientation distribution in terms of a few order parameters [Schmidt-Rohr and Spiess, 1994].

In practice, a variety of techniques to study the orientation distribution are available. Several of them, for example birefringence measurements, however, can only determine one or a few order parameters. This means the resolution of these methods is restricted, because quite different orientation distributions can have identical second moments. Also, in these methods it is very difficult to correlate the orientation of individual molecular units to their corresponding experimental data [Schmidt-Rohr and Spiess, 1994]. Wide Angle X-ray (WAX) scattering are popularly used to fully determine the orientation distribution of crystalline samples by means of „pole figure analysis“ [Balta-Calleja and Vonk, 1989], but this method is not suitable for studying amorphous materials. Due to its intrinsic supreme selectivity, NMR does not have any difficulty to correlate the orientation of individual molecular units to their corresponding experimental data, neither does it pose any restrictions for being used to study amorphous materials. This makes NMR one of the most important method for studying molecular orientation distribution of weakly ordered solid polymers.

However, What NMR can directly measure is the orientation distribution of chemical shift tensor in Principal Axis System (PAS) with respect to external magnetic field \mathbf{B}_0 instead of the orientation distribution of molecular chain axes, many complications will arise when the latter distribution is derived from the directly measured chemical shift tensor distribution.

1.2 Scope of thesis

In this work, our primary interest is to study the orientation distribution behaviour of liquid crystal side-chain polymers by the method of NMR, chemical shift anisotropic interaction is selected as the experimental tool. To obtain the necessary CSA patterns and separate them by their corresponding chemical shift isotropic values of different in-equivalent nuclear sites, a special 2D NMR correlation method - Variable Angle Correlation Spectroscopy (VACSYS) is applied [Frydman et al, 1994].

Chapter 2 is the theoretical basis for this work. Firstly, all NMR interactions in solid materials are listed and briefly discussed. Only those angular-dependent anisotropic interactions can give us information about molecular orientation distribution. Then, for the convenience of mathematical handling, several NMR relevant co-ordinates systems are discussed. Different systems are connected to each other through Euler transformations. In section 2.3, a typical example of the NMR anisotropic interactions - chemical shift anisotropic interaction and the dependence of resonance frequency on molecular orientation is thoroughly discussed for the cases of both static and macroscopic sample spinning. In section 2.4, the availability of orientation distribution information and the corresponding possible implementation procedures for different NMR anisotropic interactions, namely: dipolar interaction, quadrupolar interaction, and chemical shift interaction are discussed. In section 2.5, different approaches to extract out the orientation distribution information from CSA patterns are discussed.

Based on the discussion in chapter 2, it becomes clear that the most important step in our procedure for obtaining orientation distribution information is to get non-distorted CSA patterns. Chapter 3 gives a general discussion about the most popularly applied approaches to obtain CSA patterns, their advantages and limitations are also discussed. Due to its simplicity in mechanic aspect and its better performance comparing with multiple RF pulses approaches, VACSYS is selected by us as the method to study the orientation distribution behaviour of liquid crystal polymer samples. Chapter 4 gives the theoretical background of VACSYS, also described here are the necessary implementation procedures such as data interpolation in time domain, removal of phase artefacts, etc.

While VACSYS needs a special probe to be performed, there are some problems which would not be met in normal 2D NMR experiments. Computer simulation can answer some special questions related to VACSYS, such as: how much a spinning speed is necessary with respect the CSA value of a specified sample in order to neglect line-shape distortion? How many angle sampling steps are necessary to minimise the data interpolation error? Chapter 5

introduces a VACSY simulation program and gives all the simulation results. Only recently, VACSY probe is commercially available. In chapter 6, the necessary knowledge for constructing a VACSY probe is presented, such as: the basic theory of radio frequency engineering, single resonance and double resonance RF circuits, impedance matching, accurate angle control, etc.

Chapter 7 presents the experimental results of the application of VACSY to various samples. It is shown that VACSY can be used to reliably measure chemical shift principal values, such as in the case of glycine, dimethylsulfon (DMS), hexamethylbenzene (HMB). It is also shown that VACSY can be used to separate two very close spectral lines and measure the values of their chemical shift tensor elements respectively, such as in the case of Durene. Finally, the result of the application of VACSY to study the orientation distribution of two liquid crystal samples, hexa-hydroxytriphenylene and LCSP polyacrylates, are discussed.

NMR AND MOLECULAR ORIENTATION DISTRIBUTION

2.1 Important NMR interactions in solid materials

In solid materials, the nuclear spin Hamiltonian consists of a number of terms that describe physically different interactions. In the case of diamagnetic non-conducting substances, the Hamiltonian can be expressed as following [Haeberlen, 1976; Schmidt-Rohr & Spiess, 1994]:

$$\hat{H} = \hat{H}_Z + \hat{H}_{rf} + \hat{H}_{CS} + \hat{H}_Q + \hat{H}_J + \hat{H}_D + \dots \quad (2-1)$$

in this expression:

\hat{H}_Z :external magnetic field (Zeeman interaction)

\hat{H}_{RF} :external radio frequency (RF) magnetic field

\hat{H}_{CS} :induced magnetic fields originating from orbital motions of electrons

\hat{H}_D :spin interaction between each other, directly through magnetic dipole moments

\hat{H}_Q :internal electric field gradients

\hat{H}_J :spin interactions between each other, indirectly through electron spins

each of these interactions is briefly discussed in the following:

- Zeeman Hamiltonian. This Zeeman interaction usually is the dominant term of nuclear spin Hamiltonian, but it does not contain any structural information. For the spectroscopic application of NMR, the local fields that the nuclear spin feels are important [Mehring, 1983].

$$\hat{H}_Z = -\gamma B_0 \hat{I}_Z = -\sum_j \gamma^j B_0 \hat{I}^j_z \quad (2-2)$$

- Radio frequency Hamiltonian. The RF field is usually applied perpendicular to the static external magnetic field B_0 , without losing generality the direction of the RF field can be chosen along the x-axis:

$$\vec{B}_{RF} = (B_1(t)\cos[\omega t + \varphi(t)], 0, 0) \quad (2-3)$$

the form of \vec{B}_{RF} implies that it can be modulated in both its amplitude and phase, but it has a constant carrier frequency. The corresponding Hamiltonian is given as:

$$\hat{H}_{RF} = B_1(t) \cos[\omega t + \varphi(t)] \sum_j \gamma^j \hat{I}^j_x \quad (2-4)$$

In multiple resonance experiments \vec{B}_{RF} consists of a sum of fields that differ, in particular, in their carrier frequencies.

- Chemical Shift interaction Hamiltonian. Under the influence of the B_0 field, the electron cloud generates also an additional field B_S which in diamagnetic materials scales with the field B_0 according to:

$$\vec{B}_S = \underline{\underline{\sigma}} \vec{B}_0 \quad (2-5)$$

so that the Hamiltonian for the chemical shift interaction of nuclear spins is given:

$$\hat{H}_{CS} = \sum_j \gamma^j \hat{I}^j \cdot \underline{\underline{\sigma}}^j \cdot \vec{B}_0 = \sum_j \gamma^j (\hat{I}_x \sigma^{LF}_{xz} + \hat{I}_y \sigma^{LF}_{yz} + \hat{I}_z \sigma^{LF}_{zz}) B_0 \quad (2-6)$$

here, $\sigma^{LF}_{\alpha\beta}$ are the elements of the laboratory frame representation of the chemical shift tensor.

- Dipolar interaction Hamiltonian. The Hamiltonian of dipolar interactions between nuclear spins is given as:

$$\hat{H}_D = -\frac{\mu_0}{4\pi} \hbar \sum_{j < k} \gamma_j \gamma_k \frac{3(\hat{I}^j \cdot \vec{r}_{jk} / r_{jk})(\hat{I}^k \cdot \vec{r}_{jk} / r_{jk}) - \hat{I}^j \cdot \hat{I}^k}{(r_{jk})^3} \quad (2-7)$$

where \vec{r}_{jk} defines the vector from nucleus j to nucleus k and $r_{jk} = |\vec{r}_{jk}|$

- Quadrupolar interaction Hamiltonian. The Hamiltonian can be written in the form:

$$\begin{aligned} \hat{H}_Q &= \sum_i \frac{eQ^i}{6I^i(2I^i-1)} \sum_{\alpha, \beta=1}^3 V^i_{\alpha\beta} [\frac{3}{2}(\hat{I}^i_{\alpha} \hat{I}^i_{\beta} + \hat{I}^i_{\beta} \hat{I}^i_{\alpha}) - \delta_{\alpha\beta} (\hat{I}^i)^2] \\ &= \sum_i \frac{eQ^i}{6I^i(2I^i-1)} \hat{I}^i \cdot \underline{\underline{V}}^i \cdot \hat{I}^i \end{aligned} \quad (2-8)$$

where eQ^i and I^i are the nuclear quadrupole moment and the nuclear spin quantum number of the i th nucleus. $V^i_{\alpha\beta}$ is the second (α, β) derivative of the electric potential at the site of i th nucleus.

- Indirect spin-spin coupling Hamiltonian. This term is popularly referenced as J coupling and it plays a crucial role in solution NMR. It may be expressed as:

$$\hat{H}_J = \sum_{i < k} \hat{I}^i \cdot \underline{\underline{J}}^{ik} \cdot \hat{I}^k \quad (2-9)$$

where $\underline{\underline{J}}^{ik}$ is also a tensor of rank two.

Two properties of the NMR Hamiltonian are emphasised here: firstly, in most cases, the Zeeman interaction is the dominant term, all local fields experienced by these frequently investigated nuclei: ^1H , ^2H , ^{13}C , ^{15}N , ^{19}F , ^{29}Si , ^{31}P are smaller, so that: the energy shifts originated by these terms can be treated with first-order perturbation theory; Secondly, only those ‘secular’ parts of the local field terms which commute with \hat{I}_z are relevant for the calculation of energy shifts. After this ‘truncation’, the Hamiltonian for different local field interactions are given as:

- chemical shift interaction

$$\hat{H}_{CS} = \sum_i \gamma^i \hat{I}_z^i \cdot \sigma^{iLF}_{zz} \cdot B_0 \quad (2-10)$$

- hetero-nuclear dipolar coupling

$$\hat{H}^{IS}_D = -\frac{\mu_0}{4\pi} \hbar \sum_j \sum_{j < k} \frac{\gamma^I \gamma^S}{r_{jk}^3} \frac{1}{2} (3 \cos^2 \theta_{jk} - 1) (3 \hat{I}_z^j \hat{I}_z^k) \quad (2-11)$$

- homo-nuclear dipolar coupling

$$\hat{H}^{II}_D = -\frac{\mu_0}{4\pi} \hbar \sum_j \sum_{j < k} \frac{(\gamma^I)^2}{r_{jk}^3} \frac{1}{2} (3 \cos^2 \theta_{jk} - 1) (3 \hat{I}_z^j \hat{I}_z^k - \hat{I}^j \cdot \hat{I}^k) \quad (2-12)$$

- quadrupolar interaction

$$\hat{H}_Q = \sum_i \frac{eQ^i}{2I^i(2I^i - 1)\hbar} (V^i_{zz})^{LF} \frac{1}{2} (3 \hat{I}_z^i \hat{I}_z^i - \hat{I}^i \cdot \hat{I}^i) \quad (2-13)$$

2.2 Co-ordinates system

The characterisation of orientation distribution can be performed in terms of various angles and reference systems, all of them are interrelated to each other. However, some of them are adequate for the NMR spectroscopy, while others directly describe the distribution of the structural axes in the sample [Schmidt-Rohr & Spiess]. For the convenience of later discussion, the definitions of all these angles and co-ordinates systems are described in the following diagram of fig2-1. Here, we follow Schmidt Rohr & Spiess’s conventions.

- Laboratory frame, LF. The z axis \vec{Z}_L of the laboratory frame is defined as the external magnetic field \vec{B}_0 .
- Sample-fixed Director frame, DF. The primary order direction of the sample is denoted as the sample director and is usually chosen as the z axis \vec{Z}_D of the director frame.
- Molecular frame, MF. Molecular frame is fixed relative to the molecular repeat unit, usually the local chain axis is chosen as the z axis \vec{Z}_M of the molecular frame. The three Euler angles $(\Psi_M, \Theta_M, \Phi_M)$ describe the orientation of a given molecular frame in the

sample fixed director frame, usually these are the structurally most meaningful angles for describing the molecular orientation.

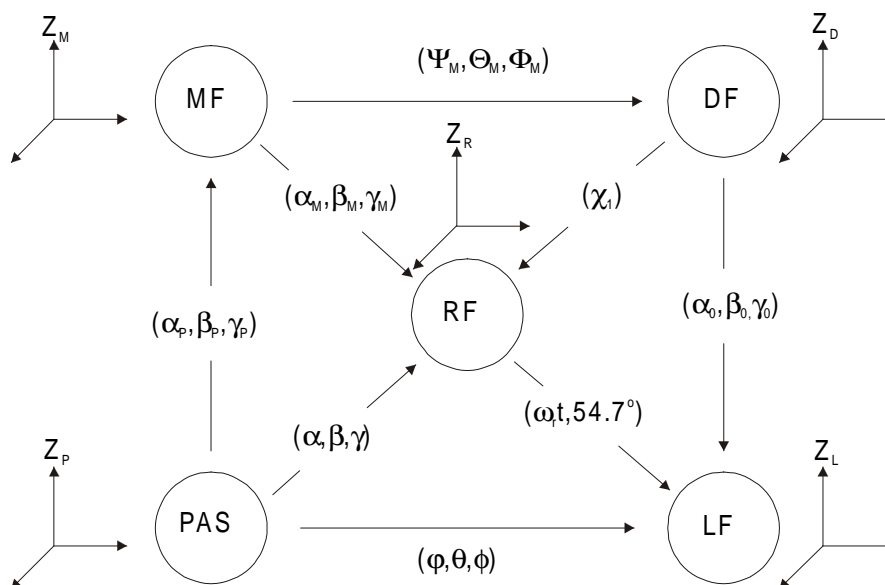


Figure 2-1 Euler angles and co-ordinates systems used in this thesis.

- Principal-axes system, PAS. Here, (θ, ϕ) are the polar co-ordinates of the \vec{B}_0 field in the PAS, so θ is the angle between the \vec{Z}_p axis and \vec{B}_0 . (Ψ, Θ, Φ) are the Euler angles define the orientation of a given PAS in the sample fixed DF. The orientation of a given PAS in the molecular frame MF is described by three Euler angles $(\alpha_p, \beta_p, \gamma_p)$. Without losing the generality of the treatment, angle γ_p can be set to $\gamma_p=0$, the argument is that: in the transformation from $PAS \rightarrow MF \rightarrow DF$, both γ_p and ψ_M describe a rotation around the a \vec{Z}_M axis, therefore only the sum of $\gamma_p + \psi_M$ is relevant, so that γ_p can be included in ψ_M when a correct null position is defined.
- Rotor-fixed frame, RF. The RF frame is a sample fixed frame whose z axis \vec{Z}_R is chosen along the rotor axis. χ_1 is the angle between the sample director \vec{Z}_D and the rotor axis \vec{Z}_R . The angles (α, β, γ) describe the relative orientations of the PAS to the RF. The similar angles $(\alpha_M, \beta_M, \gamma_M)$ relate the MF to RF. In particular, the angles γ and γ_m describe the rotations around the rotor axis. In the case of Magic Angle Spinning, the polar co-ordinates of the \vec{B}_0 field in the rotor frame is $(54.7^\circ, \omega_t)$.

2.3 Dependence of NMR frequency on Segmental-orientation

One of the important features of solid state NMR is its orientation dependence of NMR interactions as well as NMR resonance frequency. This property enables us to investigate the

molecular orientation and re-orientation of individual segments. The origin of this angular dependence lies in the tensorial nature of these interactions [Schmidt-Rohr & Spiess].

In this section, the relationship between the NMR resonant frequency and segmental-orientations will be derived for the typical case of chemical shift interaction.

2.3.1 chemical shift interaction - static case

If only Zeeman interaction and chemical shift interaction are considered, according to equation (2-2), (2-5) and using $\omega_0 = -\gamma B_0$, the Hamiltonian of a specified nuclear spin is:

$$\hat{H}_z + \hat{H}_{CS} = \omega_0(1 - \sigma^{LF}_{zz})\hat{I}_z \quad (2-14)$$

this leads to a slow precession of the magnetisation with a frequency:

$$\omega_{CS} = -\omega_0 \sigma^{LF}_{zz} \quad (2-15)$$

relative to the Larmor frequency ω_0 of the unshielded spin. σ^{LF}_{zz} is the z element of the shielding tensor expressed in the laboratory frame, which depends on the orientation of the molecular segment relative to \vec{B}_0 field. Assume that: $\vec{B}_0 = B_0(0,0,1)$, the unit vector is $\vec{b}_0 = \vec{B}_0 / B_0$, then σ^{LF}_{zz} can be written as:

$$\sigma^{LF}_{zz} = (0 \quad 0 \quad 1) \underline{\underline{\sigma}}^{LF} \begin{pmatrix} 0 \\ 0 \\ 1 \end{pmatrix} = \vec{b}^{s_0} \underline{\underline{\sigma}}^s \vec{b}^{s_0} \quad (2-16)$$

this relation is valid with both \vec{b}_0 and $\underline{\underline{\sigma}}$ expressed in any co-ordinates system \mathbf{S} , since the bilinear form of the above equation is co-ordinates independent [Schmidt-Rohr & Spiess]. Similarly, ω_{CS} can be written as:

$$\omega_{CS} = -\omega_0 \vec{b}^{s_0} \underline{\underline{\sigma}}^s \vec{b}^{s_0} = -\omega_0 \vec{b}_0^{PAS} \underline{\underline{\sigma}}^{PAS} \vec{b}_0^{PAS} \quad (2-17)$$

in the last part of equation (2-17), both \vec{B}_0 field direction \vec{b}_0 and tensor $\underline{\underline{\sigma}}$ are expressed in their principal value systems (PAS). \vec{b}_0 can be described by its polar co-ordinates (θ, ϕ) in the PAS, σ_{xx}^{PAS} , σ_{yy}^{PAS} , σ_{zz}^{PAS} are the principal values of tensor $\underline{\underline{\sigma}}$. Then, ω_{CS} can be further expressed as:

$$\begin{aligned} \omega_{CS} &= -\omega_0 \sum_{\alpha} (b_0^{PAS})_{\alpha} \underline{\underline{\sigma}}_{\alpha\alpha}^{PAS} (b_0^{PAS})_{\alpha} \\ &= \omega_0 (\sigma_{xx}^{PAS} (\cos \phi \sin \theta)^2 + \sigma_{yy}^{PAS} (\sin \phi \sin \theta)^2 + \sigma_{zz}^{PAS} (\cos \theta)^2) \end{aligned} \quad (2-18)$$

if we define the isotropic chemical shift as:

$$\sigma_{iso} = \frac{1}{3}(\sigma_{xx}^{PAS} + \sigma_{yy}^{PAS} + \sigma_{zz}^{PAS}) \quad (2-19)$$

then subtract this isotropic chemical shift from each principal values and define:

$$\begin{aligned} \sigma_x &:= \sigma_{xx}^{PAS} - \sigma_{iso} \\ \sigma_y &:= \sigma_{yy}^{PAS} - \sigma_{iso} \\ \sigma_z &:= \sigma_{zz}^{PAS} - \sigma_{iso} \end{aligned} \quad (2-20)$$

the formula for calculation the resonance frequency can be further simplified, here two cases with different tensor symmetry are discussed:

- Case 1: Tensor has axial symmetry with respect to its principal z axis. So that, $\sigma_x = \sigma_y$ and $\sigma_z = -2\sigma_x = -2\sigma_y$, the frequency formula is given as:

$$\omega_{CS,aniso} = -\omega_0 \sigma_z \frac{1}{2}(3\cos^2\theta - 1) \quad (2-21)$$

due to this dependence of resonance frequency on molecular segment orientation, in a powder sample a specific powder line-shape will be observed. In solid NMR, powder means a isotropic sample of sufficiently rigid materials.

For the case of axial symmetric tensor, the calculation of the powder spectrum is relatively easy because of the angle ϕ independence. The principle is that: the integral intensity of corresponding interval in θ and ω is equal:

$$S(\omega(\theta))|d\omega| = P(\theta)|d\theta| \quad (2-22)$$

divided both sides by $d\theta$, and re-arrange:

$$S(\omega(\theta)) = P(\theta)/|d\omega/d\theta| = P(\theta)/|3\delta \sin\theta \cos\theta| \quad (2-23)$$

for powder samples, $P(\theta)$ is solely decided by the size of the surface element, $P(\theta) = \sin\theta$

and it is normalised according to $\int_{0^\circ}^{90^\circ} P(\theta)d\theta = 1$. This leads to:

$$S_{powder}(\omega(\theta)) = \frac{1}{3\delta|\cos\theta|}, \quad |\cos\theta| = \frac{\sqrt{2}}{\sqrt{3}}\sqrt{\omega/\delta + \frac{1}{2}} \quad (2-24)$$

finally, it is given as:

$$S_{powder}(\omega(\theta)) = \frac{1}{\sqrt{6}\delta} \frac{1}{\sqrt{\omega + \frac{1}{2}\delta}}, \quad -\frac{\delta}{2} \leq \omega \leq \delta \quad (2-25)$$

the shape of this powder spectrum is shown in fig2-2, it was firstly calculated by Bloembergen and Rowland in 1953 [Bloembergen and Rowland, 1953]. The centre of the range covered by this powder spectrum is at $\omega(45^\circ) = \delta/4$, the centre of gravity is at $\omega(54.74^\circ) = 0$.

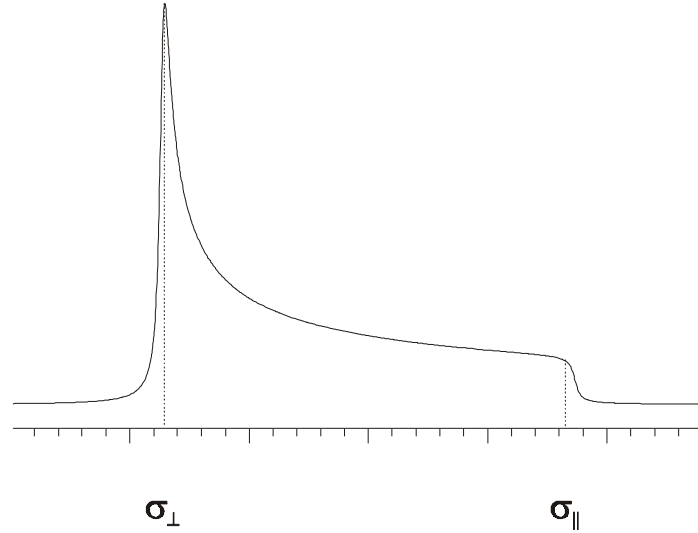


Figure 2-2: Powder spectrum for chemical shift tensor with axial symmetry.

- Case 2: Tensor has no symmetry. In this case, it is useful to introduce two popularly referenced parameters:

$$\text{asymmetry parameter: } \eta := \frac{\sigma_y - \sigma_x}{\sigma_z} \quad (2-26)$$

$$\text{anisotropy parameter: } \delta = -\omega_0 \sigma_z \quad (2-27)$$

the frequency formula is then given as:

$$\omega(\theta, \phi) = \delta \frac{1}{2} (3 \cos^2 \theta - 1 - \eta \sin^2 \theta \cos(2\phi)) \quad (2-28)$$

when $\eta = 0$ it is the case of tensor with axial symmetry. The Euler angles (θ, ϕ) of the \vec{B}_0 field in PAS are also the Euler angles $(\theta, \phi, \text{arbitrary})$ specifies the Euler transformation from PAS into laboratory frame. The third Euler angle, corresponding to a rotation around the \vec{B}_0 axis is not relevant for the frequency, since the secular interactions are invariant under a rotation around \vec{B}_0 .

The calculation of the powder spectrum for the general case of $\eta \neq 0$ is much more complicated, it has been treated by Bloembergen and Rowland (1953). Here only the result is given as shown in fig2-3. The resulting spectra span the range between $-\frac{1}{2}\delta(1+\eta)$ and $+\delta$. At σ_y the spectrum has maximum intensity which decreases with increasing η .

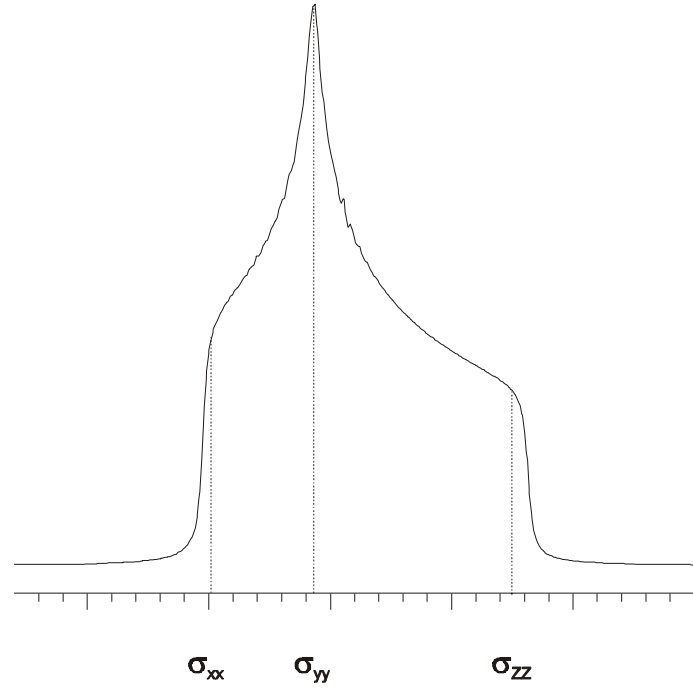


Figure 2-3: Powder spectrum for chemical shift tensor with asymmetry parameter

$$\eta = (\sigma_y - \sigma_x) / \sigma_z .$$

Additionally it must be pointed out that: any real spectrum is a convolution of the theoretical spectral distribution with the line-broadening functions of different resonance lines.

2.3.2 chemical shift interaction - macroscopic sample rotation

Macroscopic sample rotation renders the orientation of chemical shift tensor with respect to external magnetic field time dependent, this leads to a time dependence of the NMR resonant frequency. In a co-ordinate system shown in fig2-4, the sample is spun at a angular frequency ω_r around an axis at an angle ξ with respect to the external magnetic field \vec{B}_0 . Therefore, the sample feels an oscillating magnetic field which is given as:

$$\vec{B}_0 = B_0 (\sin \xi \cos \varphi, \sin \xi \sin \varphi, \cos \xi) \quad (2-29)$$

where

$$\varphi = \varphi + \omega_r t \quad (2-30)$$

according to equation (2-17), the resonant frequency of a given spin is written as:

$$\omega = -\gamma B_0 (\hat{b}_0 \cdot \underline{\underline{\sigma}}^R \cdot \hat{b}_0) \quad (2-31)$$

where $\underline{\underline{\sigma}}^R$ is the chemical shift tensor of a spin with a molecular orientation R in PAS reference system. Evaluation of equation [2-31] shows that there are three terms: one is time independent,

one oscillates with frequency ω_r , and one oscillates with frequency $2\omega_r$ [Herzfeld and Berger, 1980].

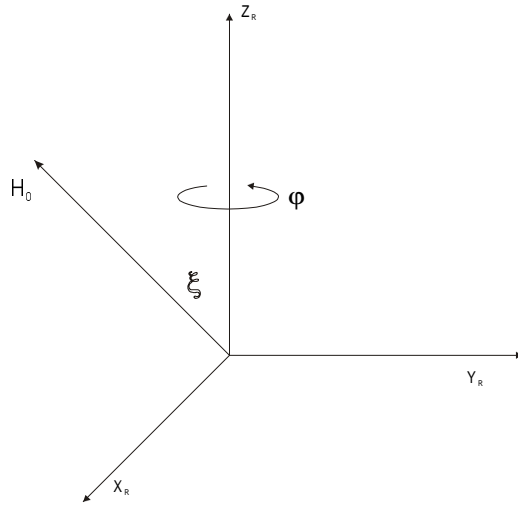


Figure 2-4: The co-ordinate system with the rotor as the frame of reference. The Z_R is the axis of rotation of the sample. H_0 is a unit vector in the direction of the applied magnetic field

$$\omega(\alpha, \beta, \gamma, \xi, t) = -\gamma B_0 \left\{ \bar{\sigma} + \frac{1}{2} (3 \cos^2 \xi - 1) (\sigma_{33}^R - \bar{\sigma}) \right\} + \sin^2 \xi \left[\frac{1}{2} (\sigma_{11}^R - \sigma_{22}^R) \cos(2\varphi) + \sigma_{12}^R \sin(2\varphi) \right] + 2 \sin \xi \cos \xi \left[\sigma_{13}^R \cos \varphi + \sigma_{23}^R \sin \varphi \right] \quad (2-32)$$

where $\bar{\sigma}$ is the isotropic chemical shift

$$\bar{\sigma} = \frac{1}{3} (\sigma_{11}^R + \sigma_{22}^R + \sigma_{33}^R) = \frac{1}{3} (\sigma_{xx} + \sigma_{yy} + \sigma_{zz}) \quad (2-33)$$

$\underline{\underline{\sigma}}^R$ depends on the relative orientation of the molecular segment R with respect to PAS system according to the following expression:

$$\underline{\underline{\sigma}}^R = R(\alpha, \beta, \gamma) \begin{pmatrix} \sigma_{xx} & 0 & 0 \\ 0 & \sigma_{yy} & 0 \\ 0 & 0 & \sigma_{zz} \end{pmatrix} R^{-1}(\alpha, \beta, \gamma) \quad (2-34)$$

where $R(\alpha, \beta, \gamma)$ is the rotation matrix for the Euler angles α, β, γ describing the orientation of the molecule segment relative to principal value system in which the chemical shift tensor is diagonal:

$$R = \begin{pmatrix} \cos \gamma & \sin \gamma & 0 \\ -\sin \gamma & \cos \gamma & 0 \\ 0 & 0 & 1 \end{pmatrix} \begin{pmatrix} \cos \beta & 0 & -\sin \beta \\ 0 & 1 & 0 \\ \sin \beta & 0 & \cos \beta \end{pmatrix} \begin{pmatrix} \cos \alpha & \sin \alpha & 0 \\ -\sin \alpha & \cos \alpha & 0 \\ 0 & 0 & 1 \end{pmatrix} \quad (2-35)$$

for further simplification, two general cases are considered:

- Case 1: $\xi = 54^\circ 44''$, sample is spun at the magic angle position

when $\xi = 54^\circ 44''$ the frequency formula of equation [2-32] is simplified to:

$$\omega = -\gamma B_0 \left\{ \bar{\sigma} + \frac{2}{3} [A_2 \cos(2\varphi + 2\gamma) + B_2 \sin(2\varphi + 2\gamma)] + \frac{2}{3} \sqrt{2} [A_1 \cos(\varphi + \gamma) + B_1 \sin(\varphi + \gamma)] \right\} \quad (2-36)$$

where the coefficients are:

$$\begin{aligned} A_1 &= \sin \beta \cos \beta [\cos^2 \alpha (\sigma_{xx} - \sigma_{zz}) + \sin^2 \alpha (\sigma_{yy} - \sigma_{xx})] \\ A_2 &= \frac{1}{2} (\cos^2 \beta \cos^2 \alpha - \sin^2 \alpha) (\sigma_{xx} - \sigma_{zz}) + \frac{1}{2} (\cos^2 \beta \cos^2 \alpha - \sin^2 \alpha) (\sigma_{yy} - \sigma_{zz}) \\ B_1 &= -\sin \alpha \cos \alpha \sin \beta (\sigma_{xx} - \sigma_{yy}) \\ B_2 &= -\sin \alpha \cos \alpha \cos \beta (\sigma_{xx} - \sigma_{yy}) \end{aligned} \quad (2-37)$$

for a powder sample, the free induction decay of the whole sample is given by:

$$g(\xi, t) = e^{-\frac{t}{T_2}} \cdot \frac{1}{8\pi^2} \int_0^{2\pi} \int_0^\pi \int_0^{2\pi} \exp \left[i \int_0^t \omega(\alpha, \beta, \gamma, t) dt \right] d\alpha \sin \beta d\beta d\gamma \quad (2-38)$$

where T_2 is the transverse relaxation time. The Fourier transform of the free induction decay consists of a central resonance at the isotropic chemical shift position and a series of spinning side bands spaced ω_r apart from each other. The principal values of the chemical shift anisotropy can be recovered from the relative intensities of the spinning side bands [Herzfeld and Berger, 1980]. When the spinning speed of the sample ω_r is larger comparing with the anisotropy δ of chemical shift interaction of a particular spin, the intensities of the spinning side bands become non-significant and only the central resonance is reserved. This is the case of high resolution solid state NMR.

- Case 2: $\xi \neq 54^\circ 44''$, sample is spun at the Off Magic Angle position

In this case, the general frequency formula of equation [2-32] is not easy to be further analytically simplified. However, in the special case of fast sample spinning: $\omega_r \gg \delta$, all spinning side bands will disappear and the frequency formula is simply given as:

$$\omega(\xi, t) = -\gamma B_0 \left[\bar{\sigma} + \frac{1}{2} (3 \cos^2 \xi - 1) (\sigma_{33}^R - \bar{\sigma}) \right] \quad (2-39)$$

the final spectrum consists of one single anisotropic line located at the isotropic chemical shift position, its shape resembles the powder line shape. However, the chemical shift anisotropy of

this line is scaled down to $\frac{1}{2} (3 \cos^2 \xi - 1) (\sigma_{33}^R - \bar{\sigma})$.

2.4 Study of orientation distribution from anisotropic NMR interactions

To study the orientation distribution of partially ordered polymer materials by the method of NMR, an angular-dependent anisotropic interaction of the interested nuclear spins must be investigated. A number of studies have been reported for partly drawn polymers, in which the constituent chains are preferentially but not fully oriented [McBrierty, V. J., et al, 1968, 1971, 1973; Kashiwagi, M., et al, 1971,1972,1973]. Three possible NMR anisotropic interactions are discussed in the following:

2.4.1 The anisotropy of dipole-dipole interaction

By means of the anisotropy of direct dipole-dipole interaction, the most often used nucleus is ^1H . In this case, the dependence of resonance frequency on the orientation of inter-nuclear vector is given as (for the case of homonuclear interaction):

$$\omega = \delta \frac{1}{2}(3\cos^2 \theta - 1) = \frac{3\mu_0}{8\pi} \hbar \frac{\gamma_1\gamma_2}{r_{1,2}^3} (3\cos^2 \theta - 1) \quad (2-40)$$

here θ is the angle between the external magnetic field \vec{B}_0 and the inter-nuclear vector connecting nucleus 1 and nucleus 2, $r_{1,2}$ is the distance between them. The advantage of this method is its large S/N ratio in the case of ^1H & ^{13}F nuclei and correspondingly a very short measuring time. The main disadvantage is that: overlapping of many dipolar pair-interactions normally make the resonance line featureless, therefore well defined line-splitting can only be observed in some special samples. Experimentally, there are several procedures to implement his strategy:

- Obtain $\langle P_2 \rangle$ from line splitting. But, in practice, well defined line splitting is hardly available in polymer materials which consist of complicated macromolecules. Due to many possible structural conformations and motional averaging, usually the final ^1H spectrum is a featureless broad line.
- Line-shape analysis. In theory, if the exact relative positions of all surrounding spins within the molecule are known, it is possible to calculate the theoretical line-shape due to dipole-dipole interactions [Hentschel, Schlitter, Sillescu, Spiess, 1977]. Then, orientation distribution can be deduced out by a comparison between theoretical and experimental line-shape. But, because the complicated structural conformations in macromolecular polymers, the position information of the surrounding spins are hardly possible to be obtained.
- Moment analysis of the wide-line spectra. This is the classical and the most successful method which is popularly applied in the case of proton NMR [Van Vleck, 1948; McBrierty, 1993]. The dependence of second and fourth moments of dipolar broadened lines on sample orientations relative to \mathbf{B}_0 is a direct reflection of molecular orientations in partially ordered

polymers. In principle, it is possible to determine all moments; in practice, constraints arise from experimental factors such as signal-to-noise ratio. Arbitrary number of experiments for different sample orientations relative to \mathbf{B}_0 over-determine the accessible moments [McCall and Hamming, 1959]. Practically, lower order moments of the distribution are evaluated first and these are used in fitting of the experimental data to determine moments of higher order.

2.4.2 The anisotropy of quadrupolar interaction

The most popular nucleus used in this scope is deuterium ^2H , this method is also referenced as ^2H NMR [Spiess, 1984, 1985]. In this case, the spectra are dominated by intramolecular quadrupole interaction between the quadrupole moment and the electric field gradient (EFG) tensor [Hentschel, 1979; Spiess, 1980]. The dependence of resonance frequency on the molecular segment orientation is given as [Schmidt-Rohr and Spiess, 1994]:

$$\begin{aligned} \omega &= \delta_Q \frac{1}{2} (3 \cos^2 \theta - 1 - \eta \sin^2 \theta \cos(2\phi)) \\ &= \frac{1}{2} \cdot 3 \cdot \frac{eQeq}{4\hbar} (3 \cos^2 \theta - 1 - \eta_Q \sin^2 \theta \cos(2\phi)) \end{aligned} \quad (2-41)$$

here Q is the quadrupolar moment. In aliphatic $\text{C}-^2\text{H}$ bond the asymmetry parameter η_Q of the electric field gradient tensor is negligible ($\eta_Q \cong 0$) due to the approximately uniaxiality of the electron density in this bond [Hentschel, et al., 1976]. This symmetry also causes the unique z axis of the PAS of the electric gradient tensor to coincide with the $\text{C}-^2\text{H}$ bond direction. This well defined tensor orientation is of great value in the interpretation of ^2H NMR spectra [Hentschel, 1981].

The advantage of this method is a very clean spectrum with good S/N, almost without any influence coming from other kinds of spin interactions. The disadvantage is: because the natural abundance of ^2H is very low, usually selective deuteration of the sample is necessary and this procedure is very expensive as well as very time consuming.

2.4.3 The anisotropy of Chemical Shift interaction

To study the orientation dependence of the chemical shift tensor in terms of structural unit distributions it is necessary to get (i) undistorted spectra and (ii) tensors are well defined in the molecular fixed system. Ideally, Chemical shifts which cover a wide range and exhibit appreciable anisotropies are preferred [McBrierty, 1993]. For this purpose, nucleus ^{13}C and ^{29}Si are frequently used. With these two nuclei, it is also possible to make Chemical Shift interaction the dominant term by suppressing all other spin interactions through various ingenious NMR methods such as dipolar de-coupling, multi-pulse sequence, etc. Several procedures are available to implement this strategy.

- Direct line-shape analysis. In this approach, the orientation distribution of structural units is obtained by a direct comparison of the experimental spectrum from the sample in oriented state and a theoretical powder spectrum. In Principle, this method can characterise the complete orientation distribution. However, due to the generally existing overlap of different lines and the „round off“ of spectral line features, it is not adequate for most complicated macromolecular polymers.
- Moment analysis. This approach is very similar as the moment analysis of ^1H spectra dominated by dipolar-dipolar interactions. With this method, the orientation degrees (up to several orders) are directly available. Due to noise in the spectrum, difficulty will arise for the analysis of higher order moments.
- Synchronised - MAS 2D procedure: site-resolved orientation measurement [Harbison, 1987]. This experiment is conducted under magic angle spinning and rotor synchronised phase delays. In the direct dimension, due to slow sample spinning the anisotropic chemical shift interaction shows up as a number of spinning side bands. Therefore, it leads to a better resolved, high resolution like spectra. In the indirect dimension, orientation information can be obtained from the side band patterns.
- 3D ORDER procedure [Titman et al., 1993]. This is the 3D extension of Harbison’s 2D method. In Harbison’s 2D approach, there are apparent overlap of various sideband patterns although the differences in their isotropic chemical shifts are appreciable. In polymer systems where the sidebands are broadened by conformational and packing effects, the overlapping is particular serious. Therefore, a 3D experiment which separate spinning sidebands of different order according to their isotropic chemical shifts is desirable. In principle this 3D approach gives a better resolution, but at the expense of long experimental time.
- DECODER (Direction Exchange with Correlation for Orientation Distribution Evaluation and Reconstruction) procedure. In this method, the orientation dependent frequency for each individual segment is measured two or three times by means of 2D or 3D NMR spectroscopy with a sample flip between the evolution and detection periods [Henrichs, 1987]. In principle, full orientation distribution can be obtained through the final 2D or 3D correlation spectra [Schmidt-Rohr et al., 1992; Chmelka et al., 1993], However, in 2D cases overlapping often impedes the further orientation distribution analysis.
- VACSY procedure, this is the method we selected for the investigation of molecular orientation distribution of liquid crystal polymers in solid state. In this method, the separation & correlation of isotropic and anisotropic interactions is achieved through a number of independent variable-angle-spinning (VAS) experiments [Frydman et al., 1992]. In the direct direction, there is no overlapping and all spectral lines are separated according to their

Chemical Shift isotropic values; In the indirect direction, the complete orientation distribution can be derived from the CSA line-shape at different isotropic positions.

2.5 Procedures to extract orientation distribution from NMR line-shape of chemical shift interaction

There are several procedures available to extract the information about orientation distribution of chemical shift tensors from the NMR line-shape of chemical shift anisotropic interaction. Two most popularly applied methods are discussed in the following:

- direct reconstruction
- moment analysis

2.5.1 Direct reconstruction procedure

Direct reconstruction is the most direct and most convincing method to obtain the orientation distribution. In this approach, the orientation distribution of chemical shift tensors is obtained by a direct comparison of the experimental spectrum from the sample in oriented state and a theoretical powder spectrum [Hempel G., 1982]

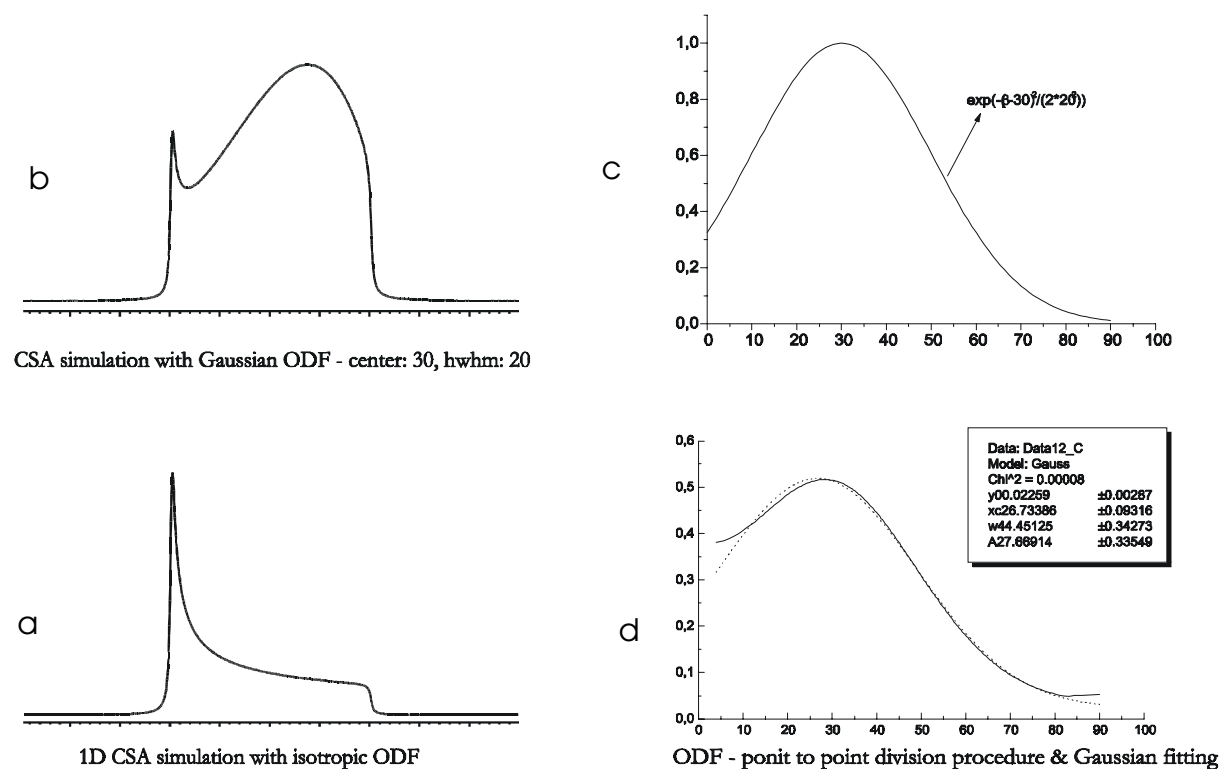


Figure 2-5: Simulation result of the direct reconstruction approach, the chemical shift tensor elements used are $(\sigma_x, \sigma_y, \sigma_z) = (100, 100, -100)$ (ppm). (a) spectrum of isotropic powder. (b) spectrum with an orientation distribution of Gaussian function centred at 30° , hwhm is 23° . (d)

the extracted orientation distribution with application of the direct reconstruction approach to spectra in (a) & (b)

One simulation example is given in fig2-5. The parameters used for this simulation are: $\sigma_{\parallel} = -100 \text{ ppm}$, $\sigma_{\perp} = 100 \text{ ppm}$, $\sigma_{iso} = 33.3 \text{ ppm}$. (a) is the isotropic powder spectrum, (b) is the spectrum with a Gaussian orientation distribution function of the chemical shift tensor, which is centred at 30° with respect to the \mathbf{B}_0 direction and with a half width at half maximum (hwhm) of 23° , its mathematical expression is:

$$u(\cos\theta) = \exp(-\sin^2(\theta - \theta_0)/(2 \cdot \sigma_{\theta}^2)) \quad (2-42)$$

Here θ is the angle between the z axis of the PAS system and the external magnetic field \mathbf{B}_0 direction. ODF function is drawn in (c). (d) is the result of the direct ‘point to point’ division of spectrum (b) by spectrum (a), where the solid line is the direct result and the dash line is the corresponding Gaussian function fitting. The result of the Gaussian fitting is: centre at 26.7° , hwhm is 44.5° . The difference between the fitting results and the input orientation distribution parameters for simulation is due to the broadening effects of the spectra and digital calculation noise.

With this direct reconstruction procedure, in principle, the complete orientation distribution function can be obtained; in practice, due to noise and spectra rounding, the result might be totally meaningless. Nevertheless, the most important advantage of this procedure is its simplicity. It does not need any experimental data fitting, therefore very robust. The disadvantage of this procedure is that: it can be applied only to a sample with axially symmetric CS tensor, only in this case the NMR spectrum contains a direct image of the angular distribution. That means: a single spectral peak corresponds to a single angular peak, no degeneration of spectral peaks occurs. Therefore, the angular distribution can be directly reconstructed from the spectral intensity [Schmidt Rohr & Spiess, 1994].

2.5.2 Moment analysis procedure

Moment analysis is the classical method to analyse the orientation distribution of partially ordered samples NMR [Van Vleck, 1948; McBrierty, 1993]. The moments of a NMR resonant line is defined as:

$$M_n = \int (\omega - \omega_{iso})^n S(\omega) d\omega \quad (2-43)$$

where M_n is n th moment of the NMR spectral line $S(\omega)$, ω_{iso} is isotropic chemical shift frequency. From the values of these moments M_n , the orientation degrees or the moments of the distribution of chemical shift tensors can be calculated. In the following, the cases with transversal symmetry and the general case without any symmetry are discussed separately.

2.5.2.1 Moment Analysis for a uniaxial system

Here, we assume that the investigated sample exhibits transverse symmetry, both macroscopically and microscopically. So that the orientation distribution can be described by a single angle θ which specifies the tensor symmetry axis direction \vec{Z}_p relative to the external magnetic field direction \vec{Z}_L . This distribution function $R(\theta)$ can be expanded in terms of Legendre polynomials $P_L(\cos\theta)$, which form a complete set of orthogonal basis functions for $\cos\theta$ over the interval $[0...1]$.

$$R(\theta) = \sum_L (2L+1) \langle P_L \rangle P_L(\cos\theta) \quad (2-44)$$

the range $0 \leq \cos\theta \leq 1$ corresponds to the angle range $0 \leq \theta \leq 90^\circ$ which is sufficient for the analysis of NMR second-rank tensor orientations [Schmidt-Rohr & Spiess, 1994]. The coefficients $\langle P_L \rangle$ in (2-44) are often referenced as orientation degrees. Because $P_L(\cos\theta)$ functions are orthogonal, $\langle P_L \rangle$ can be easily calculated as:

$$\langle P_L \rangle = \int_0^1 R(\theta) P_L(\cos\theta) d \cos\theta \quad (2-45)$$

the distribution function is normalised according to:

$$\langle P_0 \rangle = \int_0^1 R(\theta) d \cos\theta = \int_{0^\circ}^{90^\circ} R(\theta) d\theta \sin\theta = 1 \quad (2-46)$$

$\langle P_0 \rangle$ is considered as representing the isotropic part of the distribution. The orientation degrees $\langle P_L \rangle$ for $L > 0$ contain the information about orientation distribution. Particularly, if the orientation is centred around $\theta = 0^\circ$, $\langle P_2 \rangle$ characterise the width of the distribution: the smaller the $\langle P_2 \rangle$, the larger the width of the orientation distribution $R(\theta)$. However, if the distribution contains isolated δ functions which means very sharp peaks, the Legendre Polynomial expansion is not convergent. For example, if the distribution is $\delta(\theta)$, all the orientation degrees $\langle P_L \rangle = 1$ for $L > 1$.

For the convenience of data analysis, a few basic properties of the orientation degrees in the Legendre polynomial expansions and several representative orientation cases are summarised in the following.

- if normalisation condition $\langle P_0 \rangle = 1$, all other orientation degrees are in the range $[1, -0.5]$
- if all orientation degrees $\langle P_L \rangle = 0$ when $L > 0$, then $R(\theta)$ is isotropic.
- if all orientation degrees $\langle P_L \rangle = 1$, the distribution is perfect uniaxial with $R(\theta) = \delta(\theta)$

Usually, Gaussian distribution function is used to approximate a real distribution:

$$R(\theta) = N \exp(-\sin^2 \theta / 2\sigma_\theta^2) \quad (2-47)$$

for Gaussian distribution, all orientation degrees are positive as can be easily proved by actually evaluating the integrals of equation (2-45). The values of the orientation degrees decrease monotonically with increasing order L. The orientation degrees of Gaussian distributions as a function of σ_θ is shown in fig2-6:

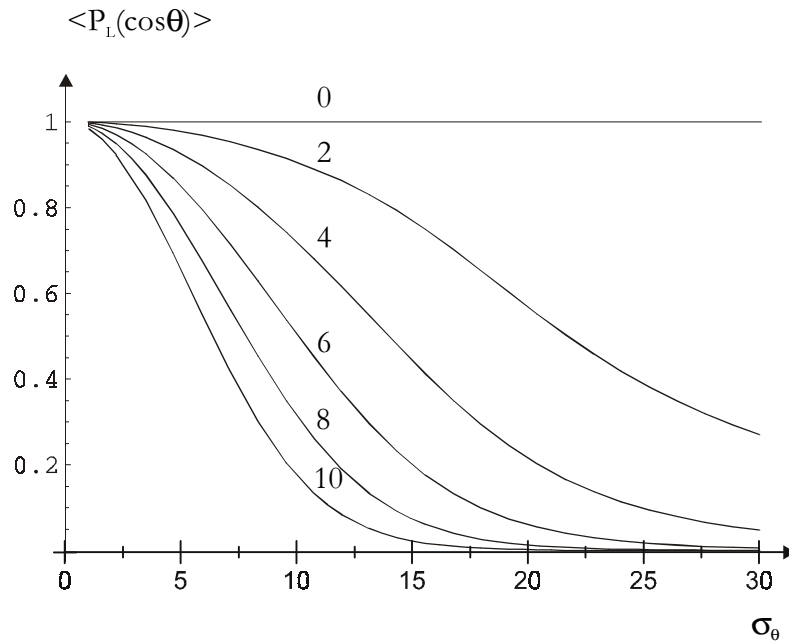


Figure 2-6: dependence of order parameters on the width σ_θ of a Gaussian orientation distribution. For this specific type of distribution, the order parameters decrease with increasing L. For comparing widths of distributions as given in different publications, it may be important to remember that the full width at half maximum of the Gaussian is $2.35 \sigma_\theta$.

For the convenience of later analysis, the values of second order orientation degree $\langle P_2 \rangle$ for some σ_θ values of a Gaussian orientation distribution are given in table2-1:

$\text{acos}(\sigma_\theta)$	5°	10°	15°	20°	23°	25°	30°	35°	40°
$\langle P_2 \rangle$	0.98	0.91	0.77	0.57	0.45	0.39	0.27	0.20	0.15

From the theory of spectral line-shape analysis for partially ordered polymers developed by Hentschel et al. [Hentschel, 1978; McBrierty, 1993], assume the sample has (i) fibre symmetry and the structural units are also transversely isotropic (ii) axially symmetric coupling tensors, the relationship between the moments M_n of NMR line-shape and orientation degree $\langle P_L \rangle$ is derived in the following [Hempel, 1998]. The number of tensors which have their

symmetry axes in the interval $[\cos\theta, \cos\theta + d(\cos\theta)]$ is given as $R(\cos\theta)d(\cos\theta)$, they contribute to NMR line-shape in the resonant frequency region $[\omega, \omega + d\omega]$ with relative intensity $S(\omega)d\omega$. That is:

$$R(\cos\theta)d(\cos\theta) = S(\omega)d\omega \quad (2-48)$$

replacing the integrand of equation (2-43) with equations (2-48) and (2-21), we get:

$$M_n = \left(\frac{2}{3} \Delta\sigma \right)^n \langle P_2^n \rangle \quad (2-49)$$

define:

$$m_n = \frac{M_n}{\left(\frac{2}{3} \Delta\sigma \right)^n} = \langle P_2^n \rangle$$

and by expanding the powers of P_2 into linear sum of Legendre polynomials, for some n values we get:

$$\begin{aligned} m_1 &= \langle P_2 \rangle_{cs} \\ m_2 &= \frac{18}{35} \langle P_4 \rangle_{cs} + \frac{2}{7} \langle P_2 \rangle_{cs} + \frac{1}{5} \langle P_0 \rangle_{cs} \\ m_3 &= \frac{18}{77} \langle P_6 \rangle_{cs} + \frac{108}{385} \langle P_4 \rangle_{cs} + \frac{3}{7} \langle P_2 \rangle_{cs} + \frac{2}{35} \langle P_0 \rangle_{cs} \\ &\dots \end{aligned} \quad (2-50)$$

therefore, the steps to reconstruct the orientation distribution function are:

- calculate out M_n according to equation [2-43]
- calculate out $\langle P_L \rangle$ according to equation [2-50]
- reconstruct orientation distribution according to equation [2-44]

2.5.2.2 Full expansion for non-axial systems

Until now we have restricted our discussion to the case of uniaxial samples with transverse symmetry in coupling tensors, then the orientation distribution can be expanded in terms of the Legendre polynomials $P_L(\cos\theta)$. The general case is based on the same principle but more complicated. In this case, three Euler angles (φ, θ, ϕ) are necessary to describe the relative orientation of chemical shift tensors with respect to LF reference system.

For the general case, the suitable set of basis functions are the Winger functions, the expansion is given as:

$$R(\varphi, \theta, \phi) = \sum_{L=0}^{\infty} \sum_{m=-L}^L \sum_{n=-L}^L P_{Lmn} D^L_{mn}(\varphi, \theta, \phi) \quad (2-51)$$

the Winger functions are orthogonal and the orientation degrees P_{Lmn} are the averages of the orientation-distribution function weighted with the D^L_{mn} .

$$P_{Lmn} = \frac{2l+1}{8\pi^2} \int_0^{2\pi} \int_{-1}^1 \int_0^{2\pi} R(\varphi, \theta, \phi) D^L_{m,n}{}^*(\varphi, \theta, \phi) d\varphi d(\cos\theta) d\phi \quad (2-52)$$

$R(\varphi, \theta, \phi)$ is normalised according to:

$$\int_0^{2\pi} \int_{-1}^1 \int_0^{2\pi} R(\varphi, \theta, \phi) d\varphi d(\cos\theta) d\phi = 1 \quad (2-53)$$

then, similar steps as in the case of samples and coupling tensors with transverse symmetry could be used to reconstruct the orientation distribution function.

As mentioned at the beginning of this section, moment analysis is the most frequently applied procedure to obtain ODF information from ^1H NMR spectra. The advantage of this method is that it is not sensitive to noise. However, when comes to higher moments, the influence of the noise is drastically enlarged by the term $(\omega - \omega_{iso})^n$ in the definition formula of the moments.

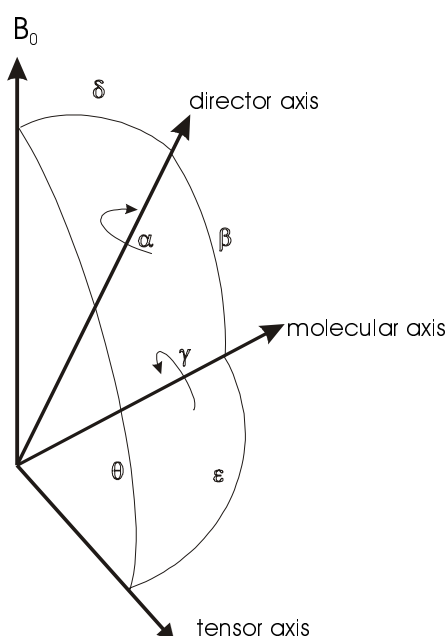


Figure 2-7: The angles used to describe the sample's orientation distribution. θ describes the angle of chemical shift tensor symmetry axis with respect to external magnetic field \mathbf{B}_0 . δ describes the angle of the sample director direction with respect to the external magnetic field \mathbf{B}_0 . ϵ is the angle describes the orientation of chemical shift tensor symmetry axis relative to molecular segment. β is the most important angle which describes the orientation distribution of molecular segments with respect to the sample director direction.

Until now we are only talking about the orientation distribution of chemical shift tensors, this is the information which can be directly obtained from the NMR spectra under some reasonable assumptions. However, this orientation distribution information does not have too much practical meaning, what most interesting to material scientists is the orientation distribution of molecular segments (MF reference system) with respect to sample director direction (DF reference system). In order to get molecular segment orientation distribution, some additional information, such as the angle ε between the tensor symmetry axis \vec{z}_p and the molecular symmetry axis \vec{z}_M as indicated in fig2-7, must be available.

NMR METHODS TO MEASURE CHEMICAL SHIFT ANISOTROPY

3.1 Introduction

Cross-Polarisation-magic-angle-spinning (CPMAS) with high-power proton decoupling [Schaefer, 1976] has been widely applied to obtain high resolution NMR spectra of dilute spin-1/2 in solids. This method averages out all anisotropic NMR interactions which transform as second-rank tensors, such as chemical shift anisotropical interactions. However, the principal elements of chemical shift anisotropy tensor contain useful information on structure, dynamics and orientation of molecular segments. Attempts to recover these CSA parameters in high resolution solid-state NMR appeared almost at the same time with the introduction of CPMAS technique [Lipmaa, 1976; Stejskal, 1977].

Among the different CSA reconstruction schemes, except for the most simplest materials, overlap of patterns from different groups prevents the valuable information from being extracted out from one dimensional spectra. Therefore, a variety of two dimensional separation methods have been proposed to resolve anisotropic line-shapes according to the isotropic frequencies of individual sites. Some of these techniques rely on static or quasi-static detection and generate the isotropic evolution by mechanical sample motions, such as: stop-and-go [Zeigler et al., 1988], magic-angle hopping during evolution [Bax et al., 1983a], flipping of sample rotation axis from MAS to OMAS [Bax et al., 1983b; Terao et al., 1984; Maciel et al., 1985], variable-angle correlation spectroscopy (VACS) [Frydman et al, 1992a, 1992b, 1993, 1994; Lee et al., 1994; Sachleben, 1997], ultra slow MAS with three periods of evolution [Gan, 1982; Harper et al., 1998; Hu et al., 1994; McGorge et al., 199], etc. The reliability and good resolution of the quasi-static spectrum obtained by using these methods are very important. Except the recently introduced ultra-slow MAS approach, all the techniques mentioned above can not be performed on standard MAS equipment.

Another category of methods that are based on re-introducing the anisotropic interaction by 180° pulses synchronised with sample spinning at magic angle position are developed to avoid the severe requirements on hardware equipment. These pulses usually involve the evolution period of the experiments, while the detection period acquires the normal MAS signal. In general, due to the multiple 180° pulses applied during the evolution, these techniques are very sensitive to experimental imperfections, which can severely distort the powder patterns; the resolution is also reduced compared with the methods of static detection.

In order to explain why we choose VACSYS for this work, some of the above mentioned methods are briefly discussed in the following.

3.2 Methods to retrieve CSA patterns

3.2.1 Stop-and-go

This is a conceptually simple but mechanically demanding technique, this method has been implemented by Maciel and co-workers [Zeigler et al., 1988]. The idea of this method is: after an evolution period for a static sample, the spinner is turned on and the signal is detected under MAS. In principle, the experiment could also be performed with MAS evolution and stopping of the rotor to detect the signal from the static sample in t_2 .

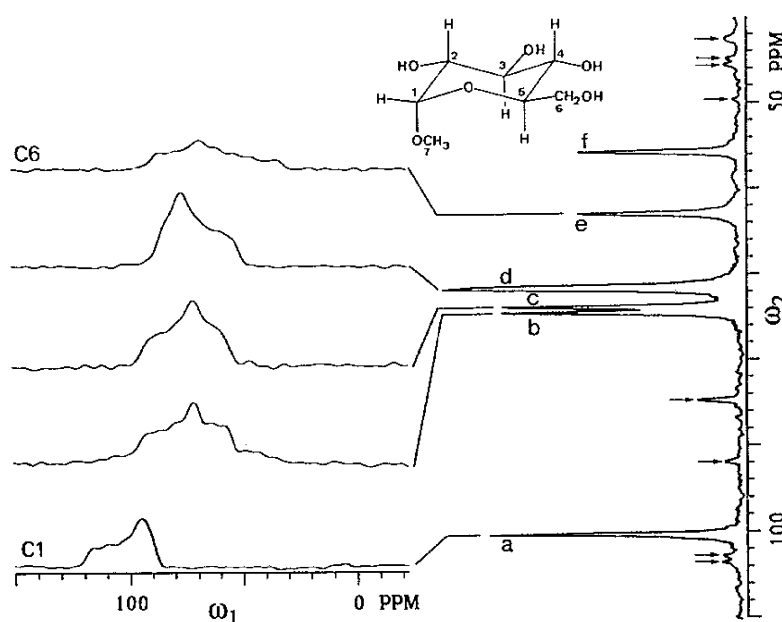


Figure 3-1: Stop-and go spectrum of Methyl- α -D-glucopyranoside taken at a Lamor frequency of 50MHz and a spinning speed of 1.7kHz; arrows mark spinning sidebands. The turn-on time of the rotor was three to five seconds (adapted from Zeiger et al., 1988).

This experiment yields reliable static spectra in the anisotropic dimension. However, there are limitations on either the spinning speed or the swiftness of the angle change between stopping and spinning. In the literature, a rotation frequency of 2k Hz and a turn-on time of 3 seconds have been reported. Due to the friction forces occurred in the rapid spinning speed changes, wear of the spinner assembly is inevitable. One example spectrum of this stop-and-go method from Zeigler et al. (1988) is shown in fig3-1.

3.2.2 Magic-Angle-Hopping, Magic-Angle-Turning (MAT)

Magic angle hopping [Bax et al., 1983a] is a conceptually interesting approach which consists of averaging the chemical shift anisotropy to zero by allowing the magnetisation evolve

at three suitable orientations of the sample relative to the \mathbf{B}_0 field. After such an effectively isotropic evolution, the static anisotropic pattern is observed in the detection period. The pulse sequence in fig3-2 shows the three dipolar de-coupled evolution periods and the intermittent sample flipping periods during which one component of the magnetisation is aligned along the z direction. While in these three flipping periods, not the whole magnetisation is flipped to the Z direction, therefore there is a considerable loss of sensitivity in the final spectrum. The rotation axis is at the magic angle with respect to \mathbf{B}_0 , this indicates its intrinsic relationship with magic angle spinning.

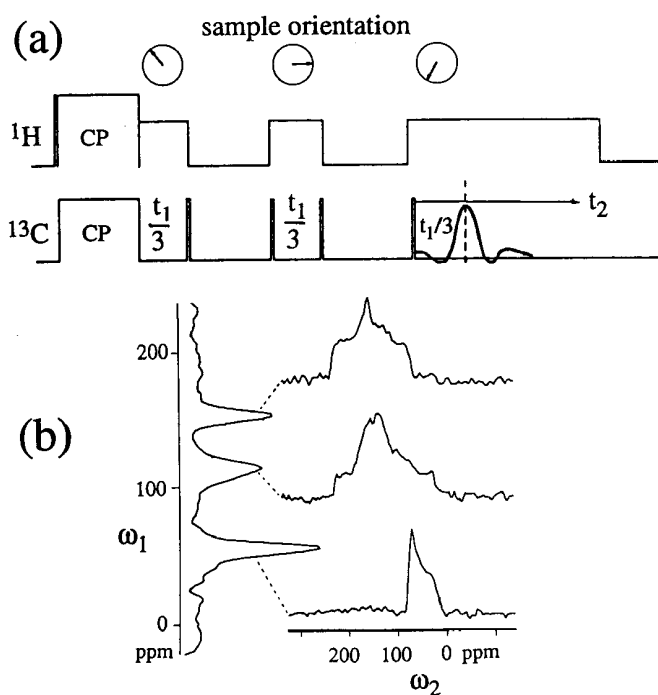


Figure3-2: Magic-angle hopping. (a) Pulse sequence. (b) Slices along the anisotropic-shift dimension and absolute-mode projection onto isotropic-shift axis of a 2D spectrum of 1,4-dimethoxybenzene taken at a ^{13}C Larmor frequency of 25MHz (adapted from Bax et al., 1983b).

The magic angle hopping technique requires a special flip equipment to swiftly rotate the sample from one position to another during one scan, therefore found little application. Recently, it was introduced by Gan [Gan et al., 1992] that the principle of three period evolution at rotor orientations γ , $\gamma+120^\circ$, $\gamma+240^\circ$ can also be applied under ultra-slow MAS conditions. Actually, the sample spinning is so slow that during the detection of the NMR signal the rotor appears to be quasi-static. The higher the \mathbf{B}_0 field, the better the quasi-static approximation, since the chemical shift anisotropies increase proportional to \mathbf{B}_0 .

The ultra-slow magic angle rotation technique has potential for a wide application, since it yields well resolved anisotropic patterns in standard MAS equipment without rotor synchronisation. Disadvantages are the loss of the intensity due to the 'incomplete' flipping and

the relaxation of the transverse magnetisation components in the storage periods of the evolution.

3.2.3 Fast flipping between MAS and Off-MAS

From the discussion in section 2.3, it is not difficult to understand that quasi-static chemical shift anisotropy spectra can be obtained in rotating samples if the sample is spun off the magic angle. This suggests a switching angle sample spinning (SASS) 2D experiment with OMAS evolution, flip of the sample spinning axis to the magic angle, and MAS detection. The magnetisation is stored along the z axis during the sample flip, producing an $\cos(\omega_1 t_1)$ or $\sin(\omega_1 t_1)$ amplitude modulation of the magnetisation detected during t_2 . With an angle θ between the rotation axis and \mathbf{B}_0 , the OMAS spectrum corresponds to the static spectrum scaled by $\frac{1}{2}(3\cos^2\theta - 1)$, if the signal is sampled at multiples of the rotor period, that means $t_{dw} = t_r$. However, if the signal is not sampled at multiples of the rotor period and the sample spinning speed is smaller than the anisotropy parameters, spinning sidebands appear in both direct and indirect dimensions. Moreover, the line-shape of the central band or any arbitrary sideband is not the same as its corresponding static CSA line-shape [Tekely, 1998].

The anisotropic spectrum can always be fitted into the restricted spectral range of $1/t_r$ by choosing a sufficient small OMAS scaling factor, typically used is $\theta_r = \theta_m + 4^\circ$. This is actually very convenient in practice, since it involves only small flip angles. If the isotropic shift is outside the $1/t_r$ range, the spectrum is aliased, but the information is not lost. Through re-arranging the ω_1 data cyclically, the standard representation can be recovered. The pulse sequence for implementing this MAS and OMAS fast flipping method is shown in fig 3-3.

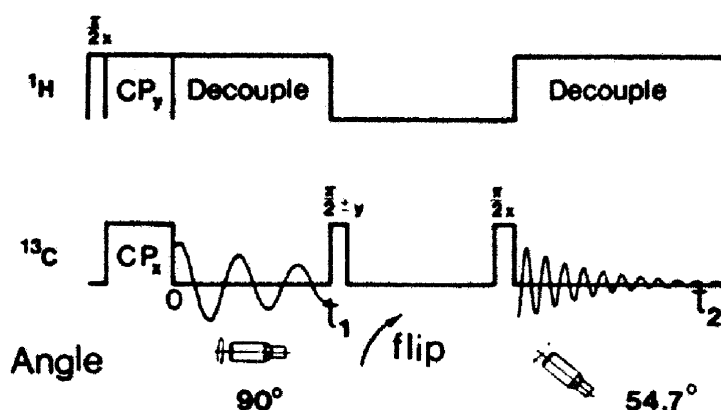


Figure 3-3: Sequence applied in 2D NMR approach for obtaining ^{13}C CSA powder patterns identifiable with individual isotropic chemical-shift averages (adapted from Gary E. Maciel, 1985).

The disadvantages of this method are twofold: (i) it requires a special equipment which can realise the swift MAS-OMAS flipping and make sample spinning stable within one scan,

this is technically very demanding. (ii) the loss of magnetisation by flipping only one component of magnetisation onto z axis and by relaxation during the storage time of the magnetisation.

3.2.4 Tycko's 4- π -pulses method

Even under the conditions of fast magic angle spinning, the complete anisotropic information is possible to be reintroduced by one or several pairs of rotor-synchronised 180° pulses per rotation period. For this category of methods, the sample spins at the magic angle at all times, the signals acquired during the detection period t_2 are modulated by spin precession during the evolution period t_1 , in which rf pulses are applied in synchrony with the sample rotation [Tycko et al., 1989]. The RF pulses prevent sample spinning from averaging out the CSA during t_1 . Fourier transformation with respect to t_1 and t_2 yields a two dimensional spectrum with CSA patterns along one axis and isotropic chemical shift along the other. The CSA patterns of in-equivalent nuclei are resolved in the two dimensional spectrum as long as the in-equivalent nuclei have resolved isotropic shifts in the one dimensional MAS spectrum.

Several versions of this two dimensional „MAS/CSA“ technique have been proposed, differing in the details of the rf pulses applied during t_1 [Alla et al., 1978; Yarim-Agaev et al., 1982; Bax et al., 1983c]. A common feature of these versions of the MAS/CSA technique is the fact that the CSA patterns in the two dimensional spectrum do not, in general, have the same shapes as do one dimensional CSA patterns of stationary sample. In a recently introduced approach from Tycko et al. [Tycko et al., 1989], it is demonstrate that: such distortions can be avoided. The minimum number of 180° pulses required is four. The pulse sequence used in Tycko's MAS/CSA approach is shown in fig 3-4:

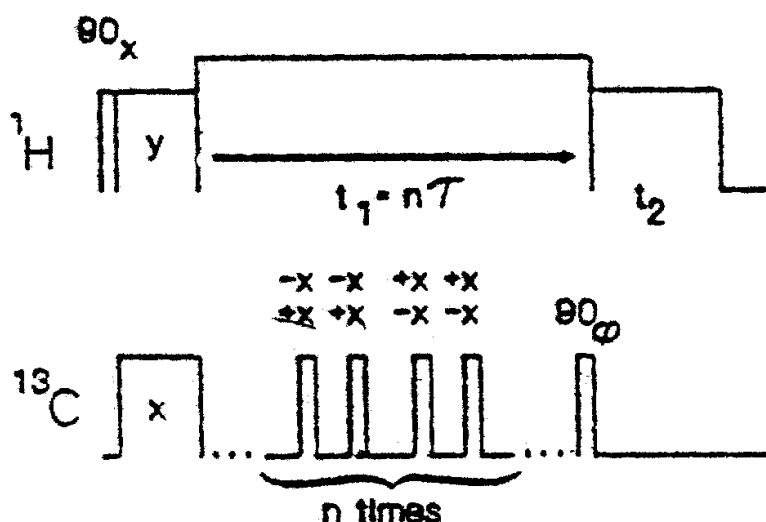


Figure 3-4: Pulse sequence for two-dimensional MAS/CSA experiment. The sample spins at the magic angle with rotation period t . During the t_1 interval, which is incremented in units of t , a sequence of p pulses (in this case, four per rotation period) applied to ^{13}C nuclei prevents the chemical-shift anisotropy from being averaged out by magic-angle spinning. If the p pulses are

given at properly chosen times within the rotation period, chemical-shift-anisotropy powder patterns with the same line-shapes as are observed in stationary samples are obtained in the t_1 dimension of the two-dimensional spectrum. The $p/2$ pulse at the end of t_1 allows purely absorptive spectra to be obtained (adapted from Tycko, 1989).

This multi- 180° pulse MAS method has the important practical advantage that it can be performed on a standard MAS equipment and it can be applied to samples with short T_1 relaxation times. The disadvantages are: firstly, the rotational resonance of ^1H dipolar interaction seriously broadens the CSA line-shape. Secondly, when comes to high speed rotation regime, the approximation: Δ (width of 180° pulse) is much smaller comparing with the rotation period t_r is not valid any more, serious CSA line-shape distortion will show up.

3.2.5 RF field modulation

A unique advantage of NMR is that nuclear spin Hamiltonian can be easily manipulated and modified to severe special purposes, such as the removal of an internal interaction for the spectral simplification and resolution enhancement, or the recovery of an anisotropic interaction in solid state MAS NMR by applying proper rf field perturbations [Ernst et al., 1987]. The predominant advantage of Hamiltonian manipulations by rf modulations is that it does not require critical adjustments of the experimental parameters like pulse width [Ishii et al., 1998].

Until now, the profiles of most rf modulations for Hamiltonian manipulations are relatively simple for the ease of the theoretical treatments, such as: switching between a small number of amplitudes, phases, frequencies and simple continuous modulation fields [Bennett et al., 1995; Hediger et al., 1997]. More general modulations will certainly provide more flexible and efficient manipulations without lengthening the cycle times. However, these more complicated rf fields can not easily be treated theoretically, nor prediction of the response is easy available. In a publication from Ishii and Terao [Ishii et al., 1998], a general procedure is proposed to design rf modulations which realise a desirable Hamiltonian manipulation. This approach provides general solutions, the wave forms of modulations are not always simple. They have a infinite number of freely adjustable parameters. By properly adjusting such parameters, the performance of Hamiltonian manipulations can be improved without lengthening the cycle time.

One example about the application of an amplitude modulation field using Ishii and Terao's approach is demonstrated in fig 3-5 to restore chemical shift anisotropy under fast MAS. While the multiple pulses method proposed by Tycko et al. [Tycko et al., 1989] for recovering CSA patterns under MAS failed at a spinning speed of 10KHz, this approach of amplitude-modulated rf field works without any difficulty.

The disadvantages of this method are: firstly, it is quite difficult to design the efficient RF modulation field for a desired hamiltonian manipulation. Secondly, the manipulation effect of

the modulated RF field is sensitive to resonant offset, that is: the difference between the carrier frequency of the RF field and the isotropic chemical shift frequencies. This makes the method not adequate for samples which have many resonant lines distributed in a big frequency range.

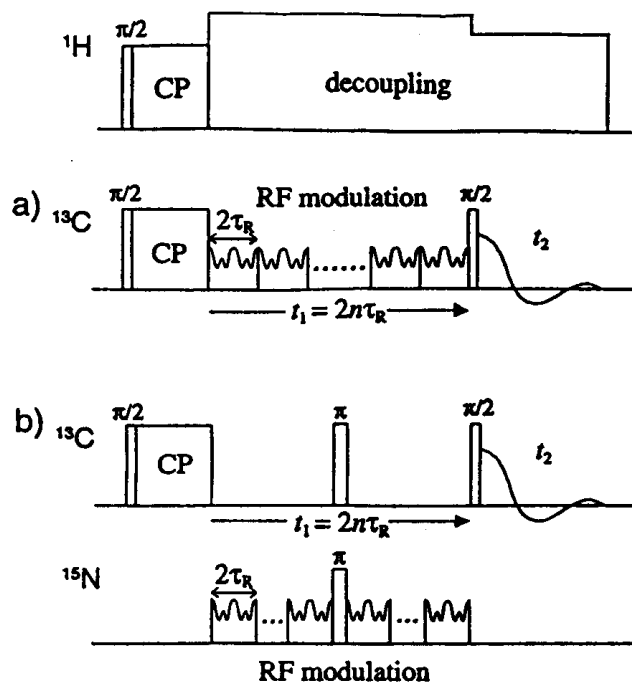


Figure 3-5: 2D pulse sequences for observation of (a) ^{13}C chemical shift anisotropy and (b) ^{13}C - ^{15}N dipolar powder patterns under MAS. After cross polarisation, in (a) the modulated rf field is applied in the t_1 period to ^{13}C spins to recover the chemical shift anisotropy under MAS, while it is applied to ^{15}N to recouple the ^{13}C - ^{15}N dipolar interaction in (b)(adapted from Ishii, 1998).

3.2.6 VACS $\underline{\text{Y}}$

Frydman et al [Frydman et al., 1992] introduced that the separation of isotropic and anisotropic Chemical shift interactions could also be achieved in an effective variable angle spinning approach. This method is termed as VACS $\underline{\text{Y}}$ (Variable Angle Correlation SpectroscopY). VACS $\underline{\text{Y}}$ is the selected method in this work to recover the CSA patterns of solid state liquid crystal samples in both isotropic state and oriented state. ODF information for different molecular segments can then be extracted out from these CSA patterns. The theory and implementation procedure of VACS $\underline{\text{Y}}$ are described in *chapter 4*.

VACSY AND INTERPOLATION OF EXPERIMENTAL DATA

4.1 Introduction

From the discussion in *chapter 3*, we know that two categories of methods are available to recover CSA powder patterns: group one - incomplete isotropic averaging is achieved by spinning fast but off the magic angle, by spinning slowly at the magic angle or by not spinning at all. This class of techniques requires both swift mechanical motions and storage of the evolving magnetisation, they are not suitable for samples with a relatively short T_1 relaxation time. Group 2 - these approaches rely on the synchronisation of magic angle spinning and radio frequency pulses. Therefore they are very sensitive to experimental imperfections such as pulse width and imperfect experimental parameters cause distortions in the final CSA powder patterns.

The effort to search for better methods which can obtain undistorted CSA line-shapes has never ended. In 1992, a new method, termed as VACSY - Variable Angle correlation Spectroscopy, was introduced by Frydman et al [Frydman et al., 1992] for correlating anisotropic and isotropic chemical shifts of in-equivalent nuclei in solid state samples.

A unique feature of this method is that the final spectra are obtained by processing signals arising from a spinning sample, acquired in independent experiments as a function of the angle between the axis of macroscopic sample rotation and the external magnetic field direction. This is in contrast to previously proposed techniques, which are based on either sudden mechanical sample flipping or multi-pulse sequences. Time evolution of the variable angle spinning signals is determined by a distribution of resonant frequencies relating the isotropic frequencies of the spins with their corresponding chemical shift anisotropies. Fourier transformation of this data results in a two-dimensional NMR spectrum. The pulse sequence of VACSY experiment is shown in fig4-1.

In VACSY, the change of the sample spinning angle is completed between two independent experiments. So, it does not put a strict limitation on the T_1 relaxation time of the investigated sample and the requirements for the mechanical performance of the probe are also relaxed. These are the predominant advantages of VACSY comparing with other approaches.

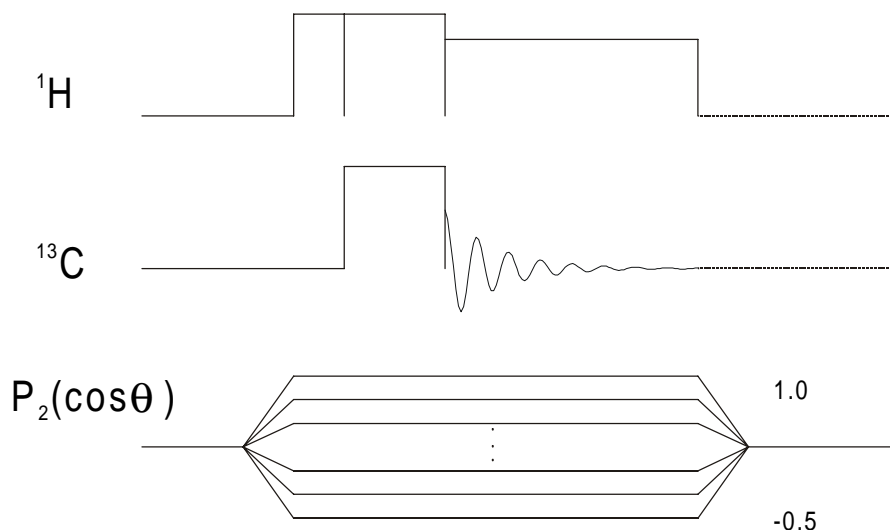


Figure 4-1: Pulse sequence of VACS Y experiment. In the direct dimension: cross polarisation between ^1H and ^{13}C , data is acquired under ^1H high power decoupling. In indirect dimension, angle θ can be sampled in an range corresponding to a range of $[-0.5, 1.0]$ for $P_2(\cos\theta)$.

4.2 Theory of VACS Y

Suppose that one wishes to obtain a 2D NMR spectrum of a sample, in which unscaled isotropic chemical shifts of different sites are correlated with their corresponding full CSA powder patterns. The usual 2D NMR approach suggests that the spins are allowed to evolve during a time t_a under the exclusive effects of anisotropic interactions, followed by a time t_i in which the spins only process at their isotropic chemical shift frequencies. Regardless of the way in which these two interactions are separated, this acquisition scheme creates a time domain space $S(t_a, t_i)$, associated with independent anisotropic and isotropic evolution frequencies.

If the time domain data $S(t_a, t_i)$ is sampled properly, the final correlation spectrum $I(\omega_a, \omega_i)$ can be calculated as:

$$I(\omega_a, \omega_i) = \iint S(t_a, t_i) \exp[-i(\omega_a \cdot t_a + \omega_i \cdot t_i)] dt_a dt_i \quad (4-1)$$

This Fourier transformation provides a 2D NMR spectrum in which slices parallel to the ω_a axis at the isotropic frequencies of the resolved sites show CSA powder patterns.

A NMR experiment like this, which can realise complete separation of unscaled isotropic and anisotropic interactions, are highly impossible in practical cases. However, it is possible and relatively simple to measure the time domain signals by acquiring a set of independent Variable-Angle-Spinning (VAS) NMR signals as indicated by the pulse sequence in fig4-1. This is the initial idea of VACS Y.

Let us consider a system composed of isolated spin $\frac{1}{2}$ nuclei, the dependence of resonance frequency on CS tensor orientation is given as:

$$\omega(\theta, \phi) = \omega_{iso} + \delta \frac{1}{2} (3 \cos^2 \theta - 1 - \eta \sin^2 \theta \cos(2\phi)) \quad (4-2)$$

As shown in fig4-2, when this spin system is spinning at an angle β with respect to the external magnetic field direction and in the fast spinning regime, this means that the rate of sample rotation is larger than the magnitude of the CSA interaction and the effects of time-dependent terms can be neglected. The instantaneous precession frequency of the spins can be approximated as:

$$\begin{aligned} \omega(\theta, \phi) &= \omega_{iso} + \delta \frac{1}{2} (3 \cos^2 \theta - 1 - \eta \sin^2 \theta \cos(2\phi)) \cdot \frac{1}{2} (3 \cos^2 \beta - 1) \\ &= \omega_{iso} + \omega_{aniso} \cdot \frac{1}{2} (3 \cos^2 \beta - 1) \\ &= \omega_{iso} + \omega_{aniso} \cdot P_2(\cos \beta) \end{aligned} \quad (4-3)$$

In this equation ω_{iso} is the difference between the isotropic chemical shift frequency of the nuclei and the transmitter offset. ω_{aniso} is the anisotropic frequency of the spins. $P_2(\cos\beta)$ is the second-order Legendre polynomial.

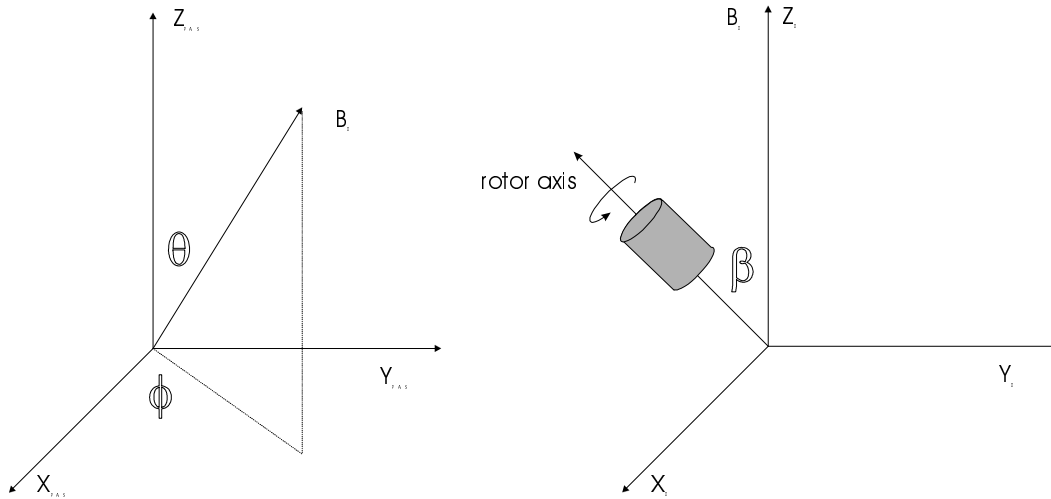


Figure 4-2: (left) Relative orientation of \mathbf{B}_0 field in the Principal Value System (PAS), θ describes the angle between tensor σ_{zz} axis and external magnetic field direction. (Right) Laboratory co-ordinate system, external magnetic field \mathbf{B}_0 is along the Z axis and the rotor spinning axis has angle β with respect to \mathbf{B}_0 .

For any particular angle β between the rotation axis and \mathbf{B}_0 , in equation [4-3] there is a $P_2(\cos\beta)$ scaling of the anisotropic chemical shift interaction. At time t after the excitation of the spins in the rotating sample, the signal observed can be written as:

$$S(\beta, t) = \iint I(\omega_i, \omega_a) \exp[i(\omega_i \cdot t + \omega_a \cdot P_2(\cos \beta) \cdot t)] d\omega_i d\omega_a \quad (4-4)$$

Define:

$$t_a = t \cdot P_2(\cos \beta), \text{ and } t_i = t \quad (4-5)$$

it is possible to rewrite the signal detected from this spin system as:

$$S(t_a, t_i) = \iint I(\omega_i, \omega_a) \exp[i(\omega_i \cdot t_i + \omega_a \cdot t_a)] d\omega_i d\omega_a \quad (4-6)$$

the FID signal $S(\beta, t)$ and the spectral $I(\omega_a, \omega_i)$ correlating the isotropic chemical shift and CSA powder patterns form a 2D Fourier pair.

Although these two experimental variables, β and t , are not capable of explicitly separating chemical shift isotropic and anisotropic interactions, they do provide a practical way of sampling the (t_a, t_i) space associated with them as shown in fig4-3:

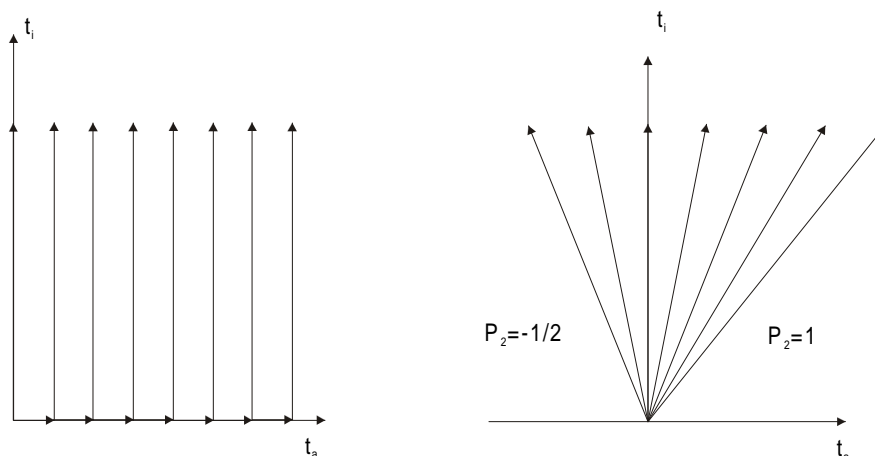


Figure 4-3: Different approaches for correlating isotropic and anisotropic chemical shifts in solids: (left) Cartesian approach - the spin system is allowed to evolve during a time t_a under the effects of the anisotropic interaction. Data are subsequently acquired as a increment of an independent time parameter t_i during which the system evolves under the isotropic interaction. (Right) Mixed-dimensions approach - the direction along which the system evolves in the (t_a, t_i) plane is along the rays originated from $(t_a, t_i)=(0, 0)$. The sampling region is confined between the two indicated values $P_2=-0.5$ and $P_2=1$, by changing the spinning axis angle β (adapted from Frydman, 1992).

4.3 Methods to implement interpolation or extrapolation

4.3.1 Normal interpolation - Frydman procedure

A normal way of evaluating equation [4-6] is the famous Fast-Fourier-Transformation algorithm (FFT) [Champeny, 1973; Elliot, 1982; William et al., 1989], but this algorithm requires an equally spaced grid of data points for the correlation of time domain data and the frequency spectra.

An obvious approach is to adjust the values of β and the dwell time t used in each individual acquisitions, to sample all points on a regular grid in (t_a, t_i) space. However, this procedure is highly inefficient. Because, even for sampling a relatively small data grid, it will require a large number of β values. Another more efficient procedure is to select a region in the

(t_a, t_i) space which is sufficient to support the desired spectral resolution, sample this region with as many different angles β as necessary to ensure an accurate interpolation of the time domain data grid points shown in fig4-4.

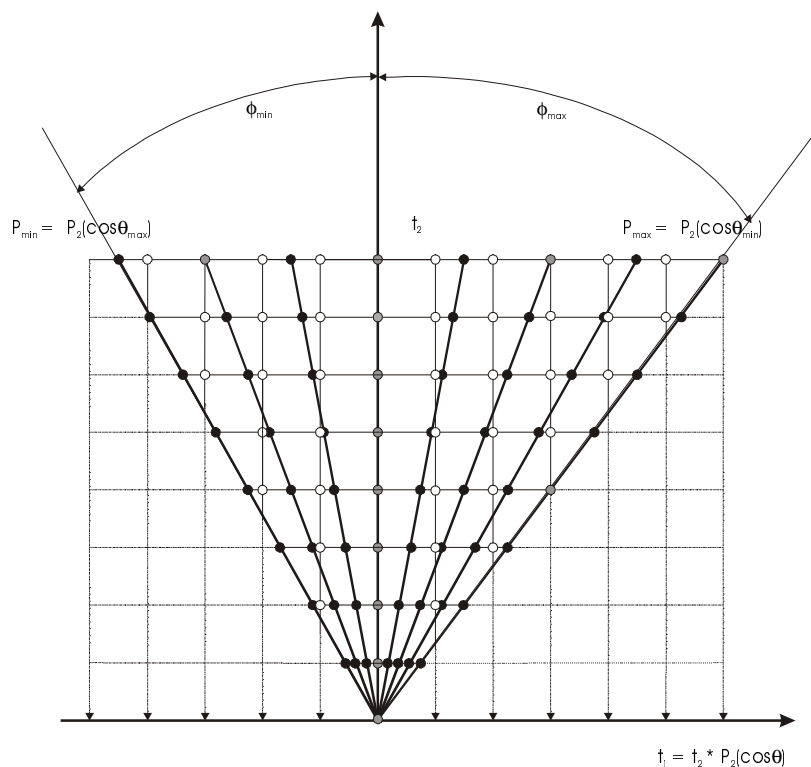


Figure 4-4: Normal interpolation procedure for obtaining isotropic-anisotropic correlation spectra from 2D VACS Y NMR data. P_{max} and P_{min} , the two maxima of $P_2(\cos\beta)$ used in the acquisition, determine a wedge in (n_a, n_i) space. Experimental data indicated by solid dots are located on the solid rays, they are acquired at multiples of the physical dwell time which also determines the grid spacing along the n_i axis. Interpolation of data values is carried out for all the grid points falling inside the wedge which are indicated by open circles, data values for the grid points falling outside this wedge which are covered within dashed grids are set to zero.

As in normal 2D NMR experiments, the spacing (dwell time) of the time domain data grids decides the range of final VACS Y spectrum; the total number of points decides its spectral resolution. Define DW_a, DW_i as the time increments (dwell times) between adjacent points along t_a, t_i axes. Sufficient resolution along the ω_i direction can be ensured by setting the practically used dwell time equal to DW_i for all acquisitions of different angles. The spinning axis angle β provides another freedom, each acquired signal corresponds to a ray in the (t_a, t_i) space.

For the convenience of further mathematical manipulations, a grid space (n_a, n_i) instead of (t_a, t_i) is used. In this grid space (n_a, n_i) , distances are scaled by units of DW_a along t_a axis and DW_i along t_i axis. Due to the properties of $1.0 \geq P_2(\cos\beta) \geq -1/2$, there are coverage limitations in (t_a, t_i) space. In a practical experiment, data is restricted in a wedge in (n_a, n_i) space limited on

the sides with the highest and lowest $P_2(\cos\beta)$ values used, $P_{2\max}$ and $P_{2\min}$. The angles ϕ_{\max} and ϕ_{\min} in (n_a, n_i) corresponding to $P_{2\max}$ and $P_{2\min}$ with respect to the isotropic axis are given as:

$$\begin{aligned}\tan(\phi_{\max}) &= P_{2\max} \cdot DW_i / DW_a \\ \tan(\phi_{\min}) &= P_{2\min} \cdot DW_i / DW_a\end{aligned}\quad (4-7)$$

if N independent variable angle spinning experiments are carried out, the angles ϕ_i which consist of a uniform sampling of the (n_a, n_i) space are given as:

$$\phi_i = \phi_{\min} + (\phi_{\max} - \phi_{\min}) \cdot \frac{i-1}{N-1}, \quad i = 1, 2, \dots, N \quad (4-8)$$

from this set of the angles $\{\phi_i\}$ the actual values of the angles $\{\beta_i\}$ used in N independent variable angle spinning experiments are given as:

$$\beta_i = \cos^{-1} \left[\frac{2 \cdot DW_a \cdot \tan(\phi_i) / DW_i + 1}{3} \right]^{1/2} \quad (4-9)$$

$$i = 1, 2, \dots, N.$$

experimental experience shows that in the range of $0.5 \geq P_2(\cos\beta) \geq -0.5$, with the total number of independent VAS experiments less than 30, satisfactory spectra can be obtained. This is due to the fact that: in the range of $1.0 \geq P_2(\cos\beta) \geq 0.5$, the angle β is small and the coil is approximately in parallel to the external magnetic field direction, therefore its efficiency to detect NMR signal is drastically reduced. Therefore, the signal intensity of the VAS experiments corresponding to the angles in this range is reduced and therefore non-significant for data interpolation.

After the finish of N independent VAS experiments, the acquired data are used to interpolate a regular 2D array in the region between ϕ_{\max} and ϕ_{\min} in (n_a, n_i) space. Because signals corresponding to different spinning angles are digitised using an equal dwell time DW_i , on the grid, the positions to be interpolated are always flanked by two data points along t_a axis. These two points are used to linearly interpolate the intermediate positions on the regular grid until a regular 2D NMR array is generated. The total number of points interpolated along the two dimensions of the grid are somehow arbitrary. The only requirement is that it should be large enough to allow the signal decay to zero to obtain maximum resolution.

4.3.2 Normal interpolation plus Linear Prediction

One disadvantage of the conventional 2D VASYS interpolation approach is that it is not possible to obtain pure-absorption-mode spectra because of phase-twist artefacts which are inherent to the experiment as shown in fig4-7. The resulting loss of resolution and line-shape distortions may impede analysis of the experimental spectra.

In 2D VACSYS experiment, a series of variable angle spinning free-induction decays are acquired and placed at angles:

$$\phi = \tan^{-1}[RP_2(\cos \beta)] \quad (4-10)$$

in (t_a, t_i) space as shown in fig4-4. Here, t_a, t_i define the anisotropic and isotropic time axes, $P_2(\cos\beta)$ is the second-order Legendre polynomial, β is the angle of the rotation axis with respect to the static field direction, R is the ratio of the anisotropic to isotropic spectral width. Typically, P_2 ranges from -0.5 to +0.5, so the signal partially spans two of the quadrants in the Fourier space. Once the FIDs are acquired and positioned in (t_a, t_i) space, the grid positions within this region can be interpolated from the experimental data points. The rest of the (t_a, t_i) space is set to zero. The phase artefacts inherent to the 2D VACSYS spectrum are due to the incomplete sampling in these two quadrants.

In general, phase artefacts in an NMR spectrum are due to the incomplete sampling of the time-domain Fourier space. Many procedures have been developed to do zero order and first order phase corrections [Wachter et al., 1989; Montigy et al., 1990; Van Vaals et al., 1990]. In the case of one-dimensional NMR signal:

$$S(t) = \int_{-\infty}^{\infty} I(\omega) \exp[i\omega t] d\omega \quad (4-11)$$

the spectral intensity distribution $I(\omega)$ and the FID signal $S(t)$ form a Fourier pair. However, the final experimental spectrum $I'(\omega)$ must take into account line broadening and truncation of the signal. Assume that all spectral components have the same Lorentzian line broadening, $I'(\omega)$ is the convolution of $I(\omega)$ with a Lorentzian-point-spread function (PSF), $P(\omega)$ [Lee et al., 1995]:

$$I'(\omega) = I(\omega) * P(\omega) \quad (4-12)$$

if the signal covers the full Fourier space for positive and negative time, $P(\omega)$ is an absorption Lorentzian line-shape. $I'(\omega)$ is then simply the broadened form of $I(\omega)$. If the signal spans only half of the Fourier space for positive time, $P(\omega)$ is complex valued function:

$$\begin{aligned} P(\omega) &= A(\omega) + iD(\omega) \\ &= \frac{\lambda}{\omega^2 + \lambda^2} + i \frac{\omega}{\omega^2 + \lambda^2} \end{aligned} \quad (4-13)$$

here $A(\omega)$ and $D(\omega)$ are the absorption and dispersion Lorentzian line-shapes, λ is the exponential relaxation factor. In both cases the real part of $P(\omega)$ has the same line-shape, the same spectral information is available from covering either all or just half of the time-domain Fourier space as shown in fig4-5.

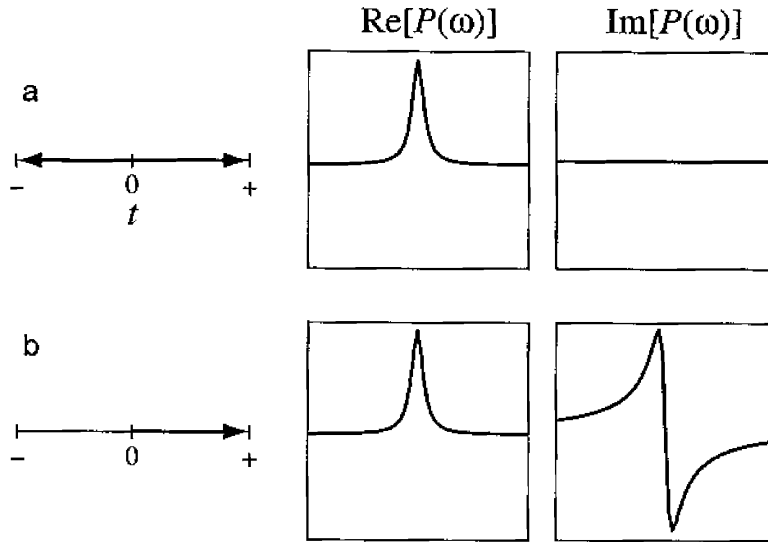


Figure 4-5: One-dimensional Lorentzian point-spread function (PSF), $P(\omega)$. (a) Complete signal acquired for positive and negative time; $P(\omega)$ is then a real Lorentzian line-shape. (b) Signal acquired only for $t > 0$. The real component is an Lorentzian line-shape, while the imaginary component becomes a dispersion line-shape (adapted from Y. K. Lee, 1995).

The same principle applies to higher dimensions. In the case of two-dimensional NMR signal:

$$S(t_1, t_2) = \int_{-\infty}^{\infty} \int_{-\infty}^{\infty} I(\omega_1, \omega_2) \exp[i2(\omega_1 t_1 + \omega_2 t_2)] d\omega_1 d\omega_2 \quad (4-14)$$

the experimental spectrum $I'(\omega_1, \omega_2)$ is a two-dimensional convolution of the spectral density distribution $I(\omega_1, \omega_2)$ with the 2D PSF function $P(\omega_1, \omega_2)$. If there is no truncation and the signal spans the complete Fourier space, $P(\omega_1, \omega_2)$ is a 2D pure absorption Lorentzian line-shape. If only half the Fourier space is acquired by truncating the signal for $t_2 < 0$, $P(\omega_1, \omega_2)$ is complex valued function:

$$\begin{aligned} P(\omega_1, \omega_2) &= 2A_1(\omega_1)[A_2(\omega_2) + iD_2(\omega_2)] \\ &= 2[A_1(\omega_1)A_2(\omega_2) + iA_1(\omega_1)D_2(\omega_2)] \end{aligned} \quad (4-15)$$

where $A_1(\omega_1)$ is the absorptive component in ω_1 , $A_2(\omega_2)$ and $D_2(\omega_2)$ are absorptive and dispersive components in ω_2 . The pure-absorptive line-shape $A_1(\omega_1)A_2(\omega_2)$ can be obtained by sampling only half of the full Fourier space. Obviously, similar results will be obtained by truncating the signal along t_1 dimension rather than t_2 dimension.

In the case of both t_1 and t_2 dimensions are truncated, that is: only one quadrant in the Fourier space is acquired, then both the real and imaginary parts of $P(\omega_1, \omega_2)$ show positive and negative lobes due to the mixing of the absorptive and dispersive components.

$$\begin{aligned}
P(\omega_1, \omega_2) &= [A_1(\omega_1) + iD_1(\omega_1)] \cdot [A_2(\omega_2) + iD_2(\omega_2)] \\
&= [A_1(\omega_1)A_2(\omega_2) - D_1(\omega_1)D_2(\omega_2)] + i[A_1(\omega_1)D_2(\omega_2) + D_1(\omega_1)A_2(\omega_2)]
\end{aligned}
\tag{4-16}$$

and pure absorption line-shapes are no longer possible as shown in fig4-6 [Lee et al., 1995].

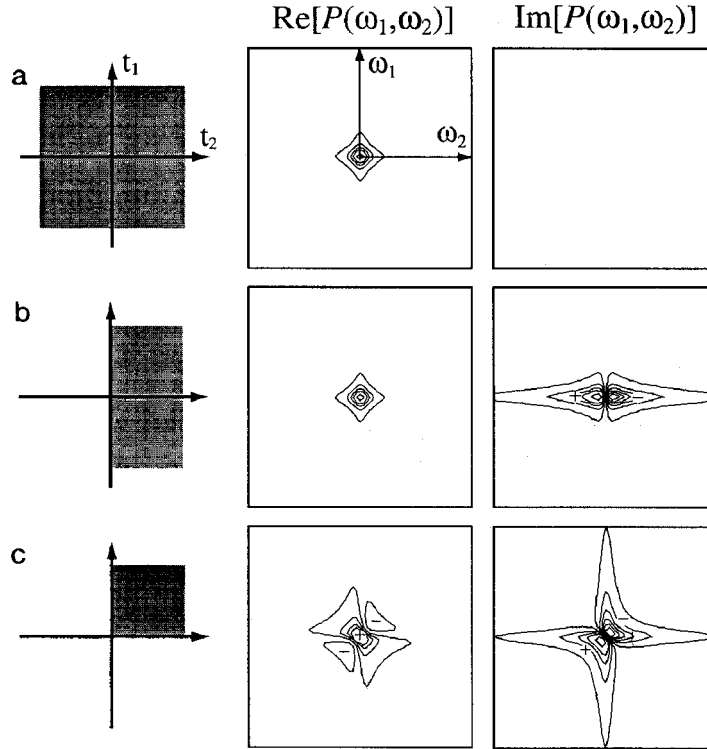


Figure 4-6: Two-dimensional Lorentzian PSF, $P(\omega_1, \omega_2)$, in conventional 2D NMR experiments. (a) $P(\omega_1, \omega_2)$ for signal acquired in all four quadrants of the time-domain, $P(\omega_1, \omega_2)$ is a real 2D Lorentzian line-shape. (b) $P(\omega_1, \omega_2)$ for signal acquired in two of the four quadrants. The real component of $P(\omega_1, \omega_2)$ remains a 2D absorption Lorentzian line-shape, $a_1(\omega_1)a_2(\omega_2)$, while the imaginary component is a mixture of absorptive and dispersive terms. (c) $P(\omega_1, \omega_2)$ for signal acquired in only one quadrant. $P(\omega_1, \omega_2)$ contains a mixture of absorptive and dispersive terms in both the real and imaginary components (adapted from Y. K. Lee, 1994)

Back to the case of VACSYS, consider the PSF function $P(\omega_a, \omega_i)$ for the case of $R=2$ and $+0.5 \geq P_2 \geq -0.5$. Since ϕ ranges from -45° to $+45^\circ$, the total area of the Fourier space covered by the VACSYS signal is equivalent to one quadrant, so $P(\omega_a, \omega_i)$ is similar in form to $P(\omega_1, \omega_2)$ in fig4-6. The artefact ridges become less intense when R increases and a larger area of the Fourier space contains experimental data. Unfortunately this is achieved at the cost of spectral resolution in the anisotropic dimension and increased interpolation error.

The spectral artefacts shown in Figure 4-7 are special to 2D VACSYS experiments due to the unconventional truncation and interpolation of time domain data. Often these artefacts may be ignored, particularly when the spectrum is dominated by broad anisotropic patterns. Because the artefacts are also broadened, then the interference between different sites becomes

negligible. This explains the success of 2D VACSYS despite the artefacts inherent to the technique. However, these artefacts can become a serious problem when the spectrum contains closely spaced isotropic shifts with small anisotropies. The ridge artefacts emerging from a narrow site may interfere with the anisotropic patterns of neighbouring sites, causing serious line-shape distortions. The removal of such artefacts becomes especially important when there are partially overlapping or a continuous distribution of isotropic shifts, or when accurate line-shape analysis is required as in the study of partial molecular ordering in this work.

Artefacts in 2D VACSYS spectra can be reduced if the missing data points in the signal Fourier space (t_a, t_i) can be extrapolated using the experimental data [Lee et al., 1995]. However, due to the large number of missing data points, the extrapolation technique must maintain accuracy over several periods of the signal. Linear prediction with singular-value decomposition LPSVD is one such technique which has been used for extrapolation and spectral estimation in NMR [Rutledge (Ed.), 1996; Barkhuijsen et al., 1985; Stephenson, 1988; Kumaresan et al., 1982, Kay, 1988].

The LPSVD method assumes the signal to be a time series represented by a sum of decaying exponentials with additional white Gaussian noise:

$$y_n = \sum_{m=1}^M a_m \exp[(i\omega_m - \lambda_m)t_d(n + \delta)] + w(n) \quad (4-17)$$

$$n = 1, 2, \dots, N-1$$

where a_m, ω_m, λ_m are the complex amplitude, frequency and damping factor of each exponential term, respectively. M is the total number of exponential components, t_d is the dwell time of the time series signal, N is the total number of points in the time series, δ is an integer that specifies the shift from the time origin to the first sample data point.

The general procedure of LPSVD computation is outlined briefly in the following. A set of linear prediction equations in the backward prediction mode is given as:

$$\begin{bmatrix} y_1 & y_2 & \cdots & y_L \\ y_2 & y_3 & \cdots & y_{L+1} \\ \vdots & \vdots & \ddots & \vdots \\ y_{N-L} & y_{N-L+1} & \cdots & y_{N+1} \end{bmatrix} \cdot \begin{bmatrix} b_0 \\ b_1 \\ \vdots \\ b_{L-1} \end{bmatrix} = - \begin{bmatrix} y_0 \\ y_1 \\ \vdots \\ y_{N-L-1} \end{bmatrix} \quad (4-18)$$

or in a compact form as:

$$Ab = -h \quad (4-19)$$

where \mathbf{b} is the vector of the backward LP coefficients, \mathbf{A} is the $(N-L) \times L$ data matrix, \mathbf{h} is the data vector with $N-L$ components. The number of LP coefficients (prediction order), L , is bounded by $N-M \geq L \geq M$, typically is set to $0.75N$ [Kumaresan et al., 1982].

The singular-value-decomposition (SVD) of the matrix \mathbf{A} is written as a product of three matrices [Kay, 1988]:

$$\mathbf{A} = \mathbf{U} \begin{bmatrix} \mathbf{S} \\ \mathbf{O} \end{bmatrix} \mathbf{V}^+ \quad (4-20)$$

where \mathbf{V}^+ denotes Hermitian conjugate; \mathbf{U} and \mathbf{V} are orthogonal matrices of dimensions $(N-L) \times (N-L)$ and $L \times L$ respectively. \mathbf{S} is a diagonal matrix with the singular values as its diagonal elements $\{\sigma_k, k = 1, 2, \dots, \min(L, N-L)\}$. \mathbf{O} is a null matrix. Denoting the column vectors of the matrices \mathbf{U} and \mathbf{V} by $\{u_1 \ u_2 \ \dots \ u_{N-L}\}$ and $\{v_1 \ v_2 \ \dots \ v_L\}$, the backward linear prediction coefficients are computed as:

$$\mathbf{b} = -\sum_{m=1}^M \frac{1}{\sigma_m} (u_m^+ \mathbf{h}) V_m \quad (4-21)$$

where the summation limit M truncates the SVD solution for \mathbf{b} . For low noise data, M is simply the total number of peaks in the spectrum; However, if the data contains significant noise, M becomes an adjustable parameter [De Beer et al., 1988; Lin et al., 1993]. Once the backward LP coefficients have been calculated, the missing data points in the time series can be extrapolated as:

$$y_n = -\sum_{k=1}^L b_k y_{n+k}, \quad n = (-1, -2, \dots, -\delta) \quad (4-22)$$

where $n = -\delta$ defines the data point at the time origin. To take advantage of the signal-to-noise ratio improvements in LPSVD, the entire time series should be reconstructed by calculating out the spectral parameters associated with the data set. The parameters, ω_m and α_m can be obtained by constructing a polynomial:

$$P(z) = 1 + b_1^* z^{-1} + b_2^* z^{-2} + \dots + b_L^* z^{-L} \quad (4-23)$$

which has roots at $z_m = \exp[i\omega_m + \alpha_m]$. The complex amplitude a_m can then be obtained by substituting ω_m and α_m into equation [4-17]. Fig4-7 shows an example of the LPSVD procedure applied to a 2D VACSYS simulation spectrum, the improvement in spectral resolution is significant.

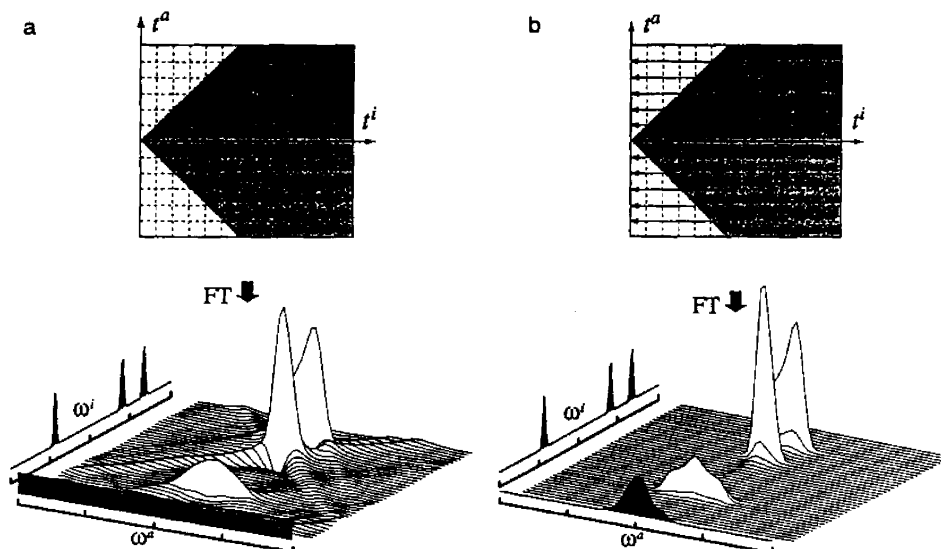


Figure 4-7: Simulation of 2D VACSYS spectra. The simulations are using $R=2$, $td=200$ us, and three sites with chemical shift tensors: $(\sigma_{xx}, \sigma_{yy}, \sigma_{zz}) = (0.3, 1.0, 2.3), (-0.5, -0.5, -1.5), (-2.5, -2.0, -1.0)$ (kHz). (a) Normal phased 2D VACSYS spectrum obtaining using $+0.5 \geq P2 \geq -0.5$ and $R=2$. The area of Fourier space outside of the shaded region is set to zero. The 2D spectrum reveals the phase artefacts inherent to the normal 2D VACSYS experiment. The projection onto the ω_a axis yields a constant function, whereas the projection onto the ω_i axis yields the pure absorption isotropic spectrum. (b) 2D VACSYS spectrum after extrapolation using LPSVD. The area set to zero in (a) is extrapolated from the interpolated simulation data in the shaded region. LPSVD is used to extrapolate the data in each slice, parallel to the t_a axis, to the $t_i=0$ point. the phase artefacts are eliminated from the 2D spectrum. The projection onto the ω_a axis yields the overlap of the different traceless anisotropic powder patterns, while the projection onto the ω_i axis again yields the isotropic MAS spectrum.

4.3.3 Non-orthogonal interpolation

The interpolation procedure introduced in section 4.3.1 can not obtain pure-absorptive 2D VACSYS spectrum, distortions of CSA line-shape patterns due to phase artefacts are impossible to be eliminated. The LPSVD procedure introduced in section 4.3.2 is capable to extrapolate the missing data points and obtain a clean pure-absorptive VACSYS spectrum. However, if the experimental data contains significant noise this procedure may fail or give apparently incorrect results.

Here, a new interpolation procedure, termed as non-orthogonal interpolation, is proposed by G. Hempel and successfully implemented by us. In this procedure, the experimental data are interpolated to a non-regular grid based on two axes z_1, z_2 :

$$\begin{aligned}
z_1 &\rightarrow P_{2\max}(\cos\theta_{\min}) = P_{2\max} \\
z_2 &\rightarrow P_{2\min}(\cos\theta_{\max}) = P_{2\min}
\end{aligned}
\tag{4-24}$$

instead of a regular grid which based on axes t_1 and t_2 as shown in fig4-8:

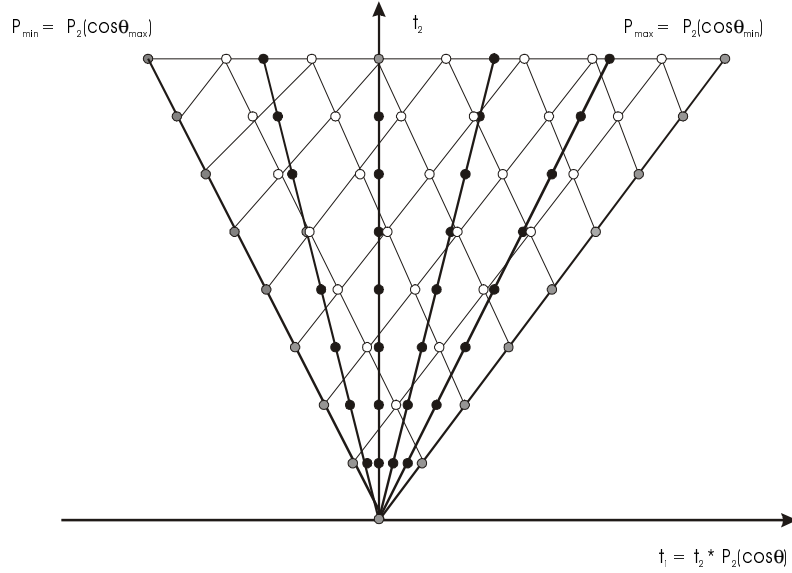


Figure 4-8: Non-orthogonal interpolation approach for obtaining isotropic-anisotropic correlation spectra from 2D VACSZY NMR data. P_{\max} and P_{\min} , the two maxima of $P_2(\cos\beta)$ used in the acquisition, determine a wedge in (t_a, t_j) space. Experimental data indicated by solid dots are located on the solid rays confined in the wedge. Interpolation of data values is carried out for all the points indicated by open circles of a non-orthogonal grid which has two characteristic axes parallel to P_{\max} and P_{\min} respectively.

2D VACSZY FID data are experimentally acquired by carrying out M independent variable-angle-spinning (VAS) experiments which corresponds to rays in the (t_1, t_2) plane and they can be mathematically expressed as:

$$\begin{aligned}
S(\theta, t_2) &= \iint I(\omega_a, \omega_i) \exp[i(\omega_i \cdot t_2 + \omega_a \cdot P_2(\cos\theta) \cdot t_2)] d\omega_a d\omega_i \\
&= \iint I(\omega_a, \omega_i) \exp[i(\omega_i \cdot t_2 + \omega_a \cdot t_1)] d\omega_a d\omega_i
\end{aligned}
\tag{4-25}$$

where:

$$\begin{aligned}
t_2 &= 0, \Delta t_2, 2\Delta t_2, \dots, (n-1)\Delta t_2 \\
t_1 &= t_2 \cdot P_2(\cos\theta), \theta = \theta_{\min}, \theta_{\min} + \Delta\theta, \theta_{\min} + 2\Delta\theta, \theta_{\max}
\end{aligned}
\tag{4-26}$$

where: variable n , changes from 1 to N , is the index of data sampling in the direct dimension, Δt is the corresponding experimental dwell time for all M different angles. Variable m , changes from 1 to M , is the index for θ angle sampling with a step of $\Delta\theta$ in the indirect dimension.

Directly after signal acquisition, an arbitrary VACSYS FID data point of the m th independent experiment at time $n \cdot \Delta t$ in co-ordinates system $\{t_1, t_2\}$ is expressed as:

$$\begin{aligned} FID(m, n)_t &= \iint I(\omega_a, \omega_i) \exp[i(\omega_i \cdot n \cdot \Delta t_2 + \omega_a \cdot P_2(\cos(\theta_{\min} + m\Delta\theta)) \cdot n \cdot \Delta t_2)] d\omega_a d\omega_i \\ &\Rightarrow \binom{nP_m}{n} \end{aligned} \quad (4-27)$$

and:

$$P_m = P_2(\cos(\theta_{\min} + m\Delta\theta)) \quad (4-28)$$

In the following discussion, the co-ordinate of this data point in co-ordinates system $\{t_1, t_2\}$ is denoted as: $\{nP_m, n\}$

Now we change the co-ordinates system from $\{t_1, t_2\}$ to $\{z_1, z_2\}$, where: z_1 is along $P_{2\max}$ direction and z_2 along $P_{2\min}$ direction, they are the two base vectors of co-ordinates system $\{z_1, z_2\}$. In co-ordinates system $\{t_1, t_2\}$, z_1 and z_2 can be expressed as following:

$$\hat{z}_1 = \begin{pmatrix} P_{2\max} \\ 1 \end{pmatrix}, \quad \hat{z}_2 = \begin{pmatrix} P_{2\min} \\ 1 \end{pmatrix} \quad (4-29)$$

therefore, the transformation matrix from co-ordinates system $\{z_1, z_2\}$ to $\{t_1, t_2\}$ is given as:

$$\begin{pmatrix} t_1 \\ t_2 \end{pmatrix} = \begin{pmatrix} P_{2\max} & P_{2\min} \\ 1 & 1 \end{pmatrix} \begin{pmatrix} z_1 \\ z_2 \end{pmatrix} \quad (4-30)$$

Because the data set $FID(m, n)_t$ obtained directly from VAS acquisitions do not fulfil the 2D FT requirements, they must be interpolated to the new data set $FID(i, j)_z$ on the non-regular grid points.

In co-ordinates system $\{z_1, z_2\}$, that is: in the non-regular grid space, if we focus on an arbitrary data point $FID(i, j)_z$, it should have a co-ordinate $(i, j)_z$. Using the transformation matrix in equation (4-30), the co-ordinate of the same data point in co-ordinates system $\{t_1, t_2\}$ can be written as:

$$\begin{pmatrix} i \\ j \end{pmatrix}_t = \begin{pmatrix} P_{2\max} & P_{2\min} \\ 1 & 1 \end{pmatrix} \begin{pmatrix} i \\ j \end{pmatrix}_z = \begin{pmatrix} i \cdot P_{2\max} + j \cdot P_{2\min} \\ i + j \end{pmatrix} = \begin{pmatrix} (i + j) \left(P_{2\max} + \frac{j}{i+j} (P_{2\min} - P_{2\max}) \right) \\ i + j \end{pmatrix} \quad (4-31)$$

from a direct comparison of equation (4-27) and (4-30), it is easy to get that: in co-ordinates system $\{z_1, z_2\}$, an arbitrary data point $FID(i, j)_z$ has the following co-ordinate in system $\{t_1, t_2\}$:

$$n = i + j$$

$$P_{m'} = P_{2\max} + \frac{j}{(i + j)}(P_{2\min} - P_{2\max}) \quad (4-32)$$

So, in $\{t_1, t_2\}$ space, the two nearest data points relative to this one have co-ordinates:

$$FID(m, n)_t = \begin{pmatrix} nP_m \\ n \end{pmatrix} \quad FID(m+1, n)_t = \begin{pmatrix} nP_{m+1} \\ n \end{pmatrix} \quad (4-33)$$

where:

$$n = i + j$$

$$P_m \leq P_{m'} \leq P_{m+1} \quad (4-34)$$

In space $\{z_1, z_2\}$, the value of this arbitrary data point $FID(i, j)_z$ can then be interpolated through these two nearby data points $FID(m, n)_t$ and $FID(m+1, n)_t$ in space $\{t_1, t_2\}$ by the following equation:

$$FID(i, j)_z = \frac{P_{m'} - P_m}{P_m - P_{m+1}} FID(m, n)_t + \frac{P_m - P_{m+1}}{P_m - P_{m+1}} FID(m+1, n)_t \quad (4-35)$$

In fig4-8, data points indicated by solid circles which are lying on rays originated from (0, 0) are acquired by M independent VAS experiments, this 2D data array does not fulfil FFT requirements. Data points which are indicated by open circles form a non-orthogonal grids and fulfil 2D FFT conditions, these are the data points which should be interpolated from experimental data by using equation (4-34).

After normal 2D FT evaluation, a non-orthogonal 2D VACSY spectrum is obtained. Due to a rotation of co-ordinate system $\{z_1, z_2\}$ relative to $\{t_1, t_2\}$ for an angle which is decided by $P_{2\max}$ and $P_{2\min}$ as shown in fig4-8, in the final VACSY spectrum the CSA powder patterns are rotated for the same angle with respect to the VACSY spectrum obtained by the normal interpolation procedure as shown in fig4-9c. CSI and CSA projections can not be directly taken from the VACSY spectrum obtained with this non-orthogonal approach, a reverse version of this non-orthogonal interpolation procedure for the VACSY spectral data is required to rotate the final spectrum to normal direction, that is: CSI and CSA are parallel to ω_1 , ω_2 directions respectively. A „four points“ interpolation formula is used to accomplish this smooth reverse interpolation as shown in fig4-9d, and in the anisotropic direction the final spectrum is scaled for a known factor comparing with the spectrum in fig4-9c.

A direct comparison of the results of these two interpolation approaches to a simulated VACSY data is presented in fig4-9. Fig4-9b shows that due to the incomplete data sampling in (t_1, t_2) space, the VACSY spectrum obtained from the normal interpolation procedure can not be displayed in phase sensitive mode. A well accepted fact is that the resolution of a spectrum displayed in magnitude mode (absolute value mode) or power mode is lower than the same

spectrum displayed in phase sensitive mode when its imaginary part is not zero like in the case of VACSY, and moreover the correct line-shape of a spectrum is also changed when it is displayed in magnitude mode or power mode. In some cases when good spectral resolution is highly desirable as in the case of closely spaced isotropic chemical shifts or when accurate line-shape analysis is required as in the investigation of partial molecular ordering, it is highly desirable that the spectra can be displayed in phase sensitive mode.

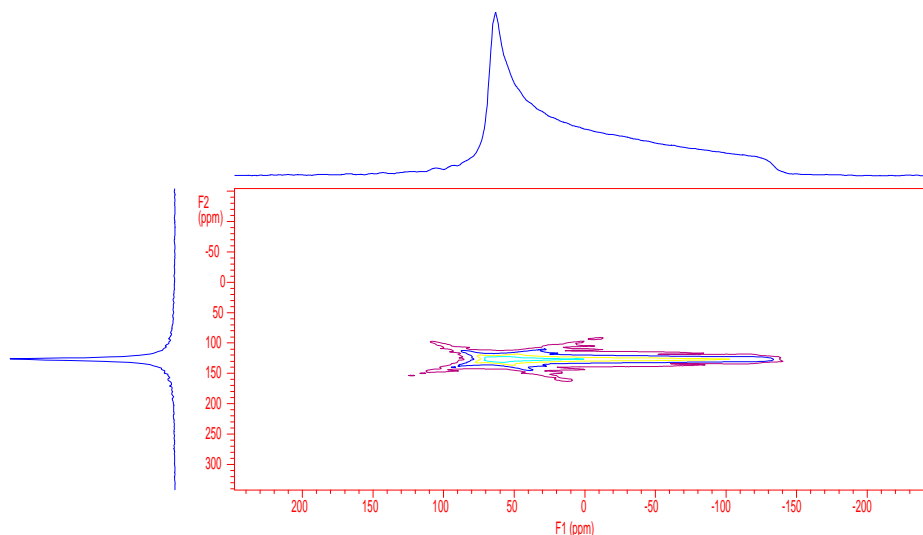


Figure 4-9a: VACSY simulation spectrum processed by normal interpolation procedure and displayed in absolute value mode, chemical shift tensor used $(\sigma_{xx}, \sigma_{yy}, \sigma_{zz})=(100, 100, -100)$ (ppm).

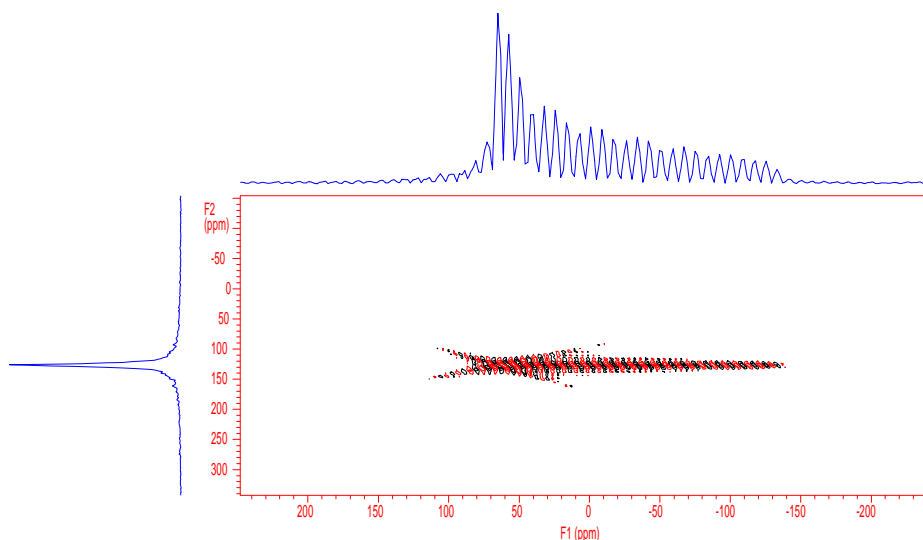


Figure 4-9b: VACSY simulation spectrum processed by normal interpolation procedure and displayed in phase sensitive mode, chemical shift tensor used $(\sigma_{xx}, \sigma_{yy}, \sigma_{zz})=(100, 100, -100)$ (ppm).

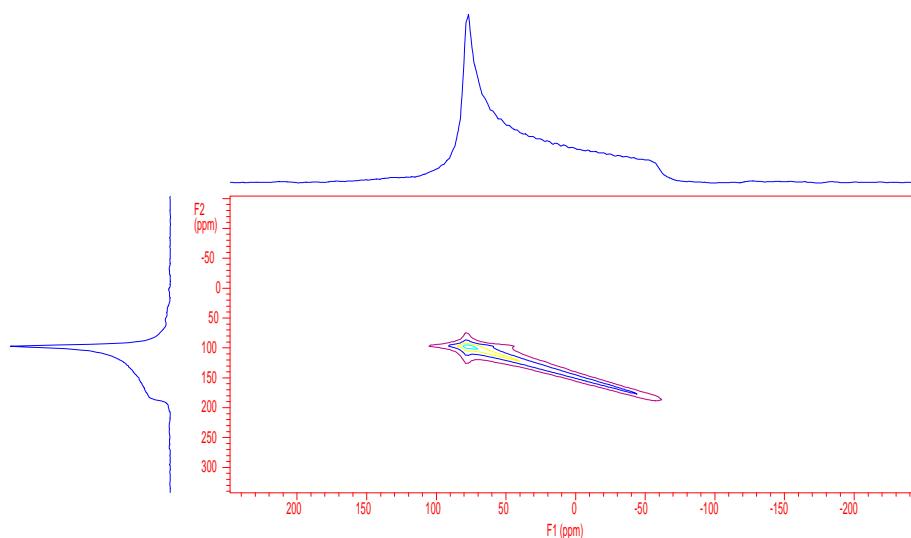


Figure 4-9c: VACSY simulation spectrum processed by non-orthogonal interpolation procedure and displayed in phase sensitive mode, chemical shift tensor used $(\sigma_{xx}, \sigma_{yy}, \sigma_{zz})=(100, 100, -100)$ (ppm).

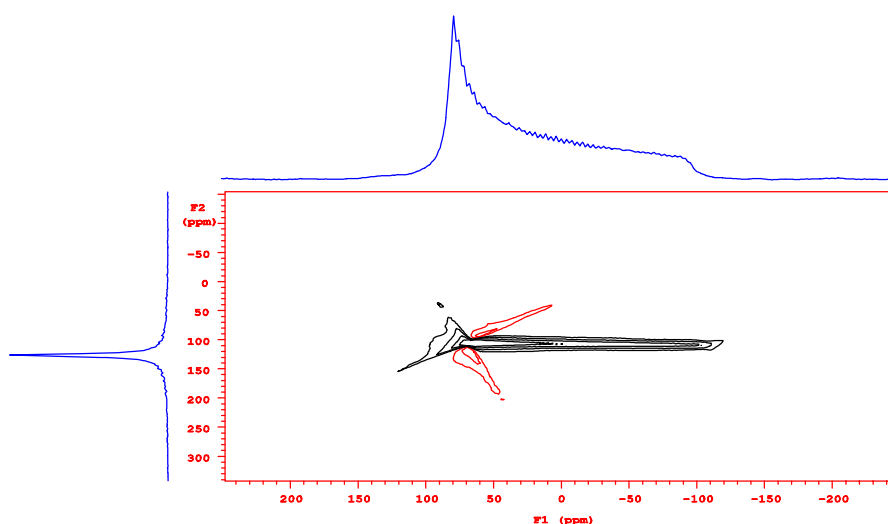


Figure 4-9d: A four-points reverse interpolation approach to rotate the spectrum in fig4-9c into normal directions, displayed in phase sensitive mode, chemical shift tensor used $(\sigma_{xx}, \sigma_{yy}, \sigma_{zz}) = (100, 100, -100)$ (ppm).

The advantages of this non-orthogonal interpolation method is that: (i) the CSA line-shape distortions are somewhat less comparing with the normal interpolation procedure; (ii) the final 2D VACSY spectrum is possible to be displayed in phase sensitive mode; (iii) comparing with the LPSVD method, this method can not completely remove phase artefacts as LPSVD does, but it can be successfully used to process noisy data.

4.3.4 VACSY transformation with eigen-coordinates

In all three above mentioned VACSY data processing methods: interpolation, interpolation plus Linear Prediction and non-orthogonal interpolation methods, the data value of the desired position in the (t_1, t_2) space is calculated from experimentally acquired data values by using various interpolation or extrapolation algorithms. From the principle of interpolation calculation, it is easy to understand that a difference always exists between the interpolation result and the theoretical magnetisation evolution. Especially when the direct digitisation index n $[1, \dots, N]$ goes to bigger value, where the data point to be interpolated is quite far apart from two adjacent acquired data points, the error of interpolation becomes bigger. A good interpolation algorithm can greatly reduce this error, but it can not totally remove this deviation.

In order to reduce the interpolation error as much as possible, G. Hempel proposed another VACSY data processing approach which obtains the final 2D VACSY correlation spectrum by directly transforming the experimentally acquired data set without doing any interpolation or extrapolation. This proposal has been successfully applied to process VACSY simulation/experimental data by me and it gives satisfied results. The procedure is termed as: VACSY transformation with eigen-coordinates.

From the mathematical expression of VACSY fid data in equation (4-25), the corresponding VACSY spectrum can be expressed as:

$$I(\omega_a, \omega_i) = \iint S(P_2, t_2) \exp[i(\omega_i \cdot t_2 + \omega_a \cdot P_2(\cos\theta) \cdot t_2)] dt_2 dp_2 \quad (4-36)$$

denote: $p = P_2(\cos\theta)$, we have:

$$I(\omega_a, \omega_i) = \iint S(p, t_2) \exp(i\omega_i \cdot t_2) dt_2 \exp(i\omega_a \cdot p \cdot t_2) t_2 dp \quad (4-37)$$

this is not a normal Fourier transformation. Here, the first time variable is t_2 , it correlates to ω_i in frequency domain; the second time variable is p multiplies t_2 , it correlates to ω_a in frequency domain. In order to be calculated by computer, the analytical equation (4-36) has to be converted into its corresponding digital form. The digitisation relation between time variables and frequency variables are given in the following:

$$\begin{aligned} \omega_a &\Rightarrow \Delta\omega_a \cdot k; & p \cdot t_2 &\Rightarrow t_2 \cdot P_2(\cos\theta + m \cdot \Delta\theta) = p_m \cdot t_2; & S(p, t_2) &\Rightarrow Z_{kn}; \\ \omega_i &\Rightarrow \Delta\omega_i \cdot l; & t_2 &\Rightarrow \Delta t \cdot n; & Z_{kn} &\Rightarrow I_{kl}; \end{aligned} \quad (4-38)$$

The complete transformation is divided into two steps, integration for $p \cdot t_2$ and for t_2 respectively.

(i) step one: the integration (this corresponds to summation in digital form) for variable $p \cdot t_2$, the intermediate result is denoted as Z_{kn} :

$$Z_{kn} = \sum_{m=1}^{M-1} [S_{mn} \exp(i\Delta\omega_a \cdot k \cdot \Delta t \cdot n \cdot p_m)] + \frac{1}{2} [S_{0n} \exp(i\Delta\omega_a \cdot k \cdot \Delta t \cdot n \cdot p_{\max}) + S_{Mn} \exp(i\Delta\omega_a \cdot k \cdot \Delta t \cdot n \cdot p_{\max})] \quad (4-39)$$

a special computer program written in C by us is required to realise this part of data calculation. The calculation result is stored in VNMR fid data format which can be directly used by VNMR software for next step processing. (ii) step two: the intermediate result of step one Z_{kn} is firstly multiplied by $t_2 = \Delta t \cdot n$, then a normal 1D Fourier transformation is performed. VNMR software is used for the calculation in this step and all later graphic manipulations. The result VACSY spectrum processed by this new approach for the same simulation data as in fig4-9 is shown in fig4-10:

From a direct comparison of fig4-10, fig4-9a, fig4-9b, fig4-9c, fig4-9d, the advantages of this ‘VACSY transformation with eigen-coordinates’ are: (i) in fig4-10, the projection onto the isotropic axis is somewhat narrower and the singularities of the projection onto the anisotropic axis are sharper comparing with the corresponding spectra of fig4-9a. This is because: fig4-10 is displayed in phase sensitive mode while fig4-9a in absolute value mode. (ii) in fig4-10 the 2D VACSY spectrum is not rotated like in fig4-9c, this makes the isotropic and anisotropic projections directly possible. (iii) in fig4-10, outside the region where spectra feature is the signal intensities are very low comparing with both fig4-9a and fig4-9d. This is due to the fact that in ‘VACSY transformation with eigen-coordinates’, there are no interpolation errors. However, the butter-fly-like phase artefacts surrounding the spectral feature in fig4-10 are still present. This is due to the incomplete sampling of (t_1, t_2) space as discussed in section4.3.2, until now the only available way to remove them is by performing Linear Prediction.

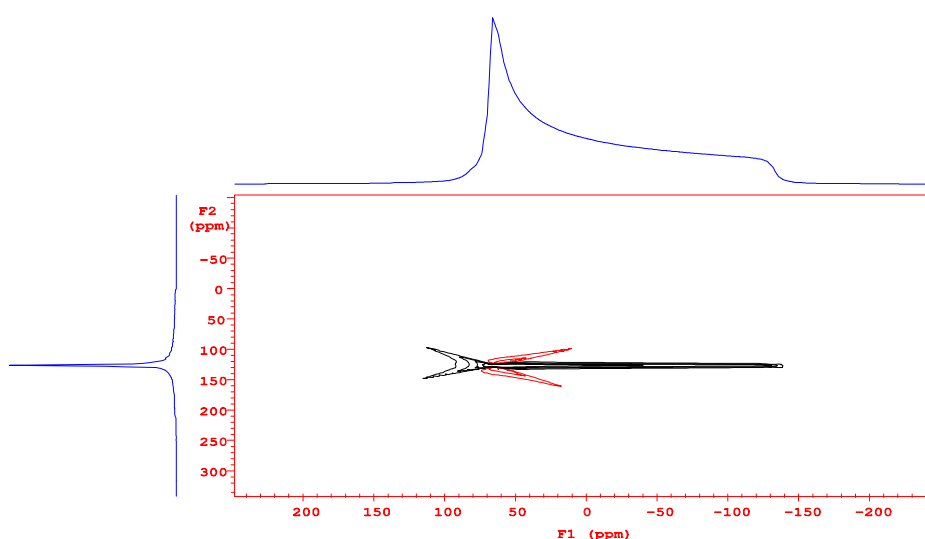


Figure 4-10: VACSY simulation spectrum processed by ‘VACSY transformation with eigen-coordinates’ procedure and displayed in phase sensitive mode, chemical shift tensor used $(\sigma_{xx}, \sigma_{yy}, \sigma_{zz}) = (100, 100, -100)$ (ppm).

SIMULATION

5.1 Introduction

VACSY is a method to reintroduce CSA patterns in one dimension and correlate them with their chemical shift isotropic values in another dimension of a 2D NMR spectrum. In *chapter 2* it has been shown that: from the NMR line-shape of chemical shift anisotropy, the complete orientation distribution function of partially ordered solid state polymer samples can be extracted out by various procedures. In all these procedures, an accurate analysis of the CSA line-shape is required. So, for a successful orientation distribution investigation the most important step is to obtain a non-distorted CSA patterns of the sample in both isotropic state and oriented state.

In practical cases, the spectra may have imperfections which originate from:

- noise
- phase artefacts arising from in-complete data sampling
- broadening caused by certain distribution of chemical shift values corresponding to different structural conformations, residual dipolar interaction from incomplete decoupling, etc.

then, many difficulties may arise in the forth-coming orientation distribution analysis. In extreme cases, some procedures may become not valid any more.

The deterioration of NMR spectra by noise, FT artefacts and broadening is common to all NMR methods. In general, noise can be reduced by improvement of the RF circuits in the probe and by using coherent addition of a large number of transitions; FT artefacts can be removed by careful zero order and first order phase corrections, linear prediction, etc; Line broadening can be relieved by optimising dipolar decoupling efficiency and by doing experiments in low temperature region. Many work have been done in this area to solve these problems, now for most samples a satisfied spectrum can be obtained.

VACSY experiments need a dedicated probe to be implemented, except the reasons mentioned above there are some special factors which might cause distortions of the CSA line-shapes if they are not correctly chosen, such as the control accuracy of the angle β which is the angle between the rotation axis and the external magnetic field direction \mathbf{B}_0 ; the deviation of

spinning speed from setting value while the rotor is flipped from one angle to another, etc. Even if the necessary hardware equipment and interpolation software are ready, before a VACSY experiment is started several important questions special for VACSY have to be understood, for example:

- How much a spinning speed is necessary with respect to the CSA value of the investigated sample to neglect the CSA line-shape distortion of the central spinning band?
- How much a control accuracy is necessary to neglect the CSA line-shape distortion due to the angle β mis-setting?
- How much a sampling range of the angle β is necessary for the acquisition of a non-distorted CSA line-shape?
- How many independent VAS experiments should be carried out for a non-distorted CSA line-shape?
- How much a fluctuation in spinning speed is tolerable to achieve a non-distorted CSA line-shape?
- etc.

Of course, these answers can be found through many times of try and error experiments. But, this will be an extremely inefficient way and it also does not guarantee that the optimised parameters will be found. A more efficient approach for answering these questions is by using computer simulation. Computer simulation provides an excellent way to deeply understand the influence on the final CSA patterns from each individual parameter of a VACSY experiment

5.2 Simulation Program

The dependence of NMR resonance frequency on molecular segmental orientations in the case of macroscopic sample spinning has been discussed in *chapter 2* and the corresponding equations are given in equations (2-32) - (2-35). For a powder sample, the free induction decay of the whole sample is given by:

$$g(\xi, t) = e^{-\frac{t}{T_2}} \cdot \frac{1}{8\pi^2} \int_0^{2\pi} \int_0^\pi \int_0^{2\pi} \exp\left[i \int_0^t \omega(\alpha, \beta, \gamma, t) dt\right] d\alpha \sin \beta d\beta d\gamma \quad (5-1)$$

where T_2 is the transverse relaxation time, (α, β, γ) are the three Euler angles which describe the orientation of PAS system relative to rotor system RF as illustrated in fig2-1. All the simulation calculations in this thesis are based on equation (5-1) and its corresponding angle definitions

given here. For all simulations, FID data are firstly calculated according to equation (5-1), then Frydman's normal interpolation procedure and VNMR software from VARIAN are used to get the final spectra through fast Fourier transformation. The calculation result of $g(\xi, t)$ from equation (5-1) corresponds to the experimental VAS acquisition where the sample spinning axis has an angle equal to ξ . A total number of M calculations of $g(\xi, t)$ corresponding to the angle ξ in a range (ξ_{\min} , ξ_{\max}) form a complete simulation VACSYSY fid data set.

Equation (5-1) shows that: in order to get the free induction decay of the whole sample corresponding to one specified angle ξ position, three integrals (powder averaging) with respect to the three Euler angles α , β , γ have to be evaluated. If the corresponding part of the simulation program for this powder averaging is not correctly optimised, the whole VACSYSY simulation might be extremely time consuming [Conroy, 1967; Eden et al., 1998; Maricq et al, 1979]]. Two available procedures to implement this powder averaging are described in the following.

5.2.1 Stepwise procedure

An obvious approach for evaluating the three powder averaging integrals is a step-wise procedure. This procedure is demonstrated as following:

$$\int_0^{2\pi} \int_0^{2\pi} \int_0^{2\pi} f(\alpha, \beta, \gamma) d\alpha \sin \beta d\beta d\gamma \Rightarrow \sum_{n_\alpha=1}^{N_\alpha} \sum_{n_\beta=1}^{N_\beta} \sum_{n_\gamma=1}^{N_\gamma} f(\alpha, \beta, \gamma) \sin\left(\frac{n_\beta \cdot 2\pi}{N_\beta}\right) \frac{n_\alpha \cdot 2\pi}{N_\alpha} \cdot \frac{n_\beta \cdot 2\pi}{N_\beta} \cdot \frac{n_\gamma \cdot 2\pi}{N_\gamma} \quad (5-2)$$

the three integrals with respect to α , β , γ are converted to three summations for the convenience of digital calculation by computer. α is digitised for N_α steps in the range $(0, 2\pi)$, β is digitised for N_β steps in the range $(0, \pi)$, γ is digitised for N_γ steps in the range $(0, 2\pi)$. The selected values for N_α , N_β , N_γ depend on the values of the CSA tensor elements of the investigated sample.

Take the case of COO^- group in glycine for example, the three principal values of chemical shift are: 238 ppm, 178ppm and 108ppm. $N_\alpha=100$ $N_\beta=100$ $N_\gamma=30$ are normally necessary for simulation to give a smooth CSA line-shape.

If the numbers of steps N_α , N_β , N_γ are relative large, the total number of calculations necessary for a smooth simulation of CSA line-shape is $N_\alpha \times N_\beta \times N_\gamma$. Then, this process might become very time consuming. On a SUN Sparc workstation, a VACSYSY simulation with 200 angle ξ steps, chemical shift tensor elements: 238 ppm, 178ppm and 108ppm, digitisation numbers: $N_\alpha=100$ $N_\beta=100$ $N_\gamma=30$, takes more than 4 days!

5.2.2 CONROY procedure

Harold Conroy proposed a new general method for the numerical integration of functions with many independent variables [Conroy, 1967]. Apply this procedure to perform powder averaging, the calculation time is drastically reduced.

In this new method the sample points are distributed systematically rather than at random. The ensemble of points forms a unique, closed, symmetrical pattern, which effectively fill the space of the multidimensional integration as shown in fig5-1. This method employs certain rational constants which control the arrangement of sample points. A table of the constants for the case of three independent integration variables is given in table 5-1.

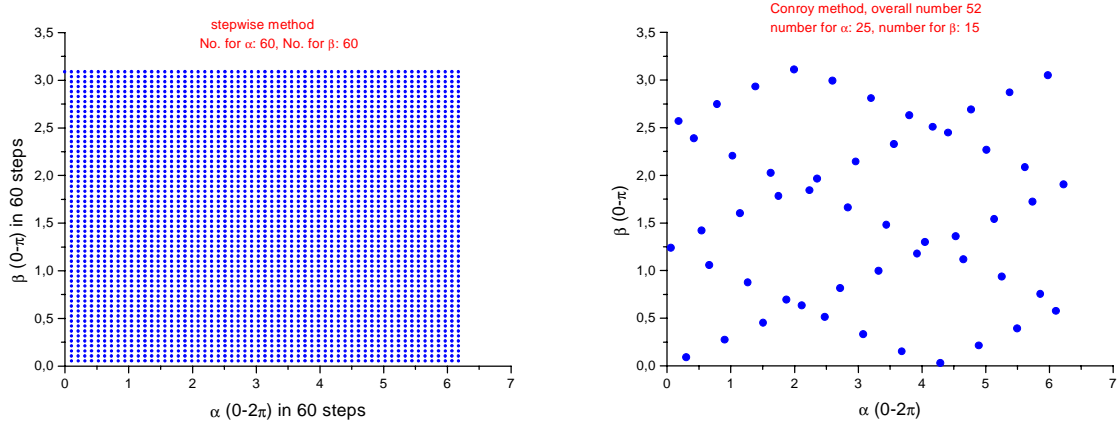


Figure 5-1: Comparison between stepwise approach and Conroy approach. (left) Stepwise approach - random distribution of calculation data points for the case 2D powder averaging, α from 0 to 2π , β from 0 to π . (Right) Conroy approach - symmetric distribution of calculation data points for the case of 2D powder averaging, α from 0 to 2π , β from 0 to π .

According to Conroy's procedure, instead of three integration/summation loops as in the step-wise procedure, only one integration/summation loop is required. In this single loop, integration/ summation is calculated from 1 to the selected general integration constant Const0. α is sampled in the range (0, 2π) with an increment of $2\pi/\text{Const1}$. If $0 \geq \alpha$ or $\alpha \geq 2\pi$ then α is mirrored back to the range of (0, 2π) by using relations $-\alpha$ or $4\pi-\alpha$. Angle β and γ are handled similarly as α but with Const2 and Const3 respectively.

Const0	Const1	Const2	Const3
52	5	7	11
538	115	241	251
1154	11	369	569
3722	653	1005	1483
6044	595	1359	1865

Table 5-1: Conroy rational constants for the calculation of powder averaging. Const0- overall rational constant; (Const1, Const2, Const3) - rational constants for angles (α , β , γ)

Two computer programs for VACSY spectrum simulation are written in C language, one uses step-wise approach, another one uses Conroy's method. A comparison of the necessary calculation time between these two methods is presented in fig5-2. With visually the same simulation result, the calculation time used by the step-wise approach is about 1000 times of the time used by Conroy's method!

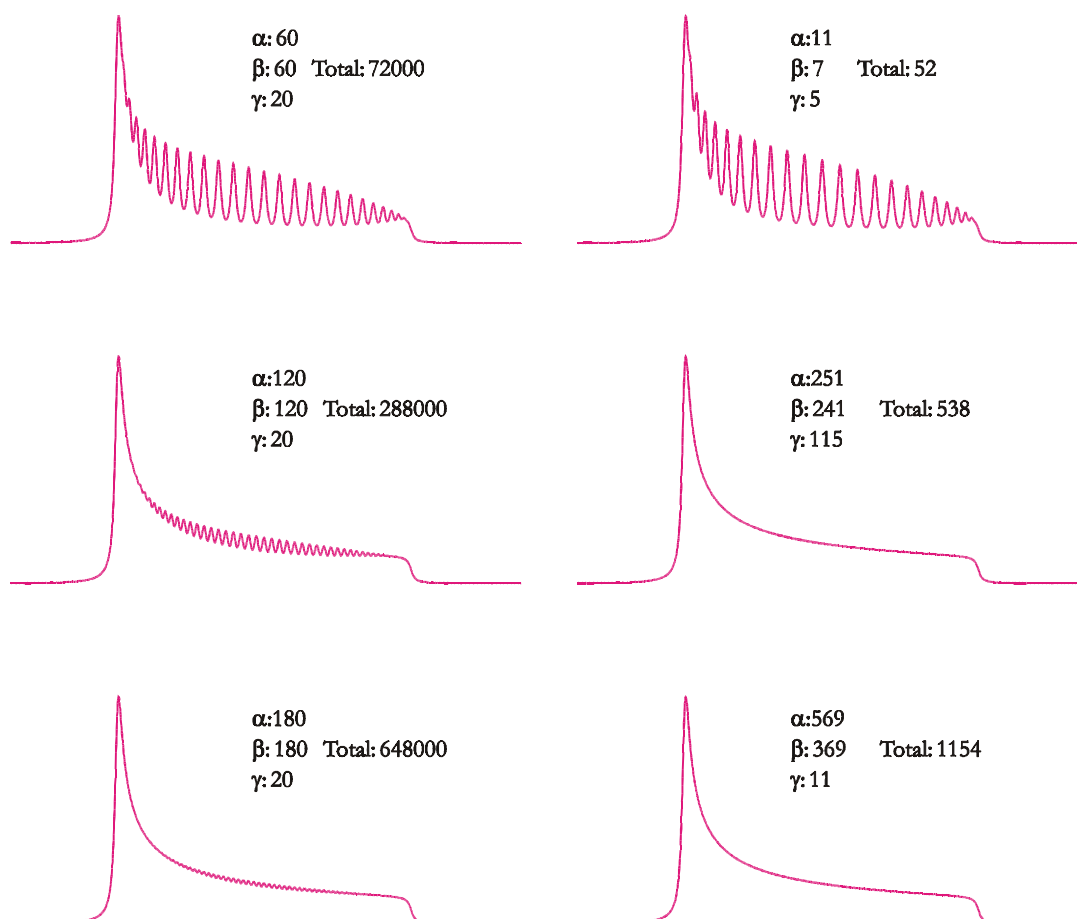


Figure5-2: Comparison of calculation time between stepwise approach and Conroy approach. (left) Stepwise method - total number of integral summation, and number of steps for each angle are given in inserted text boxes. (right) Conroy method - total number of integral summation, and number of rational constants used for each angle are also given in text boxes.

With Conroy's method for powder averaging, on a SUN Sparc workstation, the same VACSY simulation with 200 angle ξ steps, chemical shift tensor elements: 238 ppm, 178ppm and 108ppm, Conroy number used: 3722, takes less than 2 hours.

5.3 Simulation results

The VACSY simulation program using Conroy's powder averaging method is used to perform all the following simulation calculations. The global parameters used for these simulations are: Larmor frequency: 100.53MHz for ^{13}C (corresponding to 400MHz for ^1H);

spectral width for both direct and indirect dimensions are equal to 49875.3 Hz; number of points used in the direct dimension is 512; Except for the case of 1D VAS simulation to show the influence of insufficient spinning speed on the CSA line-shape, three principal values of HMB's chemical shift tensor: 12.5ppm, 185.5ppm, 185.5ppm are used. For all 2D VACSY simulations, Frydman's normal interpolation procedure is used to interpolate the data to $n_i=256$ steps in the indirect direction.

5.3.1 How much a spinning speed is necessary with respect to the CSA value of the investigated sample to neglect the CSA line-shape distortion of the central spinning band?

In the case of macroscopic sample spinning, when the spinning frequency is less than the width of the chemical shift anisotropy, spinning sidebands appear. One well accepted fact is that the centre-band and each spinning sideband contain all contributions from different parts of the static powder pattern. According to this argument, except for a scaling factor the CSA line-shapes of the centre-band and all sidebands should be exactly the same as the static CSA line-shape.

However, numerical simulation shows that, in slow spinning regime, due to the destructive interference of the magnetisation of different crystallites, their contribution to the centre-band and to each spinning sideband is strongly different. Therefore, under the condition of off-magic-angle spinning, different line-shapes will appear for the centre-band and for each spinning sideband [Tekely, 1998]. This indicates that: some crystallite orientations may not show up in the CSA line-shape of the centre-band or any spinning sideband of a slow spinning sample, therefore impede the correct characterisation of orientation distribution through the line-shape analysis procedure. In order to solve this problem, the distortion of the CSA line-shape from its corresponding static state due to a not enough spinning speed has to be minimised. Two approaches can be used: (i) increase spinning speed to remove all sidebands (ii) do experiments in a lower B_0 field, because chemical shift interaction is proportional to the B_0 field.

Therefore, for VACSY experiment a simulation program becomes useful to find out how much a minimum spinning speed with respect to the CSA value of the investigated sample is necessary to neglect the distortion of the line-shape. The simulation results using the indicated CSA parameters for 1D and 2D slow sample spinning cases are shown in fig5-3 and fig5-4 respectively. With these CSA parameters, the line-shape distortion at a spinning speed bigger than 6.0 kHz can be neglected.

– 1D simulation

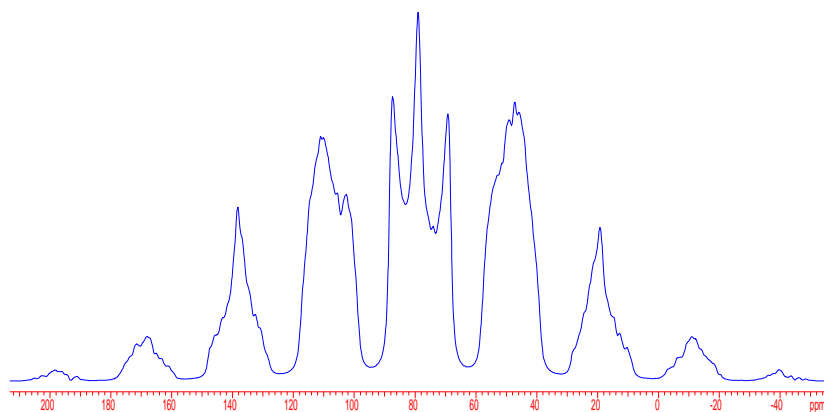


Figure 5-3a: Influence of sample spinning speed on CSA line-shape at $\beta=60^\circ$. Spinning speed: 3.0kHz. CSA tensor elements used $(\sigma_{xx}, \sigma_{yy}, \sigma_{zz})=(160, 75, 0)$ (ppm).

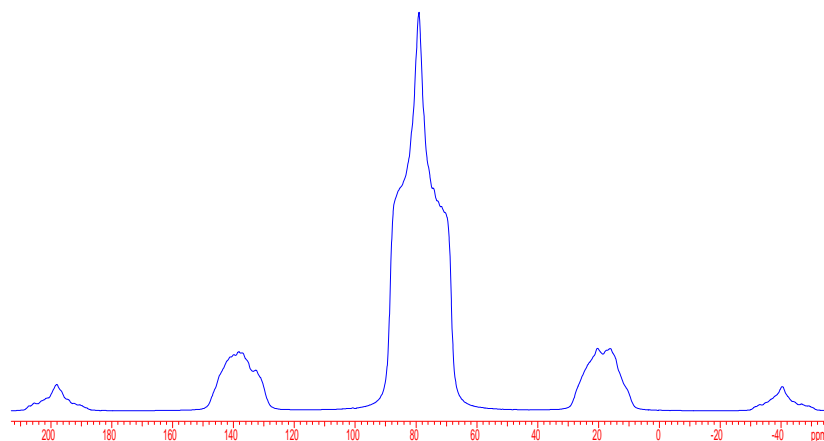


Figure 5-3b: Influence of sample spinning speed on CSA line-shape at $\beta=60^\circ$. Spinning speed: 6.0kHz. CSA tensor elements used $(\sigma_{xx}, \sigma_{yy}, \sigma_{zz})=(160, 75, 0)$ (ppm).

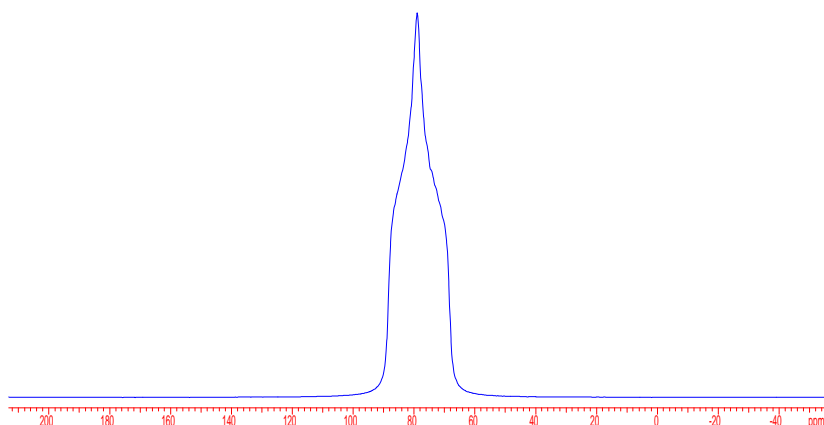


Figure 5-3c: Influence of sample spinning speed on CSA line-shape at $\beta=60^\circ$. Spinning speed: 35.0kHz. CSA tensor elements used $(\sigma_{xx}, \sigma_{yy}, \sigma_{zz})=(160, 75, 0)$ (ppm).

– 2D VACSY simulation

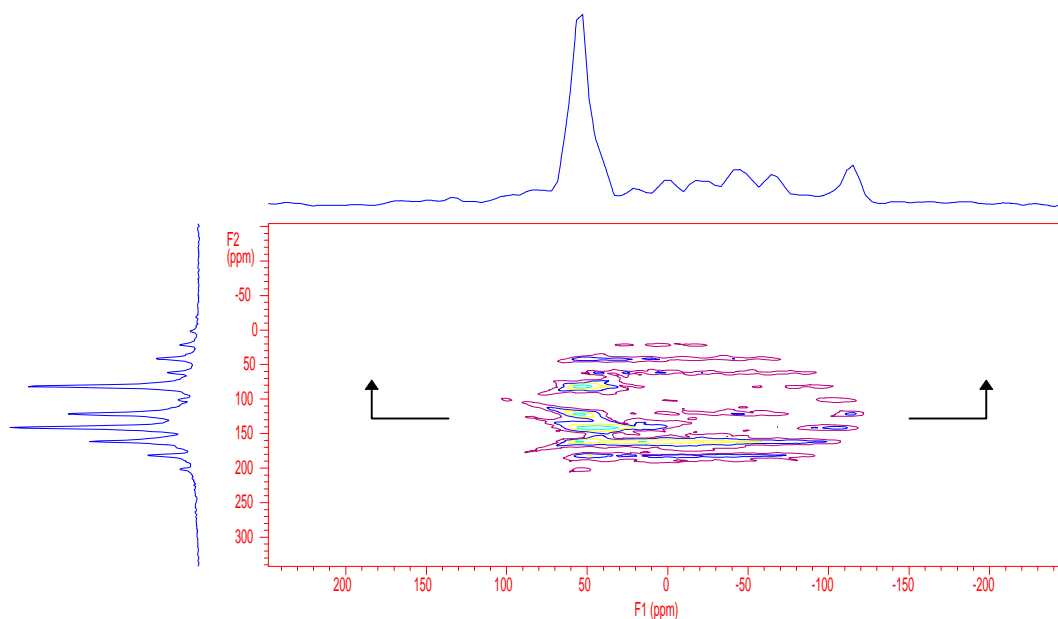


Figure 5-4a: Influence of sample spinning speed on CSA line-shape. VACSY simulation with: angle β sampling range: 35° - 90° in 120 experimental steps; CSA tensor elements used (σ_{xx} , σ_{yy} , σ_{zz}) = (185.5, 185.5, 12.5) (ppm); spinning speed: 2.0kHz.

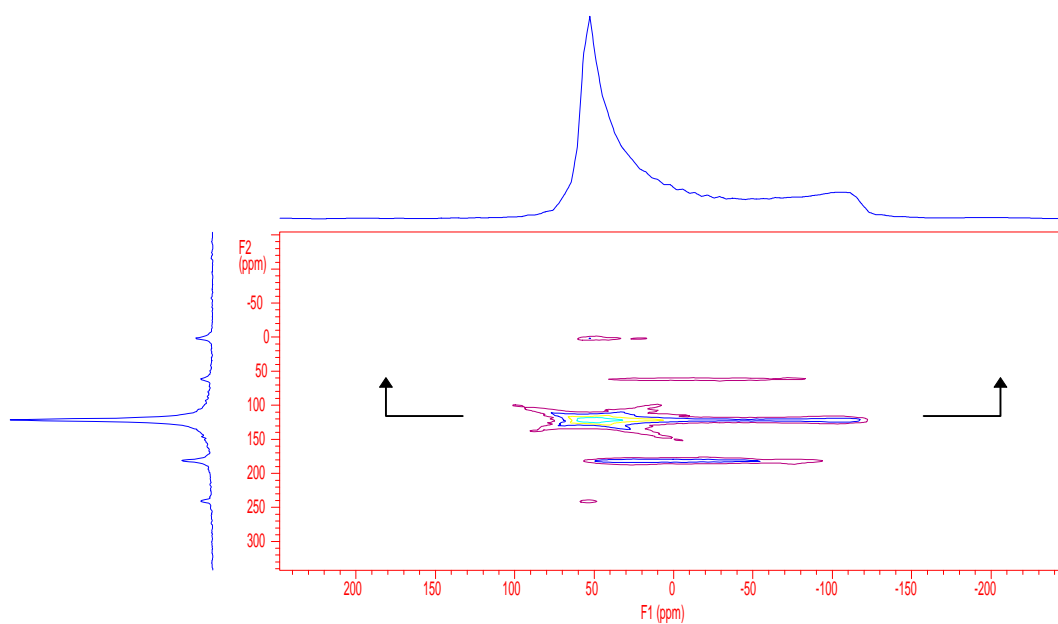


Figure 5-4b: Influence of sample spinning speed on CSA line-shape. VACSY simulation with: angle β sampling range: 35° - 90° in 120 experimental steps; CSA tensor elements used (σ_{xx} , σ_{yy} , σ_{zz}) = (185.5, 185.5, 12.5) (ppm); spinning speed: 6.0kHz.

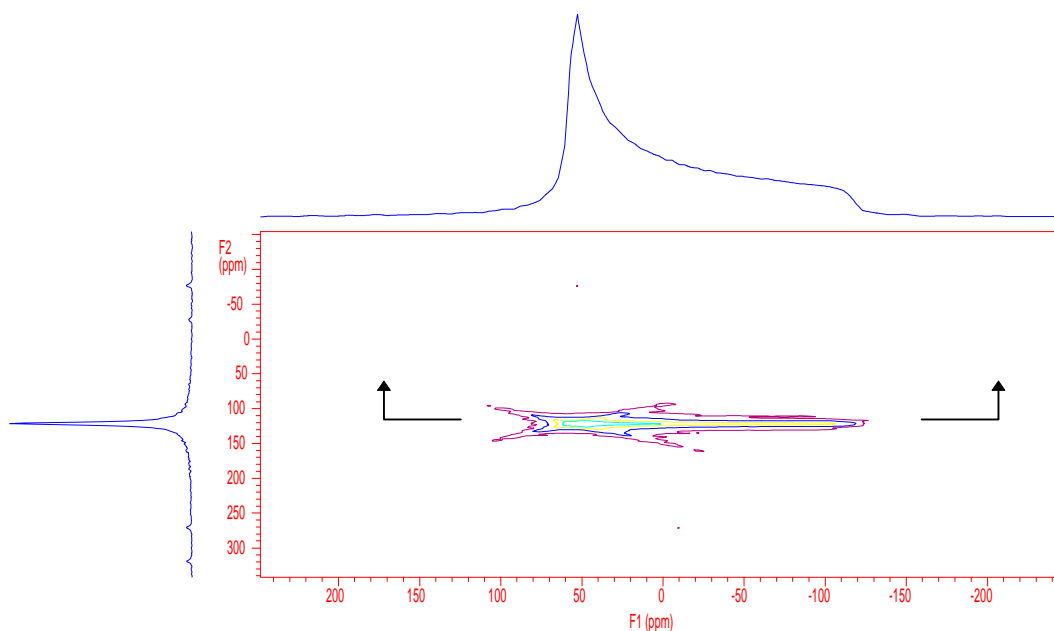


Figure 5-4c: Influence of sample spinning speed on CSA line-shape. VACSYS simulation with: angle β sampling range: 35° - 90° in 120 experimental steps; CSA tensor elements used (σ_{xx} , σ_{yy} , σ_{zz}) = (185.5, 185.5, 12.5) (ppm); spinning speed: 15.0kHz.

5.3.2 How much a control accuracy is necessary to neglect the CSA line-shape distortion due to the angle β mis-setting?

The simulation result of the CSA line-shape distortion due to the mis-setting of the sample spinning axis β is shown in fig5-5. With the indicated CSA parameters, if the uncertainty of angle β is bigger than 0.5° , significant line-shape distortion appears. Here, the angle uncertainty is randomly generated within the indicated range for VACSYS data acquisitions at different angle β positions .

In our VACSYS probe, the mechanical system used to control angle β includes a step motor, an angle encoder, a pulley and string. The motion is generated by the stepmotor located about 25cm aside from the main magnet. The stepmotor can also be put directly under the main magnet. Nevertheless, due to the magnetic property of the stepmotor a safe distance from the main magnet to the stepmotor has to be found and maintained. The motion is then coupled upwards to the sample housing through a pulley and string, where the main uncertainty in angle β control originates. Firstly, the tension of the connection string should be adjusted according to the torque of the stepmotor and the friction force existed between different moving parts of this angle β control system; Secondly, the backlash in the pulley and string system, which happens when the moving direction is reversed, has to be accurately measured and compensated in the stepmotor control program. The current angle is monitored through a angle encoder attached together with the stepmotor.

The overall angle β control uncertainty of our VACSYS probe is estimated at around 0.25° , better accuracy with further improvements of the current mechanical system is highly desirable, although practically it is not easy.

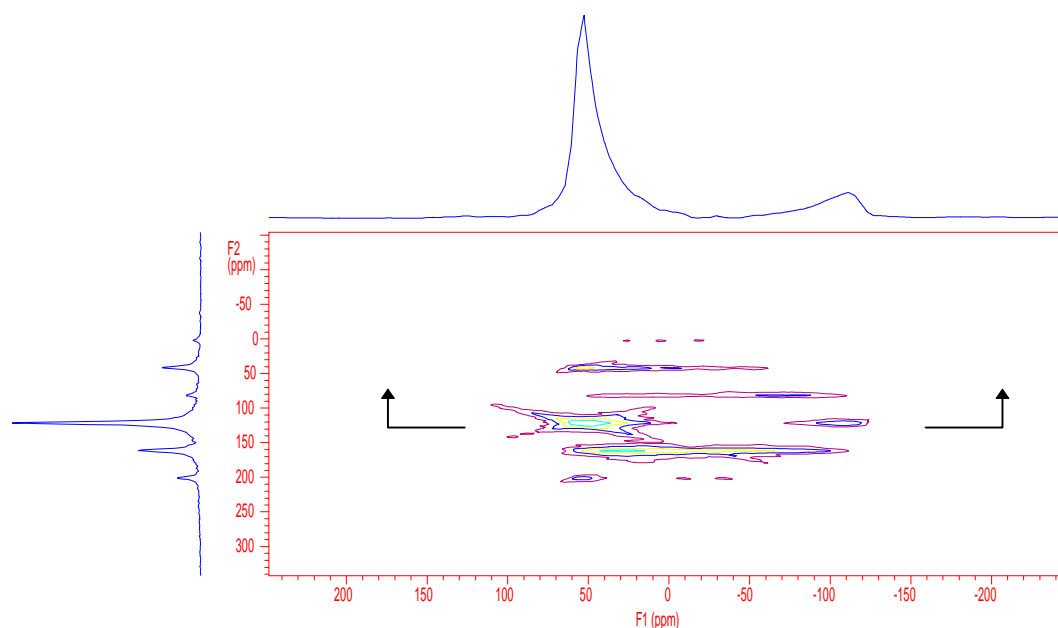


Figure 5-5a: Influence of angle β control accuracy on CSA line-shape. VACSYS simulation with: angle β sampling range: $35^\circ - 90^\circ$ in 120 experimental steps; CSA tensor elements used (σ_{xx} , σ_{yy} , σ_{zz}) = (185.5, 185.5, 12.5) (ppm); spinning speed=4.0kHz; angle β uncertainty: 0° .

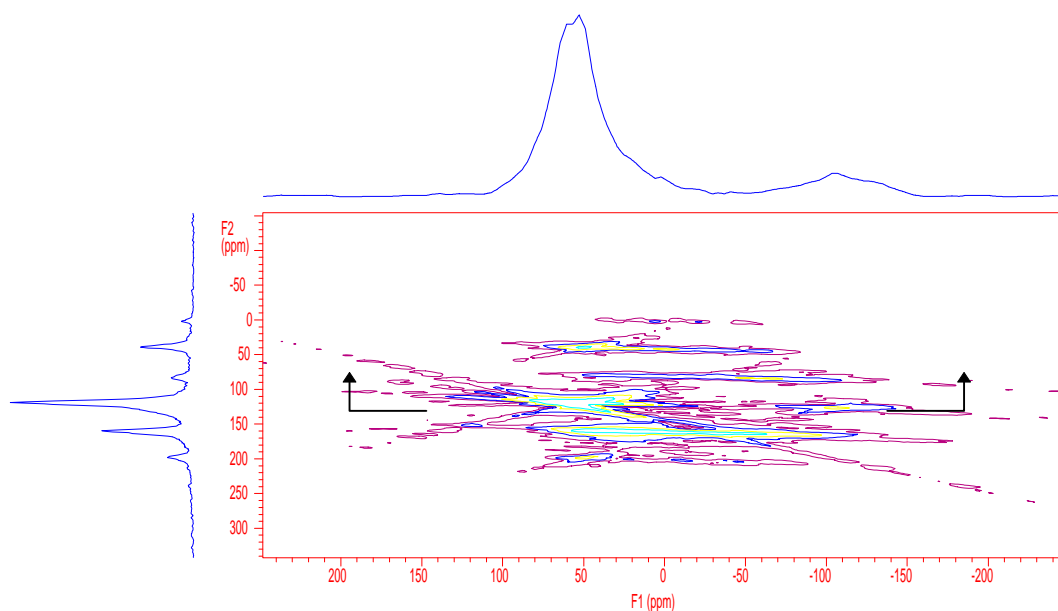


Figure 5-5b: Influence of angle β control accuracy on CSA line-shape. VACSYS simulation with: angle β sampling range: $35^\circ - 90^\circ$ in 120 experimental steps; CSA tensor elements used (σ_{xx} , σ_{yy} , σ_{zz}) = (185.5, 185.5, 12.5) (ppm); spinning speed=4.0kHz; angle β uncertainty: 0.5° .

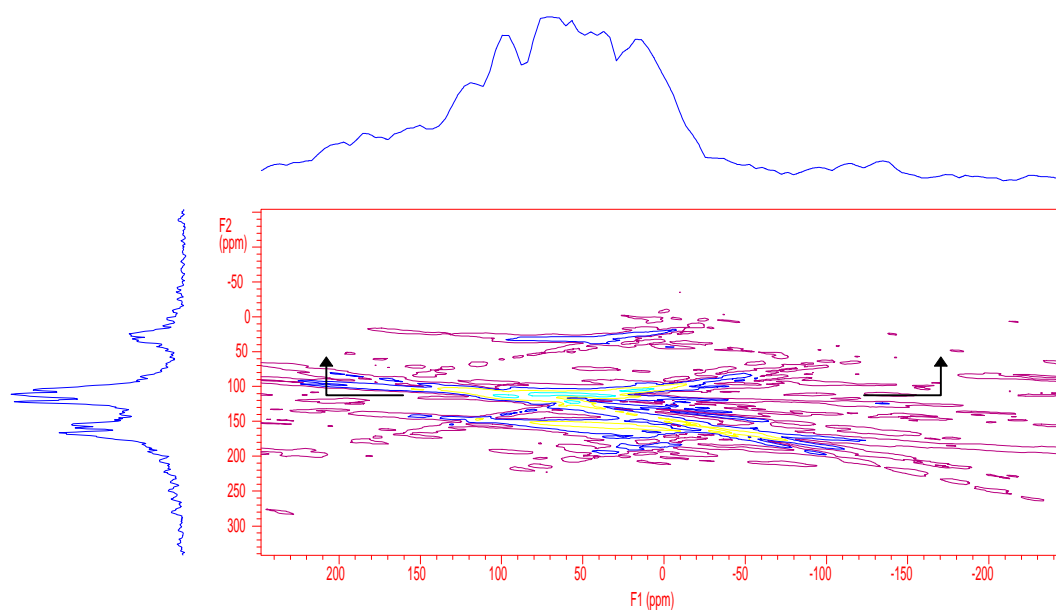


Figure 5-5c: Influence of angle β control accuracy on CSA line-shape. VACSY simulation with: angle β sampling range: $35^\circ - 90^\circ$ in 120 experimental steps; CSA tensor elements used (σ_{xx} , σ_{yy} , σ_{zz}) = (185.5, 185.5, 12.5) (ppm); spinning speed=4.0kHz; angle β uncertainty: 2.0° .

5.3.3 How much a range of the angle β is necessary for the acquisition of a non-distorted CSA line-shape?

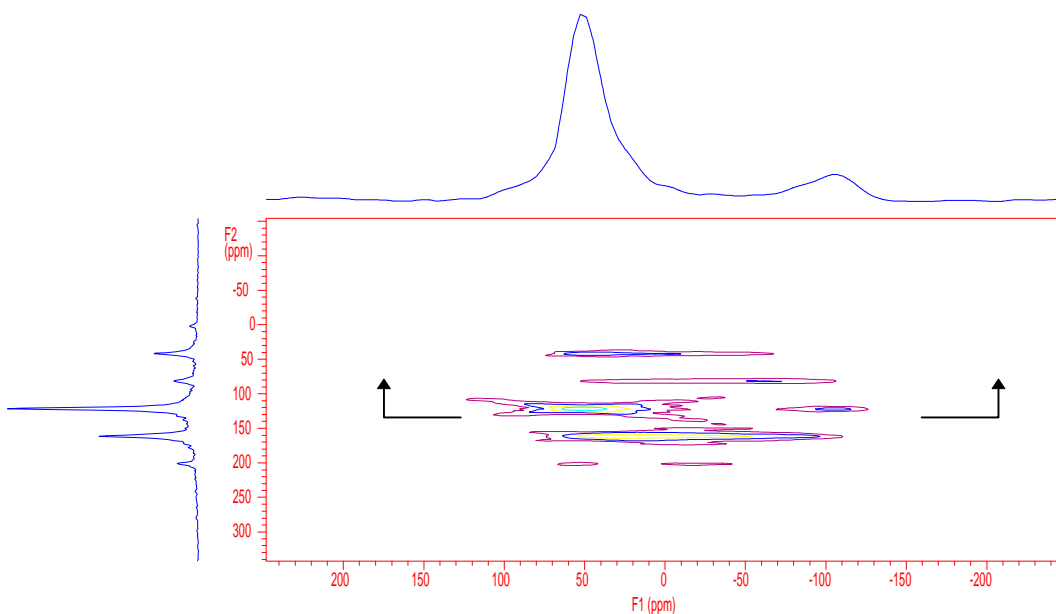


Figure 5-6a: Influence of angle β sampling range on CSA line-shape. VACSY simulation with: CSA tensor elements used (σ_{xx} , σ_{yy} , σ_{zz})=(185.5, 185.5, 12.5) (ppm); spinning speed=4.0kHz; Angle β sampling range of $45 - 63^\circ$ in 40 experimental steps;

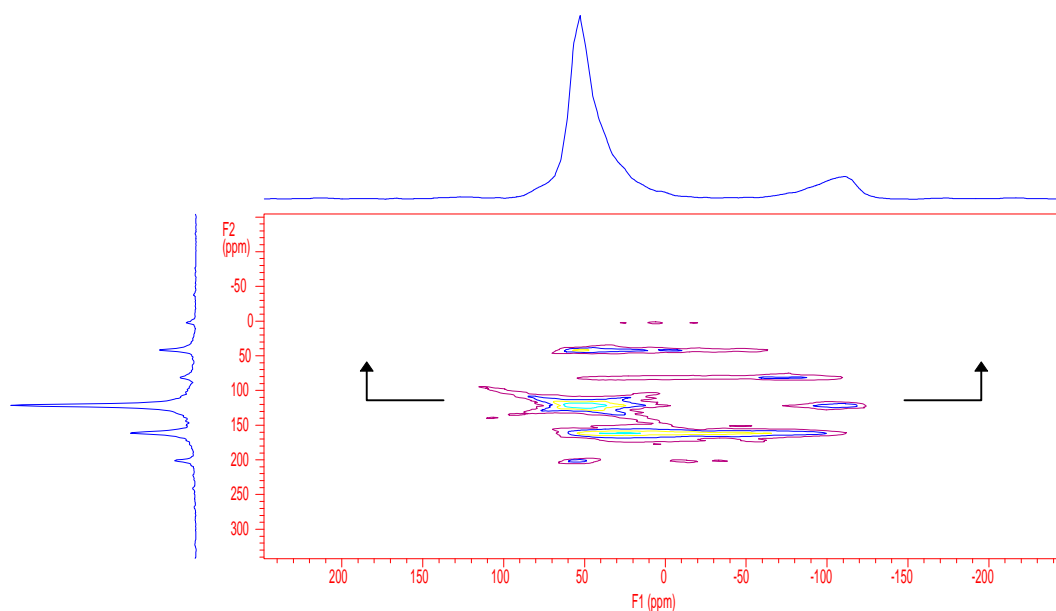


Figure 5-6b: Influence of angle β sampling range on CSA line-shape. VACSYS simulation with: CSA tensor elements used (σ_{xx} , σ_{yy} , σ_{zz})=(185.5, 185.5, 12.5) (ppm); spinning speed=4.0kHz; Angle β sampling range of 36 - 72° in 80 experimental steps;

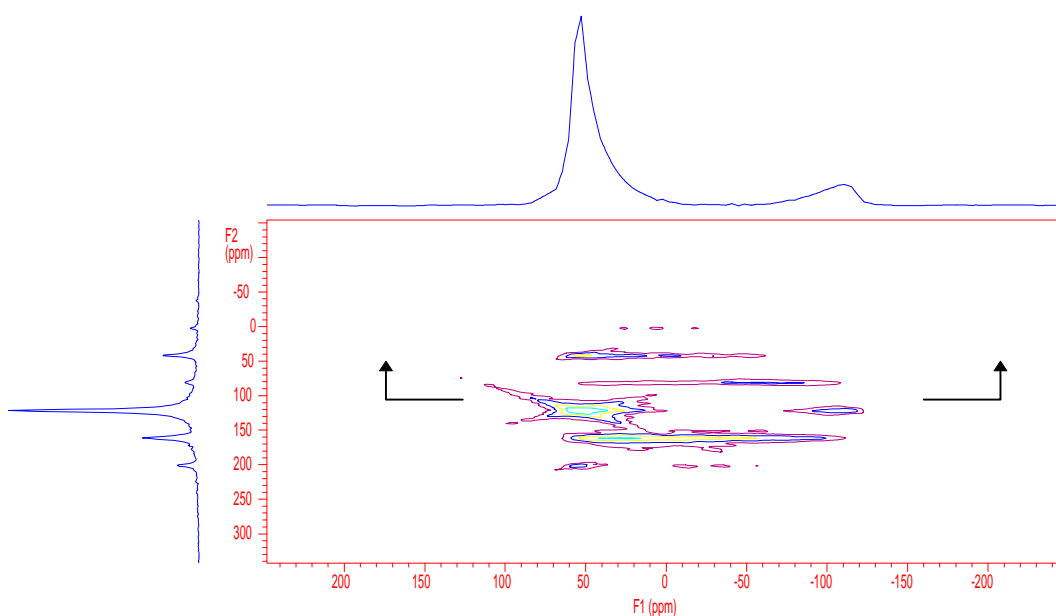


Figure 5-6c: Influence of angle β sampling range on CSA line-shape. VACSYS simulation with: CSA tensor elements used (σ_{xx} , σ_{yy} , σ_{zz})=(185.5, 185.5, 12.5) (ppm); spinning speed=4.0kHz; Angle β sampling range of 27 - 81° in 120 experimental steps.

The simulation result of the CSA line-shape distortion due to a not sufficient sampling range of angle β is shown in fig5-6. With the indicated CSA parameters, if sampling range of angle β is smaller than 20°, for example from 45° - 63°, some line-shape distortion begins to appear. This is due to a insufficient data sampling area in space (t_a , t_i) for the interpolation step as described in *chapter 4*, therefore phase artefacts and increasing interpolation error cause the resulted CSA line-shape distortion

5.3.4 How many independent VAS experiments should be carried out for a non-distorted line-shape?

The simulation result of the CSA line-shape distortion due to a not sufficient sampling numbers of angle β in a sufficient angle range is shown in fig5-7. With the indicated CSA parameters and a sufficient angle range for data acquisition $35^\circ - 90^\circ$, if the sampling numbers of angle β is less than 30, again some line-shape distortion begins to appear. The reason is the insufficient sampling number of the data area in space (t_a, t_i) corresponding to an angle range of $35^\circ - 90^\circ$ in real space, this leads to increasing interpolation error and the resulted distortion in the final spectrum.

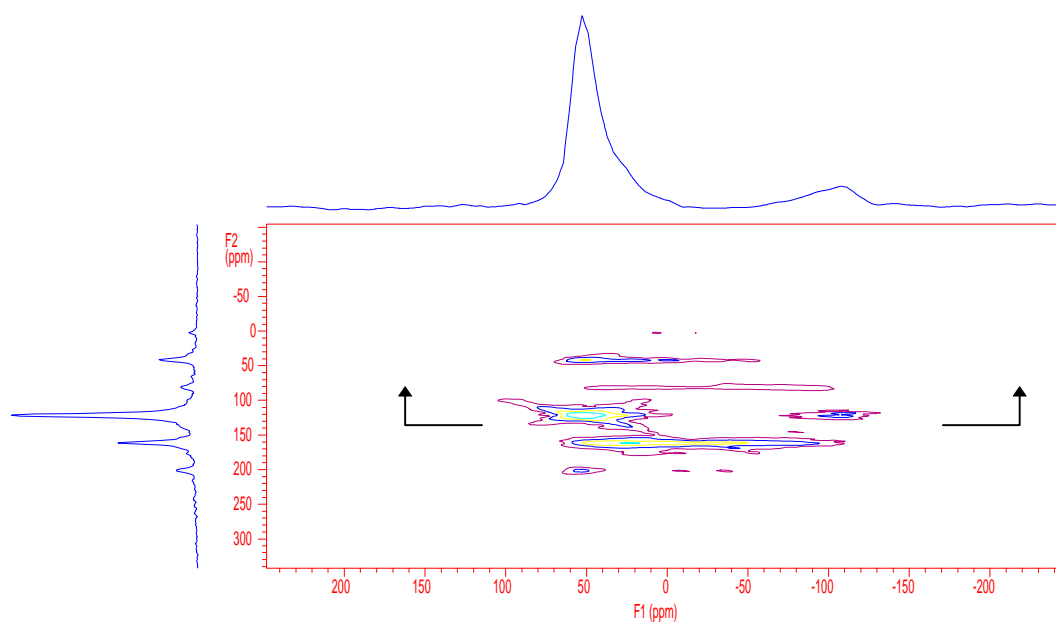


Figure 5-7a: Influence of angle β sampling number on CSA line-shape. VACSY simulation with: Angle β sampling range of $35^\circ - 90^\circ$; CSA tensor elements used $(\sigma_{xx}, \sigma_{yy}, \sigma_{zz})=(185.5, 185.5, 12.5)$ (ppm); spinning speed=4.0kHz; angle β sampling numbers: 60

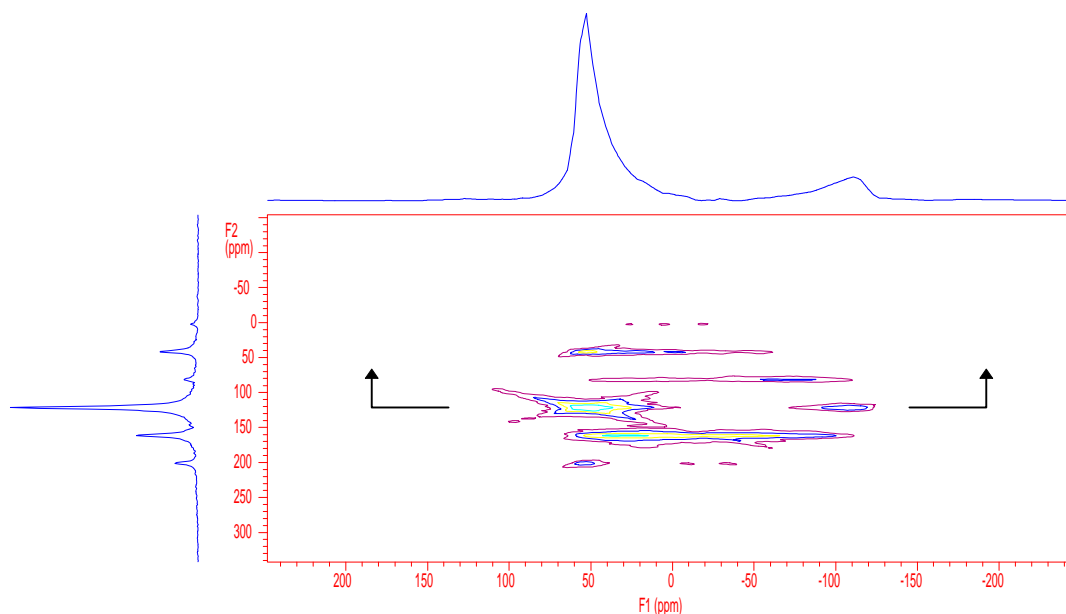


Figure 5-7b: Influence of angle β sampling number on CSA line-shape. VACSY simulation with: Angle β sampling range of $35 - 90^\circ$; CSA tensor elements used $(\sigma_{xx}, \sigma_{yy}, \sigma_{zz})=(185.5, 185.5, 12.5)$ (ppm); spinning speed=4.0kHz; angle β sampling numbers: 120

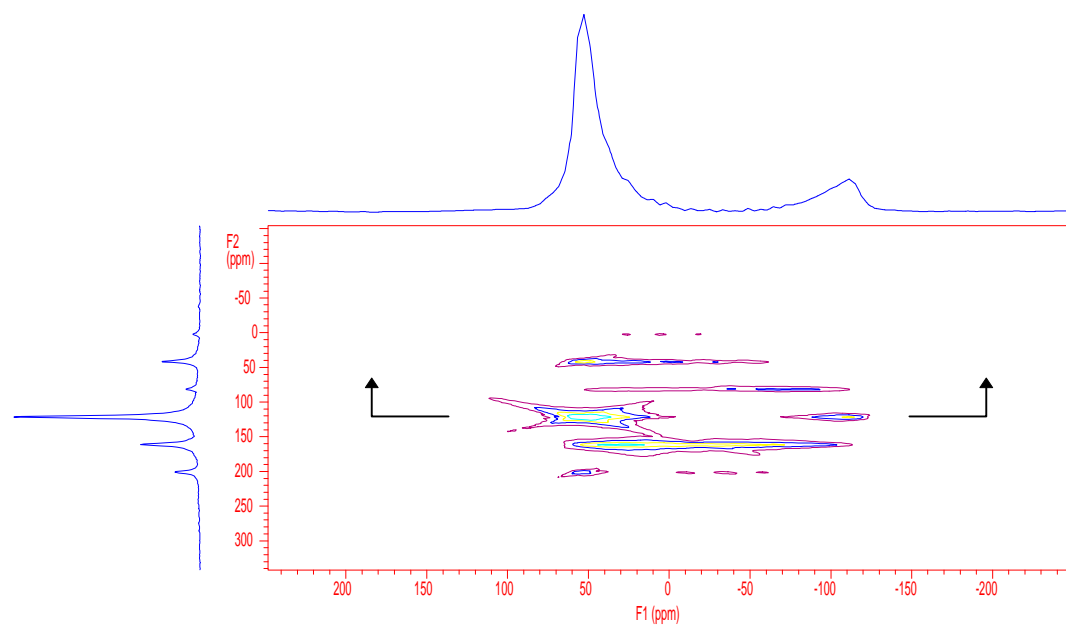


Figure 5-7c: Influence of angle β sampling number on CSA line-shape. VACSY simulation with: Angle β sampling range of $35 - 90^\circ$; CSA tensor elements used $(\sigma_{xx}, \sigma_{yy}, \sigma_{zz})=(185.5, 185.5, 12.5)$ (ppm); spinning speed=4.0kHz; angle β sampling numbers: 240

5.3.5 How much a fluctuation in spinning speed is tolerable to achieve a non-distorted CSA line-shape?

The simulation result of the CSA line-shape distortion due to the fluctuation in sample spinning speed is shown in fig5-8. With the indicated CSA parameters, if the fluctuation of the

sampling spinning speed is bigger than 500Hz, significant line-shape distortion appears. Here, fluctuation in sample spinning speed is randomly generated within the indicated range for VACSY data acquisitions at different angle β positions.

In our VACSY probe, the tribo-electric antenna design is adapted to detect the sample spinning speed while it can easily follow the movement of the whole sample housing when the experiment is swept through a certain angle range. There are two problems here (i) when the sample housing changes from angle β to another, with a constant air supply the sample spinning speed changes in the range of 0 - 500Hz. In principle, automatic spinning speed regulation can adjust it back to the setting speed. However, (ii) with the tribo-electric spinning speed detection design, there is strong interference in the spinning speed control signal when rf pulses are in action. This interference can destroy the automatic spinning speed regulation control loop and in the worst cases stop the spinning.

Recently, the spinning speed detection scheme of our VACSY probe is changed to fiber optic spinning speed detector with some careful mechanic design to allow the rigid fiber follow the movements of the sample housing. Now, during the whole VACSY experiment the spinning speed can be regulated to the setting value within an error of 10Hz. So, the line-shape distortion due to this reason is removed.

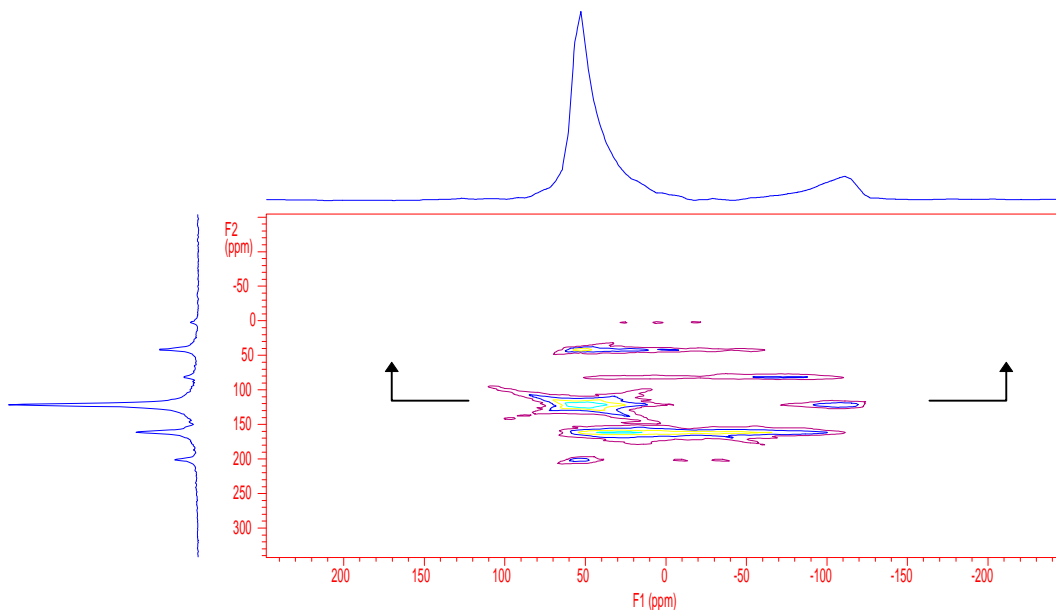


Figure 5-8a: Influence of fluctuation in spinning speed on CSA line-shape. VACSY simulation with: angle β sampling range of 35 - 90° in 120 steps; CSA tensor elements used (σ_{xx} , σ_{yy} , σ_{zz}) = (185.5, 185.5, 12.5) (ppm); spinning speed=4.0kHz; fluctuation in spinning speed: 0.0Hz

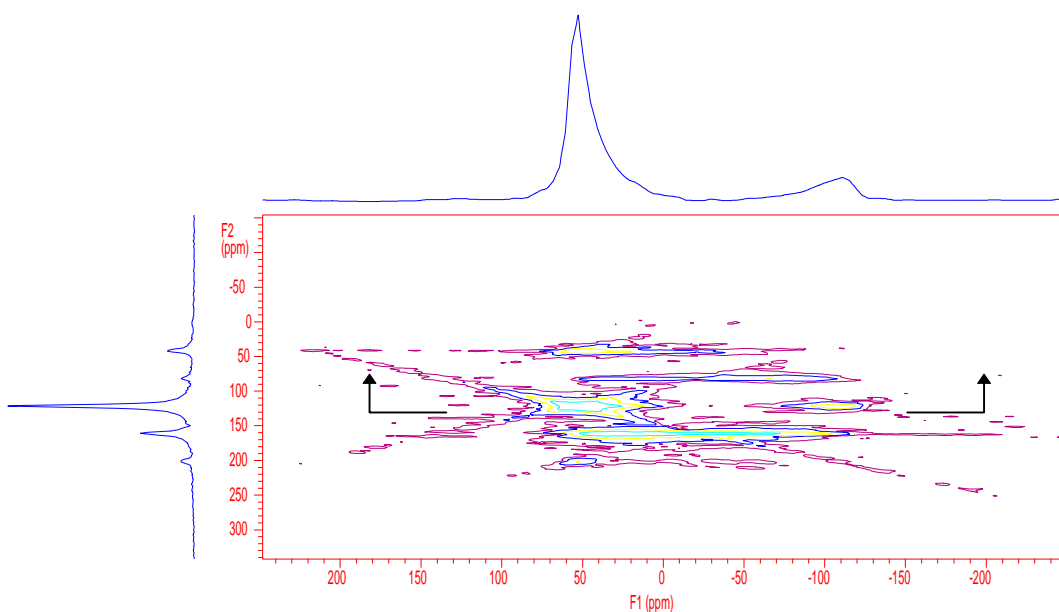


Figure 5-8b: Influence of fluctuation in spinning speed on CSA line-shape. VACSYS simulation with: angle β sampling range of $35 - 90^\circ$ in 120 steps; CSA tensor elements used $(\sigma_{xx}, \sigma_{yy}, \sigma_{zz})=(185.5, 185.5, 12.5)$ (ppm); spinning speed=4.0kHz; fluctuation in spinning speed: 100.0Hz

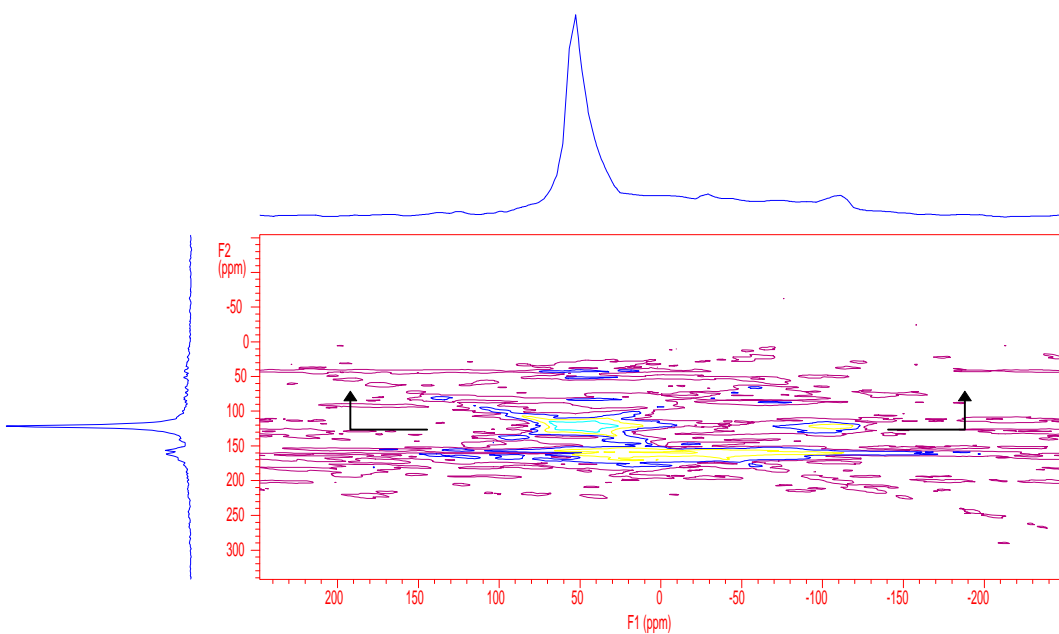


Figure 5-8c: Influence of fluctuation in spinning speed on CSA line-shape. VACSYS simulation with: angle β sampling range of $35 - 90^\circ$ in 120 steps; CSA tensor elements used $(\sigma_{xx}, \sigma_{yy}, \sigma_{zz})=(185.5, 185.5, 12.5)$ (ppm); spinning speed=4.0kHz; fluctuation in spinning speed: 500.0Hz

CONSTRUCTION OF A VACSY PROBE

6.1 Introduction

The word probe or probe-head is used to refer to the complete piece of equipment intimately associated with the sample. For the simplest experiments, the probe consists of the mechanical structure required to hold the sample in the homogeneous spot of the magnet, a coil surrounding the sample, a tuning capacitor and a rf transmission line. However, most NMR problems of interest require control over the sample environment, such as: temperature, electromagnetic irradiation, pressure, orientation, rotation and etc, apparatus associated with these functions also become parts of the NMR probe.

The modern NMR probe is a complex apparatus which is designed to accommodate all of the environmental requirements of the NMR experiment. The radio-frequency (rf) section often includes (a) an rf observe channel optimised for highest signal-to-noise ratio (SNR or S/N) at the X nucleus frequency, (b) a less efficient rf channel for hetero-nuclear decoupling (usually ^1H), (c) another low-efficiency channel for magnetic field lock (usually ^2H). Variable temperature (VT) control is achieved through a resistive heater in a gas stream that flows over the sample. In high resolution liquid probes, slow sample spinning (100-200Hz) about the external magnetic field \mathbf{B}_0 direction is required to average out azimuthal inhomogeneity. In solid state probes, high speed sample spinning (200-36000Hz) is required to average out chemical shift anisotropy and/or dipolar interactions [Doty, 1996a].

Due to the absence of molecular tumbling in solids to average out line-broadening interactions, the requirements for solid probes are more demanding than for liquid probes. Solid probes require much greater bandwidths [Hartmann et al., 1962; Mansfield et al., 1963; Vaughan, 1978]. A wide-line probe usually has spectral excitation bandwidth greater than 80KHz, that is equal to be able to generate 90° pulses less than $3\mu\text{s}$. To do this, it normally must withstand peak rf voltages in excess of 3 KV [Doty, F. D., 1996b]. Often wide-line probes are double tuned (DT) to allow cross polarisation (CP) and high power decoupling for increased sensitivity and resolution. If $\pi/2$ pulse length below $2\mu\text{s}$ can be generated, multiple pulse line-narrowing techniques may be applied to remove dipolar broadening, but this is generally only useful in single resonance probes.

Addressing the often conflicting requirements of high sensitivity, high resolution, large spectral bandwidth, low background signals, wide VT range, high speed sample spinning, intense irradiation, and uniform field gradients require careful attention to a number of problems in material science, physics, electrical engineering, and mechanical engineering [Doty, F. D., 1996a]. These efforts make a NMR probe very expensive.

The most common solid probe is the cross polarisation/magic angle spinning (CPMAS) probe, which adds high-speed sample spinning at the magic angle to the other capabilities of a DT wide-line probe for effective averaging of the chemical shift anisotropy and possibly dipolar interactions at very high speed, therefore the spectral resolution for spin-1/2 nuclei is greatly improved. Single resonance MAS probes can generate the short pulses needed for the combined rotation and multiple pulse spectroscopy (CRAMPS) line-narrowing technique for ^1H and ^{19}F . Large volume MAS rotors can achieve stable rotational spin rate which is necessary for slow MAS, where pulses are applied in precise synchronisation with rotor orientation to average out anisotropic chemical shift interactions as with high speed MAS. Extended variable temperature (X-VT) CPMAS probes allow experiments from 35K to more than 500°C [Doty, 1996b]

6.2 Basics of radio frequency engineering

For the design and construction of a NMR probe, basic understanding of rf engineering and electromagnetic field theory is necessary [Gordan, R. E., 1985; Tranficante, D. D., 1989; Jackson, 1975]. NMR signal detection is different from antenna theory and is simpler. Antennas are designed to receive electromagnetic waves in the far-field limit whereas NMR probes are designed to sense magnetic fields in the near-field limit [Hoult, D. I., 1989]. A number of articles [Hoult and Richards, 1976; Hoult, 1978; Schneider and Dullenkopf, 1977; Doty et al., 1981; Hayes et al., 1985; Doty et al., 1988; Carlson, 1988; Crozier et al, 1995] and a text book [Chen and Hoult, 1989; Fukushima and Roeder, 1996] have presented excellent discussions of general NMR probe design problems.

6.2.1 Capacitance

Capacitance (farads) is defined as electric charge per volt (V), and capacitive energy is equal to $CV^2/2$. Stray capacitance can often be estimated to sufficient accuracy from the expression for parallel plate capacitor C_p of area A (m^2), separation d (m), and dielectric constant κ_d :

$$C_p = \frac{\kappa_d \epsilon_0 A}{d} \quad (6-1)$$

or from the expression for the low-frequency capacitance of a coaxial capacitor [Doty et al., 1981] of length h , dielectric o.d. d_o , and dielectric i.d. d_i :

$$C_c = \frac{2\pi k_d \epsilon_0 (h + d_o)}{\ln(d_o / d_i)} \quad (6-2)$$

where ϵ_0 is the permittivity of free space - 8.84 pFm^{-1} . Parallel capacitors add algebraically $C_{sum} = C_1 + C_2 + C_3 + \dots$, while series capacitors add reciprocally $C_{sum}^{-1} = C_1^{-1} + C_2^{-1} + C_3^{-1} + \dots$.

6.2.2 Inductance

The definition of inductance L (henrys) is given by Farady's law - the induced voltage divided by the rate of change in current di/dt . The inductive energy is equal to $i_r^2 L / 2$. The inductance of the finite, multiturn, single layer rf solenoid in fig6-1 with a constant pitch, an integral number of turns, and a high surface coverage is given in nH, for dimensions in mm, by the following expression:

$$L_s = \frac{4n^2 r^2 (1 - 0.2/n)}{h + 1.2r^{0.9}} \quad (6-3)$$

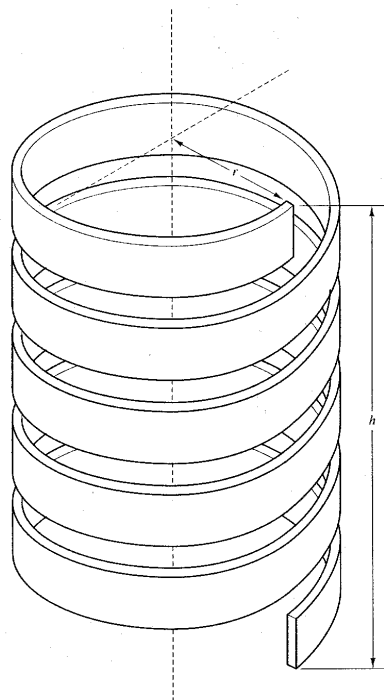


Figure 6-1: a five-turn solenoid (adapted from Doty, 1994).

where n is the number of turns (fig6-1 has five turns), h is the overall axial length, and r is the effective inside radius, which for round wire is approximately equal to the inside coil radius plus 20% of the wire radius. The last term in the numerator corrects for the fact that the helix makes the effective coil length a little less than the overall length. This expression is correct to within

several percent for $h/r > 0.2$. For a single turn solenoid, also called loop-gap resonator [Koskinen and Metz, 1987], the helix correction is dropped and the coefficient changes to 3.9 to correct for current concentrating at the ends of the ring.

Lead (parasitic) inductance is usually best estimated by calculating the inductance of a loop-gap resonator having a length equal to the diameter of the lead wire and $r^2 = A_c / \pi$, where A_c is the area enclosed by the loop formed by the leads. Sometimes lead inductance is better estimated from the expression for the inductance L_C of a coaxial transmission line:

$$L_C = \frac{\mu_0 h}{2\pi} \ln\left(\frac{d_o}{d_i}\right) \quad (6-4)$$

series inductors add like resistors $L_{sum} = L_1 + L_2 + L_3 + \dots$, while parallel inductors add reciprocally $L_{sum}^{-1} = L_1^{-1} + L_2^{-1} + L_3^{-1} + \dots$.

6.2.3 $\lambda/4$ wave length cable

The underline principle of the $\lambda/4$ wave length cable is the so called “transmission line principle”, the equation which governs the behaviour of $\lambda/4$ cable is:

$$z_i z_o = |z_c|^2 \quad (6-5)$$

where Z_i is the input reactance, Z_o is the output reactance, Z_c is the characteristic reactance of the $\lambda/4$ cable. So, it is easy to deduce that when $Z_i = 0$, then $Z_o = \infty$; when $Z_i = \infty$, then $Z_o = 0$. That means: to connect a closed $\lambda/4$ cable is equal to connect a infinite large resistance; to connect a open $\lambda/4$ cable is equal to connect a zero resistance. For example, as shown in fig6-2:

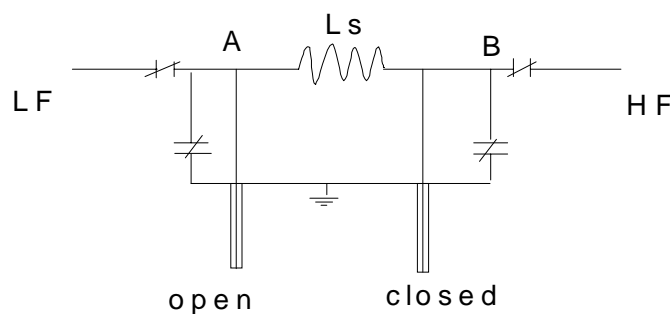


Figure 6-2: Double-tuned probe circuit using transmission lines (adapted from Doty, 1980).

the $\lambda/4$ lines depicted here are cut to the resonant frequency of the nucleus to be de-coupled. For loss-less transmission lines, the closed $\lambda/4$ line at point B presents a infinite impedance at the HF frequency, so all of the HF RF power is available to the sample coil, L_s . The open $\lambda/4$ line at point A presents zero impedance to the HF and thus serves as a virtual ground for the HF power, therefore there should be no HF power at the LF side of the probe.

However, when losses are introduced into the $\lambda/4$ lines, the situation is different. At point A the impedance is usually large enough to limit the HF rejection to less than 20 dB on the LF side of the probe. The even more serious problem is the finite impedance presented by the closed $\lambda/4$ line at point B, in it there is a dramatic loss in the HF efficiency [Doty, 1981].

A alternative for the $\frac{1}{4} \lambda$ cable is to employ a series - parallel reduction scheme on the equivalent circuit using lumped elements as demonstrated in fig6-3 [Doty, 1981].

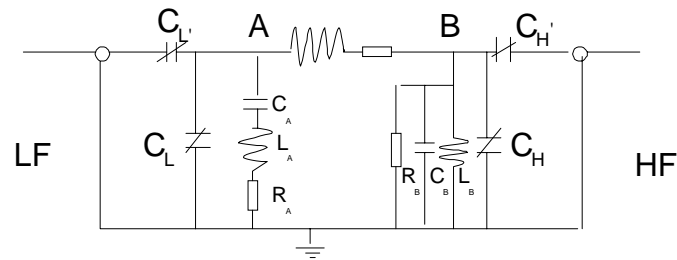


Figure 6-3: Lumped-element equivalent of figure 6-2 (adapted from Doty, 1980).

6.2.4 Single resonance circuit

Fig6-4 shows the basic RLC series and parallel circuits, respectively. The losses in the series RLC circuit are best represented by the total effective series resistance R_s (from the coil, capacitor, leads, etc). For the parallel circuit, the losses may be represented more conveniently by a total effective parallel resistor R_p .

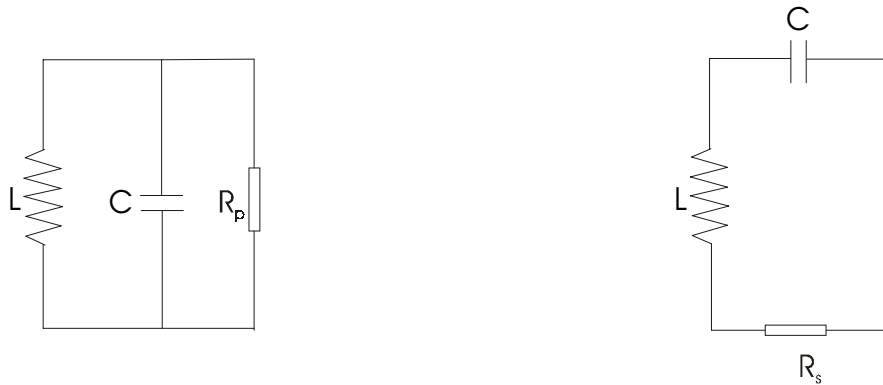


Figure 6-4: Principle of RF resonant circuits. (left) parallel resonant circuit; (right) serial resonant circuit.

In both cases, the basic equations from ac circuits apply for rms power P and peak power P_p .

$$P = \frac{P_p}{2} = \frac{i_p^2 R_s}{2} = \frac{V_p^2}{2R_p} \quad (6-6)$$

In practice, peak voltage ($2V_p$) are usually measured on an oscilloscope, and the measurements are strongly influenced by harmonic distortion, VSWR (Voltage Standing Wave Ratio), loading, and oscilloscope bandwidth. Most conventional liquid probes are excited with 100 W pulses of 10-80 μ s at the observe frequency at duty cycles below 0.1% while they are driven at 10 W at the decoupling frequency at duty cycles below 50%. Solids probes typically see LF pulses of 200-400 W with duty cycles up to 1% while irradiating with HF power of 50-200 W at duty cycles below 30% [Doty, 1996a].

For the normal high-Q condition ($Q = \omega_0 / \Delta\omega_{\frac{1}{2}}$), resonance occurs when the inductive reactance $X_L = i\omega L$ plus the capacitive reactance $X_C = 1/i\omega C$ equals to zero, therefore:

$$\omega_0 = \frac{1}{\sqrt{LC}} \quad (6-7)$$

at resonance, the series impedance of the series RLC circuit is R_s and the parallel impedance of the parallel RLC circuit is R_p . The 3dB width $\Delta\omega_{\frac{1}{2}}$ defines the quality factor of the unloaded RLC circuit. The following relationships are easily proved:

$$\begin{aligned} R_p &= QX_L \\ R_s &= X_L / Q = R_p / Q^2 \end{aligned} \quad (6-8)$$

6.2.5 Matching

Because X_L is typically 20-200 Ω , R_s is less than 1 Ω , and R_p is greater than 2000 Ω [Doty, 1996a]. For efficient coupling, the resonant circuit, transmission lines, pre-amplifier, and transmitter must all be matched to approximately the same impedance, although mismatches of up to a factor of two are often not important. The international standard for impedance is 50 Ω .

There are several methods of impedance matching, three of them are briefly introduced in the following:

- shunt inductor impedance matching method

As shown in fig6-5, the inductive matching technique has the advantage of not requiring a second high-voltage capacitor. However, due to the difficulty of adjusting very small inductor the matching range is limited. The required shunt inductor (for $R_p \gg Z_0$) is:

$$L_M = L_T \sqrt{Z_0 / R_p} \quad (6-9)$$

where L_T is the total inductance ($L_S + L_M + \text{leads}$) and Z_0 is the transmission line characteristic impedance - normally 50 Ω . The resonant frequency is decided by L_T and C .

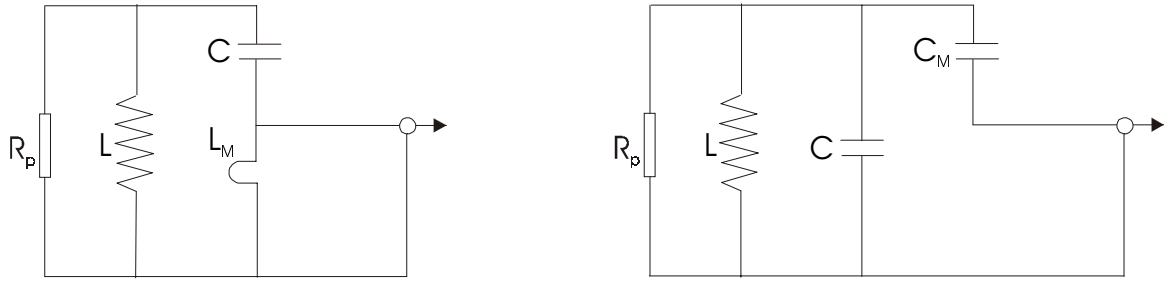


Figure 6-5: (left)shunt inductive impedance matching circuit; (right) series capacitive impedance matching circuit (adapted from Doty, 1994).

- series capacitor impedance matching

As high voltage capacitors are now readily available, capacitive matching circuit as shown in fig6-5 is popularly used. The required match capacitance (again, for $R_p \gg Z_0$) is given as:

$$X_{CM} = \sqrt{R_p Z_0} \quad (6-10)$$

- parallel capacitor impedance matching

The series resonant circuit is most often used in NMR with the addition of a capacitor in parallel for impedance matching as shown in fig6-6. If $C' \gg C$ the resonance condition remains close to $\omega^2 LC = 1$ and the impedance at resonance is $Q\omega LC^2 / (C + C')^2$. Take an example of Lamor frequency at 100MHz, if $r = 0.1\Omega$, the $C' \approx 0.005 \mu\text{F}$ for the coil to be matched to 50Ω impedance. The resonance condition should be fulfilled with the largest possible L and the smallest C to achieve the highest Q and also maintain the condition $C' \gg C$ at the same time.

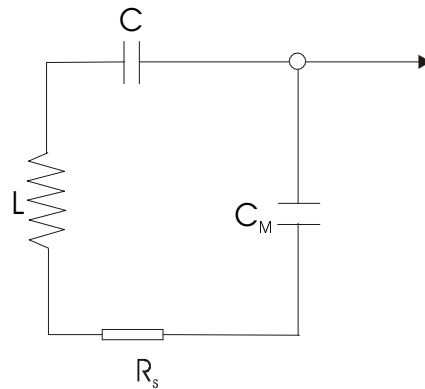


Figure 6-6: Parallel capacitive impedance matching circuit (adapted from Fukushima and Roeder, 1998).

6.2.6 Double resonance circuit

Two saddle coils, rotated 90° about the \mathbf{B}_0 axis provide a convenient method of doing double resonance NMR with good isolation. However, with this design only the inner coil can have the optimum filling factor, and sometimes it is required to have the same spatial

distribution of the two rf fields B_1 and B_2 . Also, triple- or quadruple-resonance NMR experiments are often required. Therefore it is often desirable to double-tune or triple-tune a single sample coil [Doty, 1996a].

Fig6-7 shows an example DT RF circuit which is used in Doty's NMR goniometer probe. Where, the 73nH coil is the sample coil. The 1.2PF capacitor is used to bring the resonance frequency down to the desired range. 27PF capacitor together with the second sample coil 6nH form the series 'frequency trap' for HF, that is to bypass all the HF leakage which passes through the sample coil and prevent it to reach the observe detector. Some people like to use series frequency trap, while others like to use parallel frequency trap. With respect to prevent the HF leakage, they have the same function. However, they may produce different effects on tuning and matching conditions of the LF side.

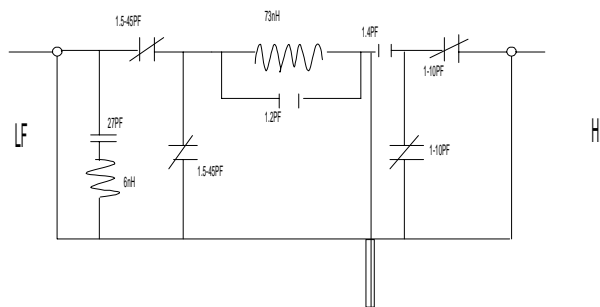


Figure 6-7: Double resonance circuit used in Doty's goniometer probe.

Another DT RF circuit example which is shown in fig6-8 is the circuit used in the NMR group of Uni. Jena. Where, two unique features are:

- Variable inductor: In Jena's design, variable inductors are used to replace variable capacitors. Comparing with variable capacitors, variable inductors have the advantages of (i)higher voltage tolerance (ii)easily adjustable in a bigger range (iii)cheaper (home made).
- a "Rod-Ring" capacitor: To give a reference ground for the HF de-coupling power, at the immediate end of the sample coil in LF side, a very small capacitor (home made and called "Rod-Ring") is added. The typical capacitance value for this capacitor is around 1 PF. It provides low impedance (good grounding) for the HF frequency.

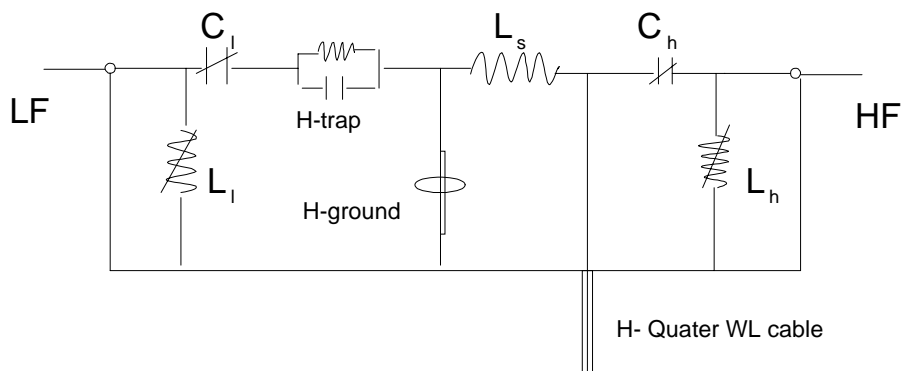
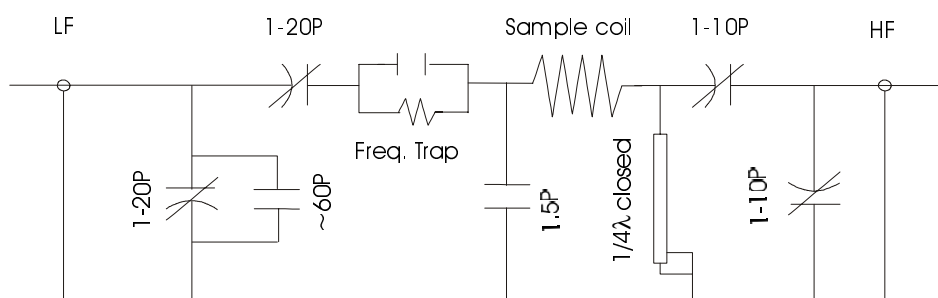


Figure 6-8: Double resonance circuit used in the NMR group of Uni. Jena.

6.3 RF design in VACSY probe

The RF circuit used in our VACSY probe is drawn in fig6-10, it is a single sample coil, double resonance circuit with parallel matching capacitors at both HF and LF sides.



RF circuit schema of VACSY probe

Figure 6-9: Double resonance circuit used in our VACSY probe.

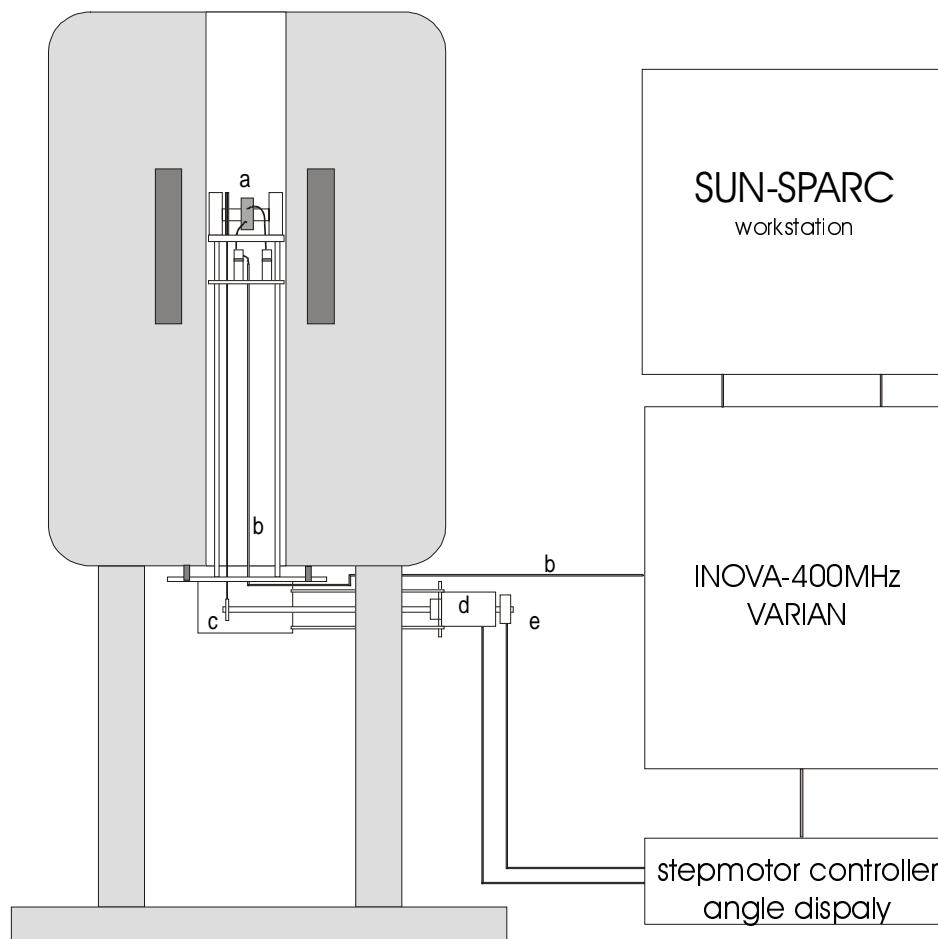
The sample coil is 4 turns and 5mm in diameter made by Doty. At high frequency (HF) side, two 1-10P variable capacitors are used for tuning and matching respectively. The $1/4$ wave length (λ) cable for 400MHz is effective to a infinite impedance for HF part. The 1.5P capacitor provides the grounding for HF part. At low frequency (LF) side, the $\lambda/4$ cable serves as the grounding for LF part. The parallel frequency trap generate the necessary isolation between LF and HF. The parallel combination of a 1-20P variable capacitor and a constant 60P capacitor is the matching capacitor which transforms the impedance to 50Ω .

From the theory of radio frequency engineering, the values of capacitors in the resonant circuit could be accurately calculated. For the purpose of NMR RF circuit, the capacitors are

normally in the range of 1~100PF, inductance in the range of 1~200nH. However, the parasitic distributive capacitance and inductance existed between different components are in the same range, and they are dependent on many practical factors such as circuit layout, connection wires and etc. In most cases, these distributive parameters are not possible to be accurately calculated except some approximate estimations. So, in general the resonant condition is hardly possible to be accurately calculated. The effective way to find out the correct capacitance and inductance values is a procedure of repeatedly ‘try and error’.

VACSYS experiment needs a special probe to be performed. A VACSYS probe adds the ability of accurate control over the angle between sample spinning axis and external magnetic field direction \mathbf{B}_0 to an ordinary double tune CPMAS probe. The general diagram of a VACSYS experiment set-up is shown in fig6-9.

instrumental setup of a VACSYS experiment



- a: Doty rotor
- b: RF- double resonance circuit
- c: pulley - string
- d: stepmotor
- e: angle encoder/display

Figure 6-10: Diagram of the overall VACSY experimental set-up.

6.4 VACSY RF circuit optimisation

During the optimisation of our VACSY RF circuit, much attention has been paid to the following things:

- Arrangement of the circuit components. A good RF circuit layout can minimise the distributive capacitance and inductance, as well as minimise noise and unwanted resonant peaks. There is no universal rule for how a good RF circuit layout should be, but experience proves that: a good RF circuit layout is the one which has fewer wire connections between individual components and fewer inner loops.
- Connection points and connection wires. For all solid NMR probes, good sensitivity (S/N - signal to noise ratio) is highly desirable, while poor S/N normally means longer experimental time or simply make some experiments not feasible. Many factors influence the S/N of a final NMR probe, such as Q values of components used (capacitors and inductors), soldering junctions, connection wires used and etc. Today, the Q values of components higher than 200 are commercially available. From our experience, the crucial connections in the circuit should use 2mm in diameter silver coated copper wire; the soldering should be performed with extreme care for a nice round shape by using soldering material with highest conductivity.
- Arching problem. The electrical theory tells us that arching most possibly happens when the gap between the positive electrode and the negative electrode (ground) is too small. To prevent arching or to remove arching: firstly, the components on the PCB should be arranged to have as large a spacing as possible, especially between different capacitors. Secondly, when arching exists in the circuit, experience proves that: wrapping the suspicious components using Teflon tape is quite successful to remove arching in some NMR probes. Thirdly, when arching is caused by a defected component and very strong, it can be located easily by direct vision: Take out the probe from the magnet, remove cover, perform tuning and matching as normal, then apply normal NMR de-coupling pulse sequence. In a dark room, if arching is strong ‘flashing’ near that point should be seen by eye.

6.5 Angle control

As described in *chapter 5*, in VACSY accurate control of the angle between the sample spinning axis and the external magnetic field direction \mathbf{B}_0 is very important. VACSY simulation

spectra tell us that: if the control accuracy is worse than 0.5° , there are serious distortions of the CSA line-shape. The instrumental set-up for realising accurate angle control is shown in fig6-11 and fig6-12.

The movement of the sample housing is generated by a stepmotor from Oriental Motor Co., Ltd, which has a accuracy of $0.9^\circ/8$ per step. Because both the main magnet and the stepmotor are magnetic, care has to be taken to prevent the interference on stepmotor from main magnet by putting the stepmotor at a position far enough away from the magnet, either vertically or horizontally. In our case, the stepmotor is put about 25cm away horizontally. The probe body and the stepmotor form an integrated device, therefore it is not necessary to re-align the mechanical connection for every experiment.

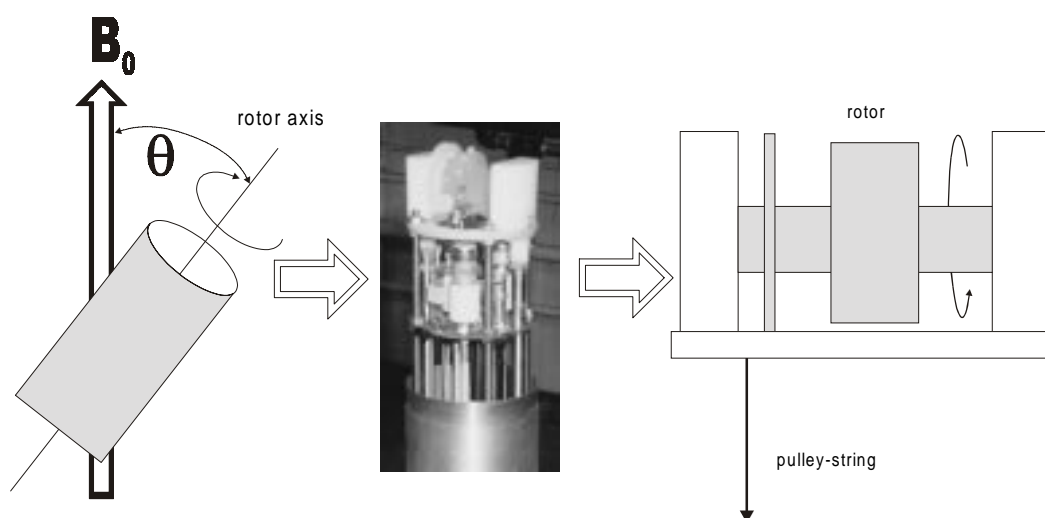


Figure 6-11: The control of angle β between rotation axis and external magnetic field \mathbf{B}_0 direction in a VACSYS probe.

The stepmotor is then connected to a pulley. The lower wheel of the pulley is fixed to the stepmotor axis, the upper wheel is fixed to the sample housing, a string connects the two wheels. This device allows the angle of the sample housing with respect to \mathbf{B}_0 to be changed in a range of 0° - 90° . The exact angle of the sample housing is monitored by an angle encoder attached at the end of the stepmotor, the angle encoder is from HENGSTLER of type 'signo 727 SSI' which has a resolution of better than $360^\circ/4096$. The HEMGSTLER angle encoder is an absolute encoder which can remember the current angle even when the power is shut down. As long as the mechanical connection between stepmotor and angle encoder is not lost, the encoder always gives the correct value for the current angle. This is of much practical convenience for us. Because of the using of an absolute angle encoder, in principle, it is not necessary to calibrate the angle before every experiment. In practice, the angle is regularly calibrated using enriched (COO^-) Glycine.

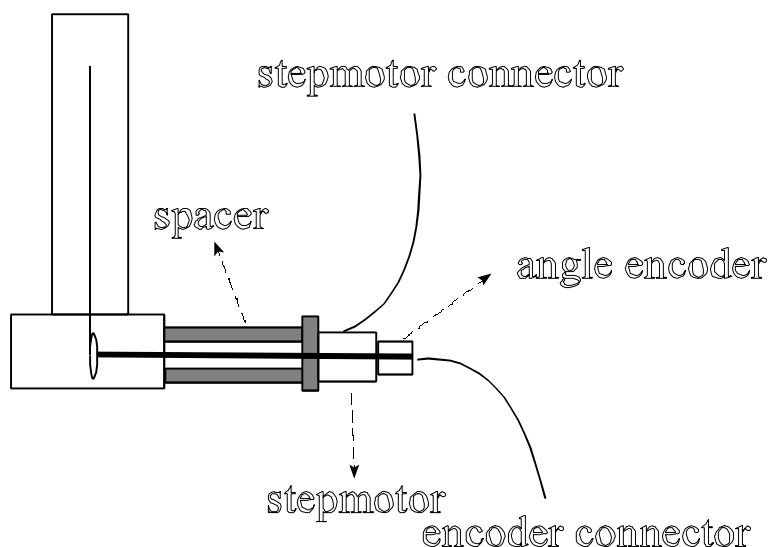


Figure 6-12: General diagram of a VACSYS probe with stepmotor and angle-encoder.

The final angle control accuracy is decided by several factors, to improve the accuracy the following steps have been undertaken:

- check the location of the stepmotor to make sure that there is no interference of the main magnet on the stepmotor.
- the tension of the connection string is carefully adjusted by a very sensitive optical method. When the tension is too high, there occurs slippery and some stepmotor steps would be missed. On the other hand, when the tension is too low, due to the problem of backlash a number of starting steps will generate no motion of the sample housing .
- minimise friction between different parts in the sample housing by replacing direct contact bearing with micro glass ball bearing form MMB Bearing Co.

The final angle control accuracy is estimated to be better than 0.25° by comparing the results of line width measurements of enriched (COO^-) Glycine using VACSYS probe and VARIAN 7mm MAS probe. Other basic specifications of my VACSYS probe are: ^1H channel tuning range 390 MHz - 460 MHz, ^{13}C channel tuning range 97.5 MHz - 110M Hz; ^1H $\pi/2$ pulse with a RF output power of 360 Watt is $2.5 \mu\text{s}$ (100 kHz), ^{13}C $\pi/2$ pulse with a RF output power of 61 Watt is $4.0 \mu\text{s}$ (63kHz); Angle of rotation axis can be changed from 0° - 90° , angle control accuracy is less than 0.25° (estimated from experiment performance).

EXPERIMENTAL RESULTS AND DISCUSSION

7.1 Introduction

All following experiments are carried out on a VARIAN 400 MHz INOVA spectrometer with 1KW linear high powder amplifier for solid-state applications. The VACSYS probe is a self built double resonance probe. It uses a standard Doty 5 mm sample spinning module, the maximum spinning speed can reach about 7.0 kHz. The change of the angle between the sample spinning axis and the external magnetic field is realised through a stepmotor and pulley-string mechanism. The accuracy of angle control is estimated at 0.25 degree. All VACSYS experimental data are interpolated to $n_i=250$ steps in the indirect direction by using Frydman's normal interpolation procedure and then transformed by VNMR's FFT software to get the final spectra.

7.2 VACSYS to measure chemical shift tensor elements

VACSYS is a promising method to correlate the chemical shift anisotropies with their corresponding chemical shift isotropic values. So, one of the basic applications of VACSYS would be to measure the values of chemical shift tensor elements, for example the values of ^{13}C chemical shift tensor elements. If the sample has only one in-equivalent ^{13}C nuclei, the values of chemical shift tensor elements can be easily measured by a simple static dipolar decoupling(DD) cross-polarisation(CP) experiment. Another popular method for measuring values of chemical shift tensor elements is to carry out a CPMAS experiment with dipolar decoupling, when the sample spinning speed is smaller than the anisotropic value of the chemical shift tensor, a series of spinning sidebands will appear. From the relative intensities of these spinning sidebands with respect to the central band, the values of chemical shift tensor elements can be obtained by applying the Herzfeld-Berger procedure. However, if there are more than one in-equivalent ^{13}C nucleus in the sample and their chemical shift anisotropies overlap each other, both methods become inadequate. In these cases, alternatives which can separate lines according to their isotropic chemical shift values and correlate each with their corresponding chemical shift anisotropies must be selected.

7.2.1 1D VAS experiment to measure CS tensor elements of glycine

The first alternative is 1D VAS experiment: the sample is spinning at an off-magic angle position and the spinning speed is larger than the biggest chemical shift anisotropic value of all spectral lines, FID data acquisition is carried out under CP and DD. From *chapter 3* we know,

when the sample is in fast spinning at an off-magic angle position the chemical shift anisotropic value is scaled down according to the second Legendre polynomial of the angle θ between rotation axis and the external magnetic field direction:

$$\omega(\theta) = -\gamma B_0 \left[\sigma_i + \frac{1}{2} \sigma_a (3 \cos^2 \theta - 1) \right] \quad (7-1)$$

The measured chemical shift anisotropic value σ'_a and the theoretical chemical shift anisotropic value σ_a is related by the following equation:

$$\sigma_a = \sigma'_a / \left(\frac{1}{2} (3 \cos^2 \theta - 1) \right) \quad (7-2)$$

An example is given in fig7-1 of enriched (COO⁻) glycine measured at angle equal to 80.26° for the spinning axis relative to the external magnetic field direction. The scaled anisotropic chemical shift value measured at 80.26° is $\sigma'_a = 65.5$ ppm, the calculated full anisotropic chemical shift value is $\sigma_a = 143.3$ ppm. In fig7-1 there is an apparent deviation from the theoretical CSA line-shape, this is due to an insufficient sample spinning speed and two weak spinning sidebands are also visible at each side of the centre band in fig7-1.

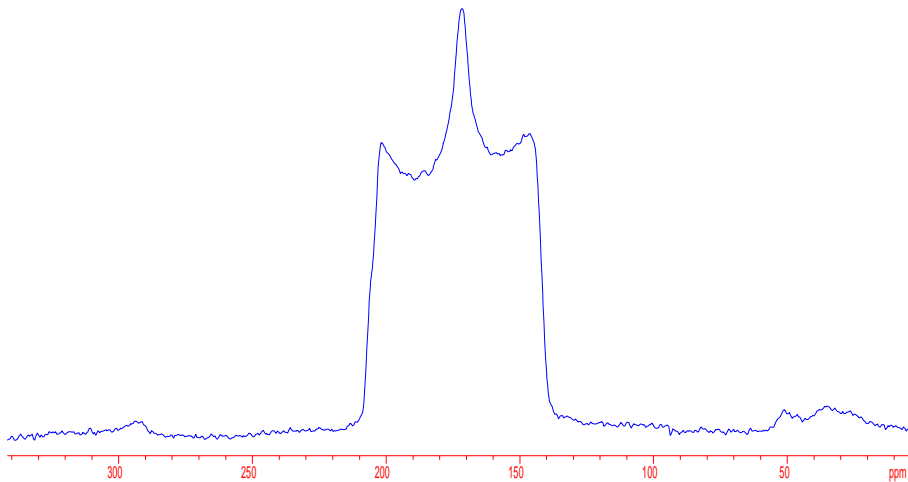


Figure 7-1: VAS ¹³C (100 MHz) NMR spectrum of enriched (COO⁻) Glycine, measured at an angle $\beta=80.26^\circ$ between the sample rotation axis and \mathbf{B}_0 direction, spinning speed used is 6.0 kHz.

Because the angle between sample rotation axis and \mathbf{B}_0 field direction is controlled better than 0.25 degree, we have reasons to believe that this method is more reliable than the normally applied Herzfeld-Berg method. However, VAS 1D method can only partially relieve the overlapping problem due to the scaling of chemical shift anisotropy at off-magic -angle position. In most practical cases, overlapping from lines with slightly different isotropic values still restrain this procedure to be successfully applied to more complicated polymer samples.

7.2.2 VACSY experiment to measure CS tensor of HMB and DMS

The second alternative for measuring the values of chemical shift tensor elements is a complete VACSY experiment. In the 2D VACSY spectrum, the projection along the isotropic dimension gives a high resolution CPMAS spectrum, all lines are separated according to their individual isotropic chemical shift values; their chemical shift anisotropic patterns are given in the projections from the slices along the anisotropic dimension. An example of VACSY used to measure values of chemical shift tensor elements in enriched Glycine is demonstrated in fig7-2

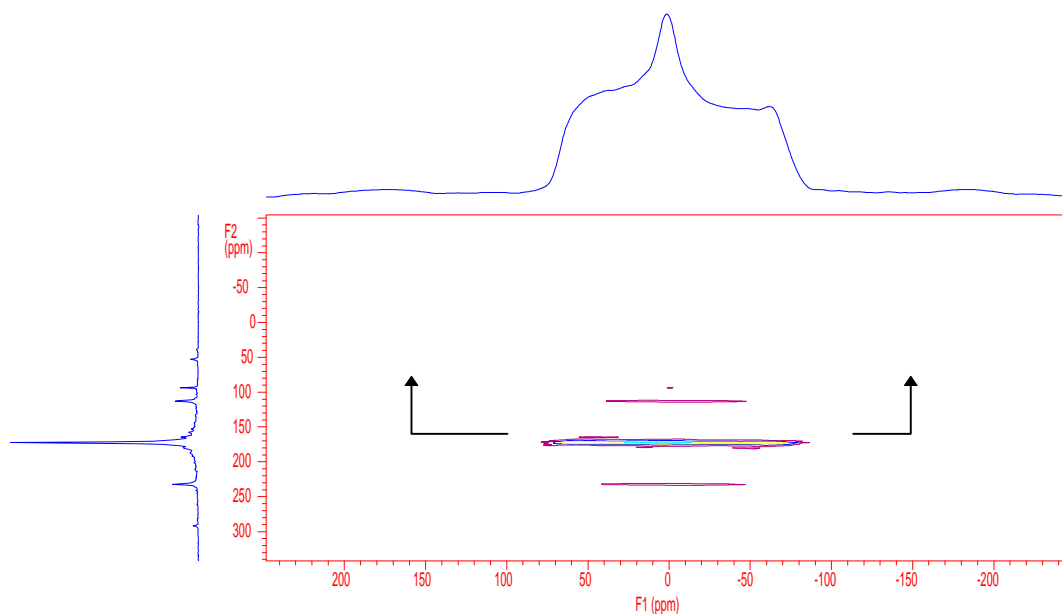


Figure 7-2: VACSY ^{13}C (100 MHz) NMR spectrum of enriched (COO^-) glycine, data acquired for angle β sampling angle of 35° - 90° in 120 steps, sample spinning speed is 6.0 kHz.

Because the ^{13}C nuclei of carbonyl group has a very large chemical shift anisotropy, the spinning speed used to acquire the corresponding VACSY spectrum is 6.0 kHz (still smaller than the anisotropic chemical shift value), so the spectrum of the sky-line projection along the isotropic dimension includes the isotropic line and two higher order spinning sidebands. The spectrum along the anisotropic dimension is the sky-line projection of the central spinning sideband. The anisotropic chemical shift value is directly measured from the singularities of this projection spectrum: 145.0 ppm. This result agrees very well with the result obtained from 1D VAS measurement. The 3D plot of the above analysed glycine VACSY spectrum is given in fig7-3, it demonstrates more clearly the correlation of chemical shift isotropy and anisotropy.

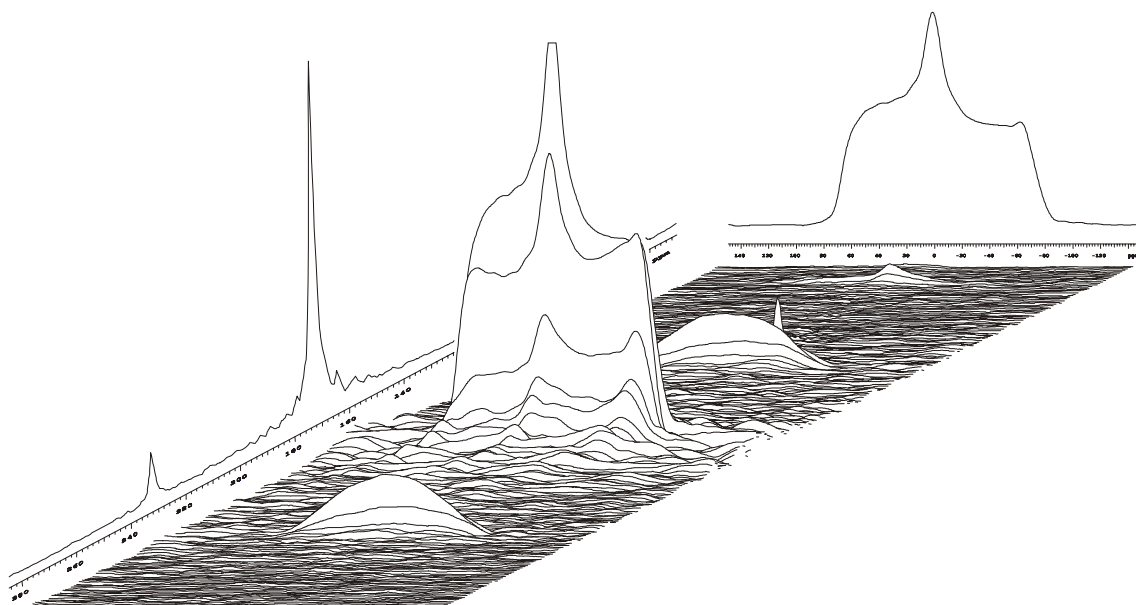


Figure 7-3: 3D plot with projections of the VACSY ^{13}C spectrum in figure 7-2. The (sky-line) projection onto the anisotropic axis is from the slice at central spinning band (isotropic chemical shift position). The (sky-line) projection onto the isotropic axis is the same as 1D CPMAS spectrum.

Two more measurement examples are given for HMB in fig7-4 and DMS in fig7-5. The measurement result of anisotropic chemical shift value of HMB is: 161.2 ppm. The spin rate used to get this VACSY spectrum is 3.9 kHz and is much smaller than the chemical shift anisotropic value of the aromatic carbons in HMB. So, the line-shape of the central spinning sideband is strongly distorted and two higher order spinning sidebands appear in the spectrum at each side of the centre band. For the methyl carbons, due to its strong intensity and the smaller chemical shift anisotropic value, serious artefacts show up as explained in section 4.3.2.

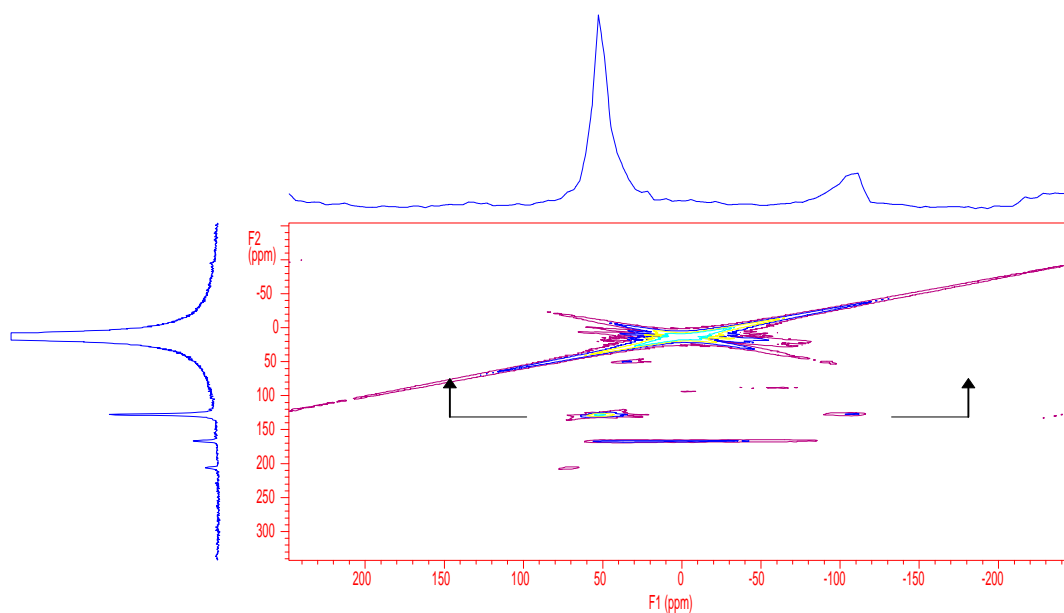


Figure 7-4: VACSY ^{13}C (100 MHz) NMR spectrum of Hexamethyl Benzene (HMB), data acquired for angle β sampling range of 38° - 80° in 180 steps, sample spinning speed is 3900 Hz.

The measurement result of the chemical shift anisotropy of DMS is 52.5 ppm, the spin rate used is 3.9 kHz and it is comparable with DMS's chemical shift anisotropic value. So, only a very weak spinning sideband is visible here. Due to thermal motions with a rate comparable with ^{13}C NMR frequency present in DMS sample around room temperature, this VACSY experiment is carried out at a temperature below 0°C with the help of a special cooling device. Otherwise, there is very strong spectral rounding at the two singularity frequency positions.

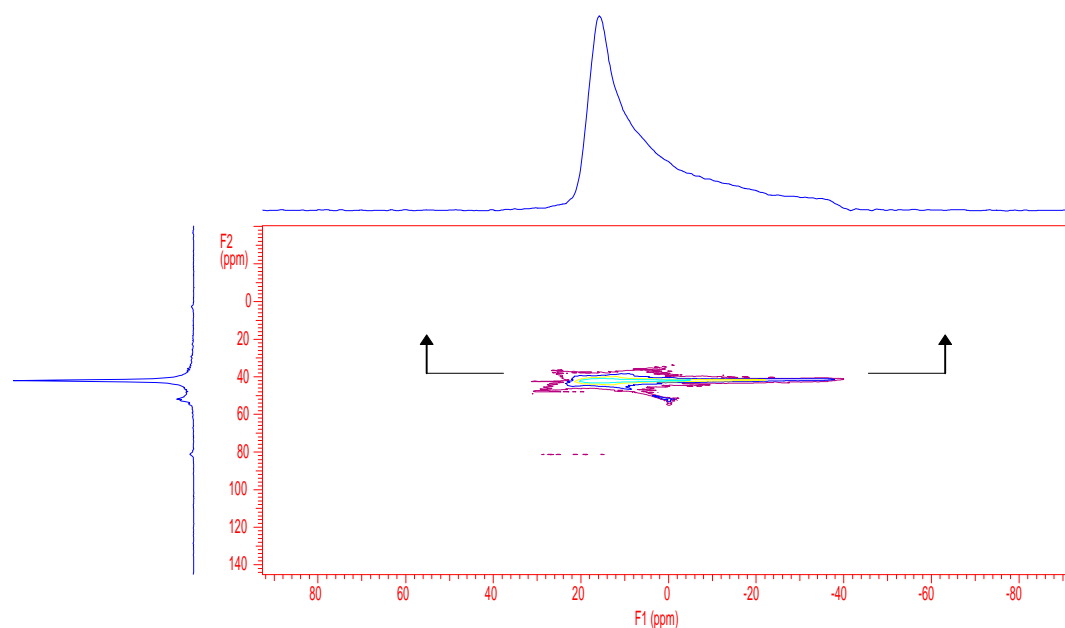


Figure 7-5: VACSY ^{13}C (100 MHz) NMR spectrum of dimethylsulfon (DMS), data acquired for angle β sampling range of 27° - 81° in 240 steps, sample spinning speed is 3900 Hz.

7.2.3 VACSY experiment to measure CS tensors of Durene

All three above measured samples: glycine, HMB and DMS are relatively simple substances from the NMR point of view. They have only one resonant line in the aromatic region, the overlapping problem does not exist. In these cases, 1D NMR methods such as static, CPMAS and VAS are enough to measure the values of chemical shift tensor elements. However, if two or more resonant lines have very close isotropic chemical shift values their anisotropic chemical shift patterns will overlap each other, then all 1D methods become not adequate. In these cases, special designed 2D correlation methods such as VACSY have to be applied. An example of VACSY used to measure the chemical shift tensor elements of two very closely located resonant lines in Durene is shown in fig7-6. The experiment is performed with a spinning speed of 3.5 kHz, the angle between the spinning axis and the external magnetic field is sampled in a range of 35° - 90° with 120 steps. Four spinning sidebands for each isotropic line show up due to the apparently not sufficient spinning speed comparing with their anisotropic chemical shift values.

From the chemical structure of Durene we know that there are two inequivalent carbons within the phenyl ring, one has a CH₃ group as attachment, another simply has a ¹H as attachment. This slight structure difference shows up in their corresponding chemical shift isotropic and anisotropic values. The measurement results of VACSYS are: the first line has an isotropic chemical shift of 130.4 ppm, chemical shift anisotropy is: 206.8 ppm; the second line has an isotropic chemical shift of 127.1 ppm, chemical shift anisotropy is 164.2 ppm. This example demonstrates very well the power of VACSYS as a method to separate closely spaced lines and to correlate them with their corresponding chemical shift anisotropic patterns at the same time. The ¹³C in the methyl group has a isotropic chemical shift of 15.3 ppm in the aliphatic region, its chemical shift anisotropy value is about 34 ppm with a axial-symmetric line-shape.

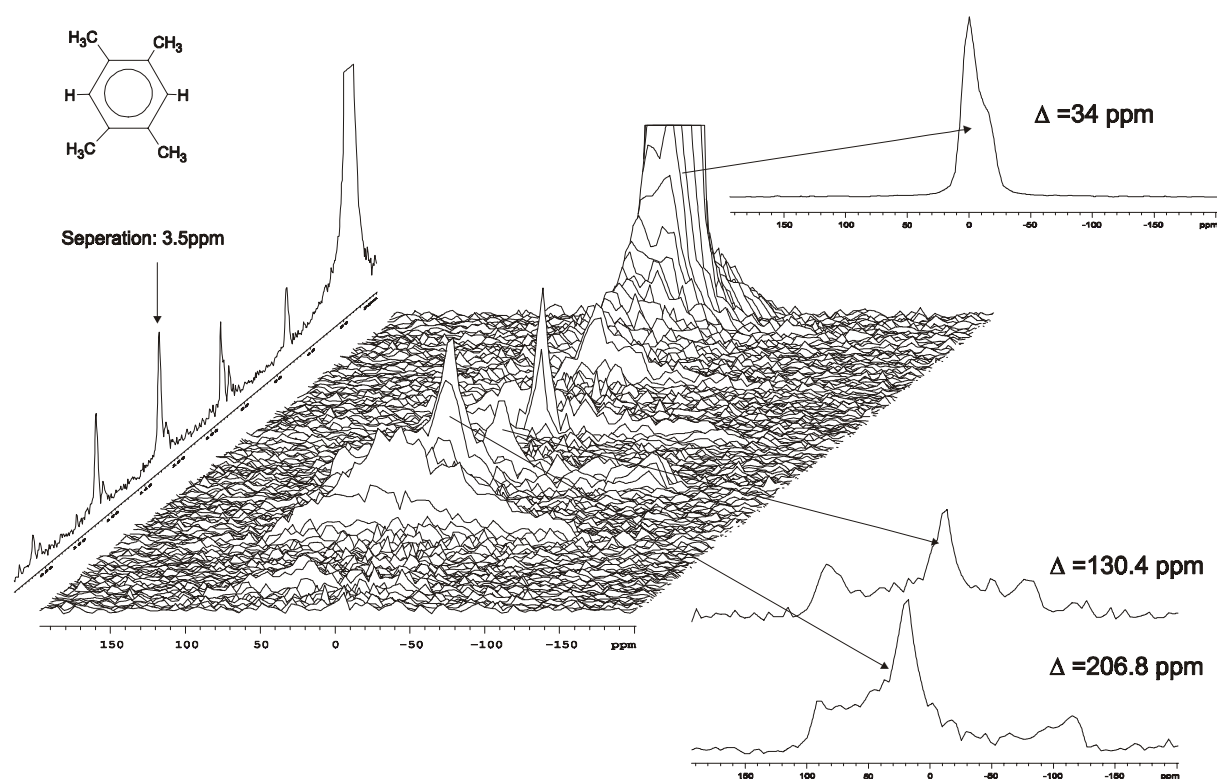


Figure 7-6: 3D plot of VACSYS ¹³C (100 MHz) NMR spectrum of Durene, data acquired for angle β sampling range of 35°-90° in 120 steps, sample spinning speed is 3500 Hz, total experimental time is 17 hours.

7.3 Liquid Crystal phase and polymer Liquid Crystal materials

7.3.1 Liquid Crystal phase

Liquid crystal phase is a special phase of materials which was discovered by an Austrian botanist Friedrich Reinitzer. The distinguishing characteristic of the liquid crystalline state is the tendency of the molecules (mesogens) to point along a common axis, called the director. This is in contrast to molecules in the liquid phase, which have no intrinsic order. In the

crystalline(solid) state, molecules are highly ordered and have little translational freedom. The characteristic orientational order of the liquid crystal state is between the traditional crystalline and liquid phases and this is the origin of the term mesogenic state, used synonymously with liquid crystal state. Note the average alignment of the molecules for each phase in the following diagram fig7-7.

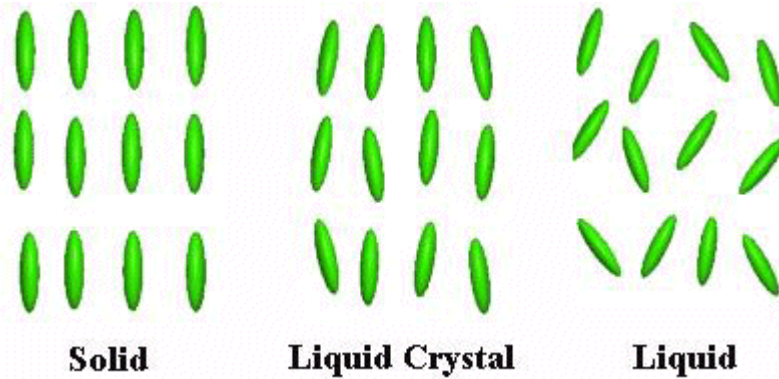


Figure 7-7: Average alignment of molecules in solid phase (left), liquid crystalline mesophase (middle) and in isotropic liquid phase (right).

It is sometimes difficult to determine whether a material is in a crystal or liquid crystal state. Crystalline materials demonstrate long range periodic order in three dimensions. By definition, an isotropic liquid has no orientational order. Substances that are not as ordered as a solid, yet have some degree of alignment and have a limited viscosity are properly called liquid crystals. To quantify just how much order is present in a material, an order parameter (S) is defined. Traditionally, the order parameter is given as follows in fig7-8:

$$S = \frac{1}{2} \langle 3 \cos^2 \theta - 1 \rangle$$

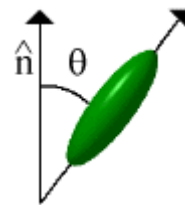


Figure 7-8: Definition of order parameter to describe the average alignment of molecules.

where theta is the angle between the director and the long axis of each molecule. The brackets denote an average over all of the molecules in the sample. In an isotropic liquid, the average of the cosine terms is $1/3$, and therefore the order parameter is equal to zero. For a perfect crystal, the order parameter evaluates to one. Typical values for the order parameter of a liquid crystal range between 0.3 and 0.9, with the exact value is a function of temperature, as a result of kinetic molecular motion.

The liquid crystal state is a distinct phase of matter observed between the crystalline and isotropic (liquid) states. There are many types of liquid crystal states, depending upon the

amount of order in the material. Two of them are most often observed: nematic phase and smectic phase:

- Nematic Phases

The nematic liquid crystal phase is characterised by molecules that have no positional order but tend to point in the same direction (along the director). In the following diagram fig7-9, notice that the molecules point vertically but are arranged with no particular order.

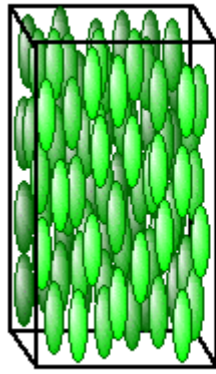


Figure 7-9: Liquid crystalline nematic phase.

Liquid crystals are anisotropic materials, and the physical properties of the system vary with the average alignment with the director. If the alignment is large, the material is very anisotropic. Similarly, if the alignment is small, the material is almost isotropic.

- Smectic Phases

The smectic state is another distinct mesophase of liquid crystal substances. Molecules in this phase show a degree of translational order not present in the nematic. In the smectic state, the molecules maintain the general orientational order of nematics, but also tend to align themselves in layers or planes. Motion is restricted to within these planes and separate planes are observed to flow past each other. The increased order means that the smectic state is more "solid-like" than the nematic. This is shown in fig7-10.

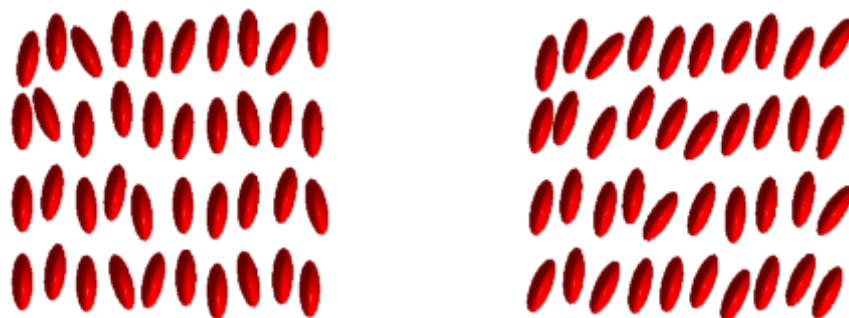


Figure 7-10: Liquid crystalline smectic phase. (left) smectic A phase; (right) smectic C phase.

7.3.2 Polymer Liquid Crystal materials

Polymer liquid crystals (PLCs) are a class of materials that combine the properties of polymers with those of liquid crystals. These "hybrids" show the same mesophases characteristic of ordinary liquid crystals, yet retain many of the useful and versatile properties of polymers.

In order for normally flexible polymers to display liquid crystal characteristics, rod-like or disk-like elements (called mesogens) must be incorporated into their chains. The placement of the mesogens plays a large role in determining the type of PLC that is formed. Main-chain polymer liquid crystals or MC-PLCs are formed when the mesogens are themselves part of the main chain of a polymer. Conversely, side chain polymer liquid crystals or SC-PLCs are formed when the mesogens are connected as side chains to the polymer by a flexible "bridge" (called the spacer.) as shown in fig7-11

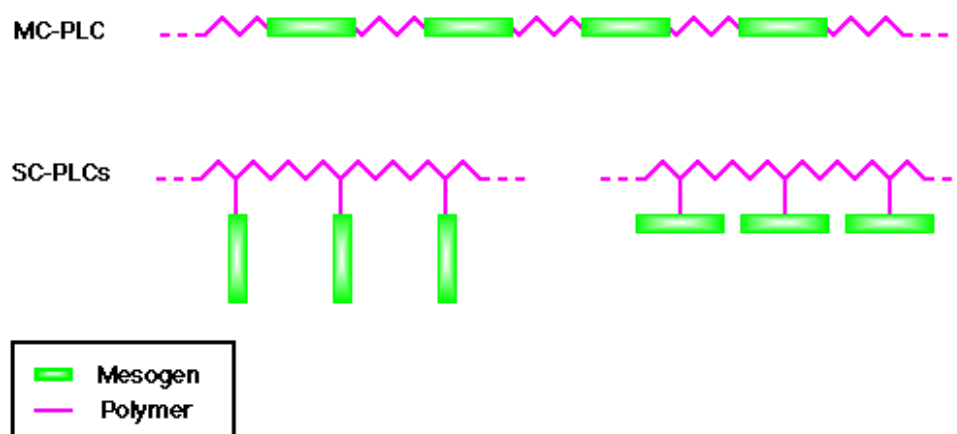
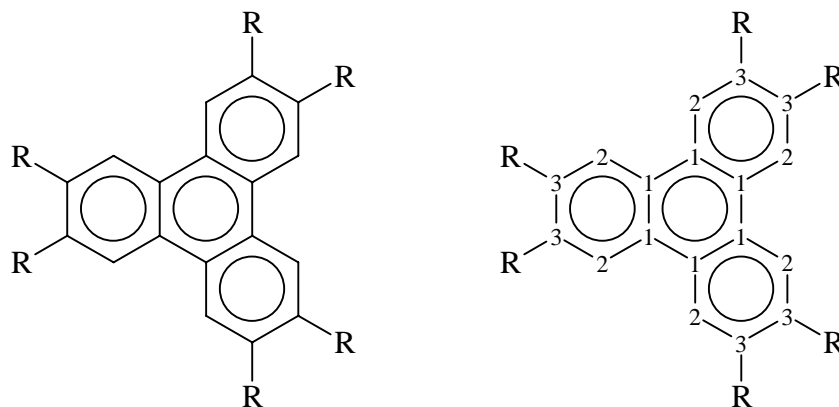


Figure 7-11: Two common polymer liquid crystalline material: main-chain polymer liquid crystal and side-chain polymer liquid crystal.

7.4 VACSYS to study orientation distribution of PLC sample - hexa-hydroxytriphenylene

The existence of a new type of liquid crystalline phase in compounds composed of disc-like molecules was reported by Chandrasekhar et al. In 1977 [Chandrasekhar, 1997] and Billard et al. in 1978 [Billard, 1978]. They observed liquid crystalline mesophases on derivatives of triphenylene. In their work, the discotic phase of p-n-hexa-hydroxytriphenylene, $R=OC_6H_{13}$, as illustrated in fig7-12 is studied, its phase diagram is also given here:





Figures 7-12: (top) phase diagram of p-n-hexa-hexyloxytriphenylene; (bottom) Chemical formula of p-n-hexa-hexyloxytriphenylene, R=OC₆H₁₃.

here Isotropic stands for isotropic liquid and Discotic stands for discotic mesophases. The ¹³C 1D CPMAS spectrum is shown in fig 7-13, the spinning speed used here is 6.0 kHz. There are three ¹³C lines in the aromatic region which have isotropic chemical shifts values: 143.7ppm, 117.9ppm, 99.1ppm respectively and a number of ¹³C lines in the aliphatic region which are not well resolved. The assignment result of some resonant lines is given in fig7-13. The assignment is achieved through a comparison of two CPMAS experiments with 4.2 kHz and 6.1 kHz spinning speed receptively. In fig7-13 letters with stars, a*, b*, c*, denote their corresponding spinning sidebands of resonate lines a, b, c.

a (1/2/3) - 143.7ppm

d (-O-C- in R) - 62.8ppm

b (1/2/3) - 117.9ppm

e (-CH₃ in R) - 10.3ppm

c (1/2/3) - 99.1ppm

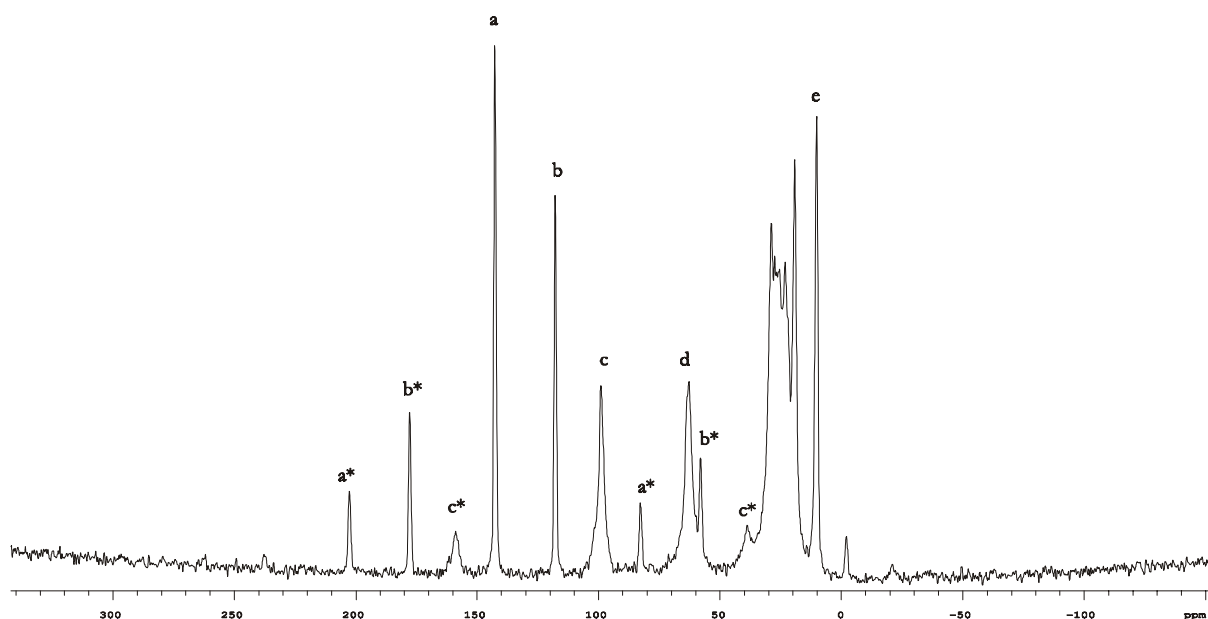


Figure 7-13: CPMAS ^{13}C (100 MHz) NMR spectrum of p-n-hexa-hexyloxytriphenylene sample in isotropic powder state, sample spinning speed used is 6.0 kHz.

In the following orientation distribution study, we focus on the ^{13}C line with the isotropic chemical shift of 143.7ppm which has the biggest spectral intensity. The procedure for creating certain orientation distribution in sample p-n-hexa-hexyloxytriphenylene is that: (i) insert the rotor with sample into the main magnet of our VARIAN INOVA 400 MHz spectrometer (9.4T), the rotor axis direction is set parallel to the magnetic field direction. (ii) heat the sample up to 10°C over its clearing temperature T_c and wait for about 20 minutes for equilibrium. (iii) at a temperature rate of 1K/min, slowly cool down the sample till below the phase transition temperature from liquid crystalline mesophase to solid phase. NMR measurements for the oriented samples are carried out at room temperature. Two VACSYS experiments are conducted, one for the sample in isotropic powder state, another for the sample in oriented state, the corresponding 2D spectra with skyline projections from the indicated slices are shown in fig 7-14. The VACSYS experiments are conducted with 5.0 kHz spinning speed, in a angle range of $35^\circ - 90^\circ$ with 60 steps. The final VACSYS spectra are obtained by firstly interpolating the experimental data to 256 points in the anisotropic dimension by using Frydman's normal interpolation procedure and then normal 2D FT.

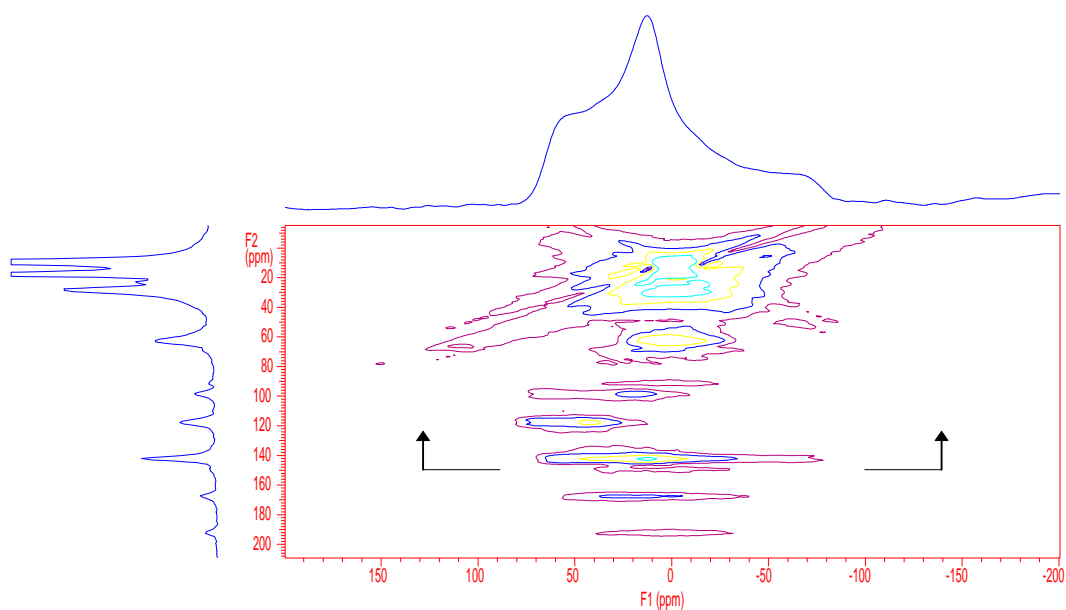


Figure 7-14a: VACSYS ^{13}C (100 MHz) NMR spectrum of p-n-hexa-hexyloxytriphenylene sample in isotropic powder state, data is acquired for angle β sampling range of $35^\circ - 90^\circ$ in 60 steps, sample spinning speed used is 5.0 kHz

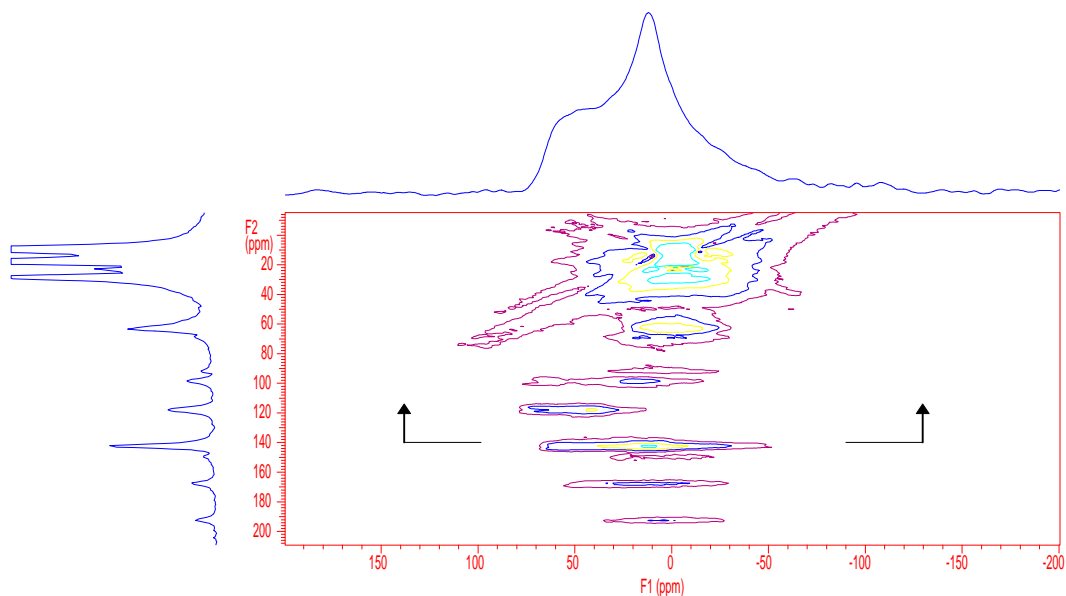


Figure 7-14b: VACSY ^{13}C (100 MHz) NMR spectrum of p-n-hexa-hexyloxytriphenylene sample in oriented state with the orientation procedure described in the text, data is acquired for angle β sampling range of 35° - 90° in 60 steps, sample spinning speed used is 5.0 kHz

From the known magnetic susceptibility tensor of the aromatic rings it is expected that the mesophase molecules prefer an orientation in which the molecular rigid planes lie parallel to the magnetic field, and the director perpendicular to it. Since all perpendicular orientations are equally probable, it is reasonable to assume that the discotic phase is broken up into many domains with their directors normal to the external field and a random azimuthal distribution [Goldfarb, 1981] as is shown in fig7-15:

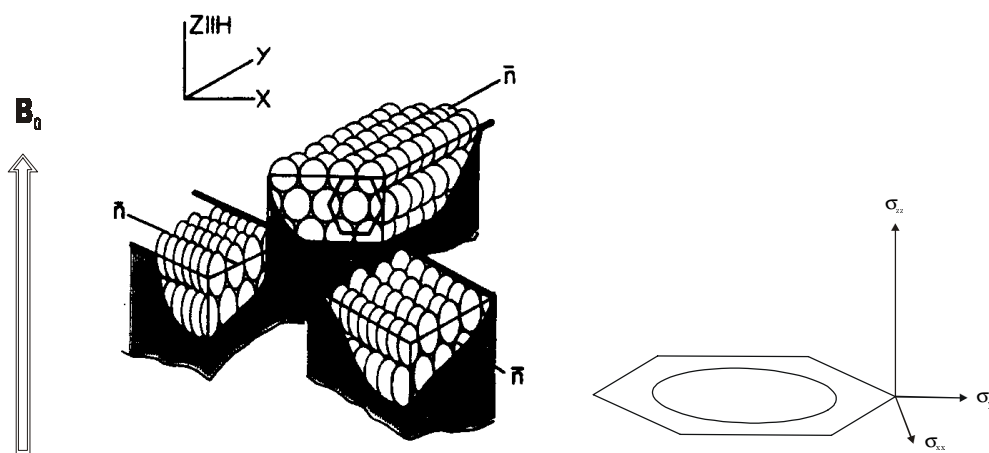


Figure 7-15: (left) Schematic diagram of the domain distribution in sample hexa-hexyloxytriphenylene by slowly cooling of the discotic mesogens in a magnetic field. The discs represent the liquid crystalline molecule and the \bar{n} is the direction of the domain. (adapted from

D. Goldfarb and Z. Luz, 1981). (right) the geometric orientation of aromatic ^{13}C chemical shift tensor relative to phenyl-ring plane

D. Goldfarb, Z. Luz and H. Zimmermann have studied the orientation behaviour of the same sample in mesophase by using ^2H NMR, the procedure which we used to create certain orientation in the sample is similar to their procedure except that they used a lower magnetic field of 6.3T. Their ^2H NMR study results show surprisingly the relative high value of order parameter S (0.90 - 0.95) and its very weak temperature dependence even close to the clearing temperature.

To evaluate the orientation distribution of p-n-hexa-hexyloxytriphenylene from VACSX spectra, the CSA line-shape simulation approach is adapted to find out the orientation distribution existed in oriented state p-n-hexa-hexyloxytriphenylene sample. The projections from slices at isotropic chemical shift position 143ppm in both isotropic state and oriented state are shown in fig7-16. For the simulation, an simple Gaussian distribution function is assumed:

$$U(\theta) = N \exp(-\sin^2(\theta - \theta_{ref}) / 2\theta^2 \sigma) \quad (7-3)$$

Here θ is the angle between the z axis of the principal value system (PAS) and the z axis of the rotor frame (RF), θ_{ref} is the centre and $1.17\theta_\sigma$ is the half width at half maximum value of the Gaussian distribution. In the particular case of p-n-hexa-hexyloxytriphenylene oriented by the above described procedure, the rigid phenyl-ring plane is parallel to the rotor's rotation axis, therefore the σ_{zz} element of the aromatic ^{13}C chemical shift tensor is in perpendicular to the rotor's rotation axis.

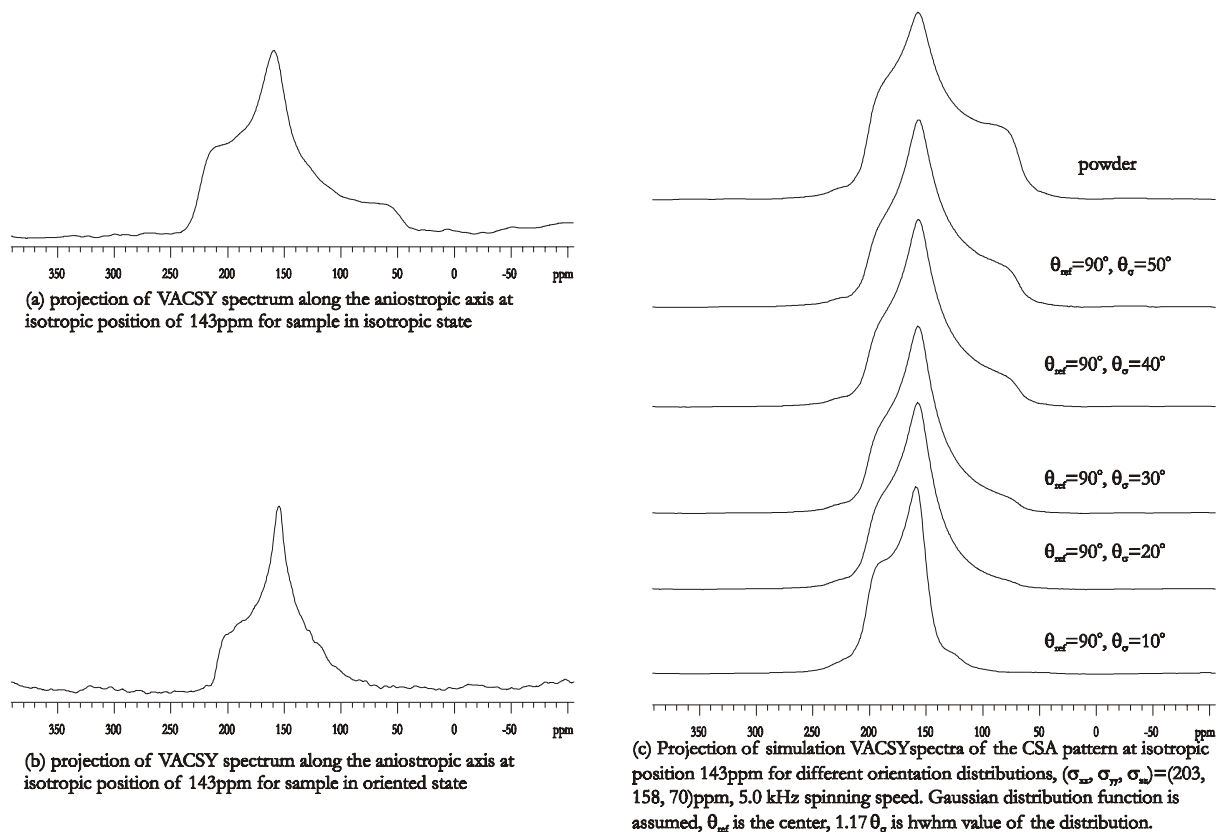


Figure 7-16: Analysis of orientation distribution in hexa-hexyloxytriphenylene by the method of line-shape fitting from VACSYS spectra of sample in isotropic state and oriented state, chemical shift tensor used for simulation is $(\sigma_{xx}, \sigma_{yy}, \sigma_{zz})=(203, 158, 70)$ (ppm) (a) projection of experimental VACSYS spectrum of sample in isotropic powder state. (b) projection of experimental VACSYS spectrum of sample in oriented state. (c) simulated CSA spectra of sample in oriented state for different orientation distributions. Comparing the spectra in (b) and in (c), the orientation distribution for the best fitting is $\theta_{ref} = 90^\circ$ and $\theta_{\sigma} \cong 20^\circ$, corresponding to an order parameter of $S=0.55\pm 0.1$.

In order to take into account the influence of a non-sufficient spinning speed on the final CSA patterns, complete VACSYS simulations with exactly the same experimental sample spinning speed, instead of simple 1D simulations, are conducted. The chemical shift tensor elements used for the simulation are obtained from the VACSYS measurement of the sample in isotropic powder state and they are: $\sigma_{iso} = 143.6$ ppm, $\sigma_{xx} = 203.3$ ppm, $\sigma_{yy} = 157.8$ ppm, $\sigma_{zz} = 69.6$ ppm. The simulation result gives the orientation distribution function as: the σ_{zz} element of the aromatic ^{13}C chemical shift tensor has a Gaussian orientation distribution function with the centre at 90° relative to the rotor's rotation axis, the hwhm is about 23° . Due to the fixed geometrical relationship between the σ_{zz} element of the chemical shift tensor for ^{13}C in a phenyl ring as shown in fig7-15, this is equal to say that: the rigid phenyl-ring planes have a Gaussian orientation distribution function with the centre parallel to the rotor's rotation axis, the hwhm is about 23° . This distribution corresponds to an order parameter of $S = 0.55\pm 0.1$.

The difference of the order parameter S obtained by Goldfarb et al. using ^2H NMR and by us using VACSYS may come from (i) Goldfarb and Luz's ^2H investigation was conducted for sample in mesophase, but our VACSYS investigation was carried out for sample in solid state. Differences in molecular structure as well as molecular orientation distribution very likely exist between these two state. (ii) in our line-shape fitting approach the selected Gaussian distribution model is too coarse. (iii) some other NMR interactions have to be considered, the strong rounding of the VACSYS spectrum for sample in isotropic powder state comparing with the theoretical powder line-shape is a strong evidence of this.

7.5 VACSYS to study orientation distribution of LCSP polyacrylates

The main interest of our work is to study the orientation behaviour of a special type of side-chain polymer liquid crystal materials, namely polyacrylates. The phase diagram of these polyacrylates is given in fig7-17:

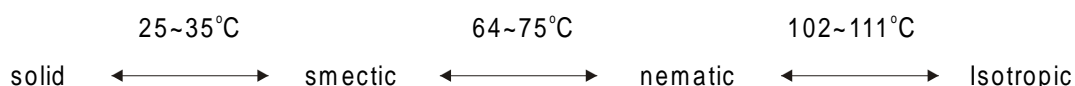


Figure 7-17: Phase diagram of polyacrylates - side-chain polymer liquid crystal samples

here smectic stands for liquid crystalline smectic phase, nematic stands for liquid crystalline nematic phase and isotropic stands for isotropic liquid phase. Its chemical formula, 1D CPMAS spectra and resonant line assignments are shown in the fig7-18.

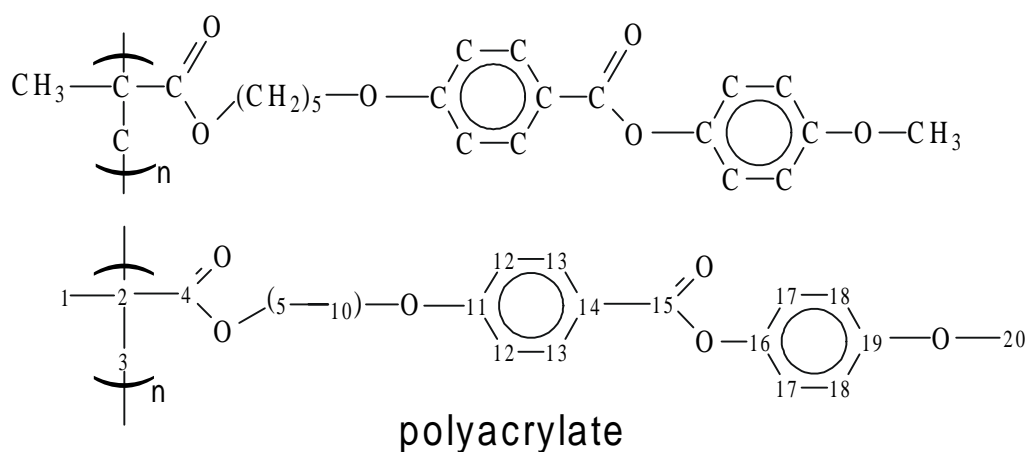


Figure 7-18a: Chemical molecular structure of polyacrylates - side-chain polymer liquid crystals

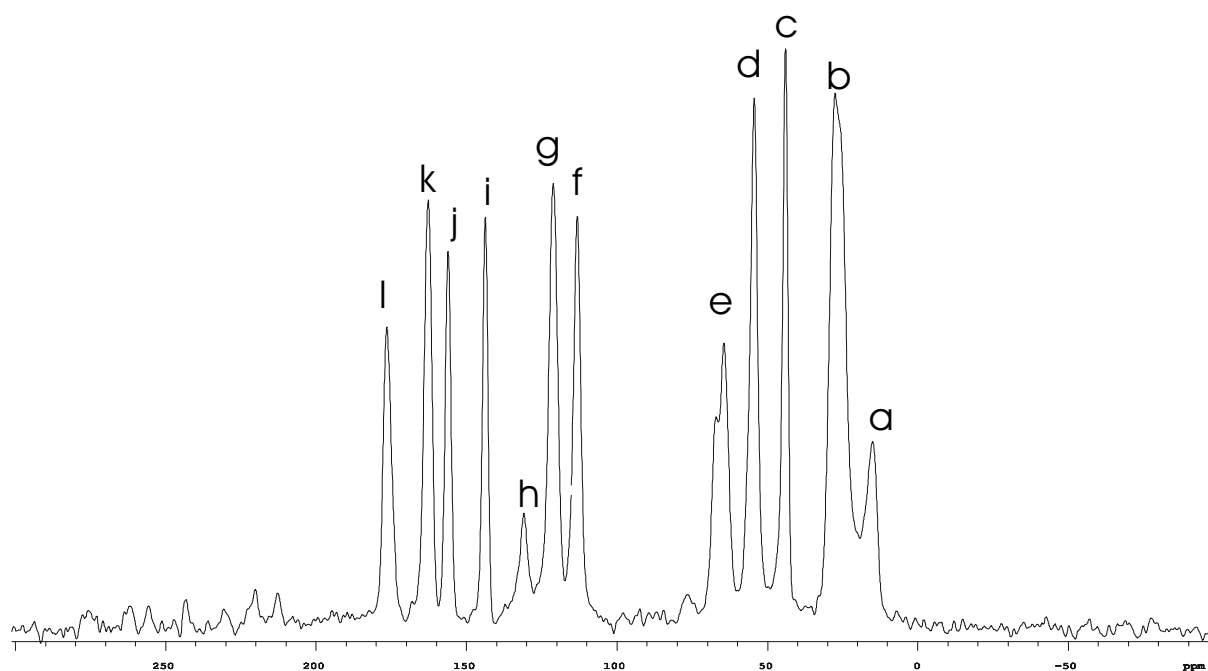
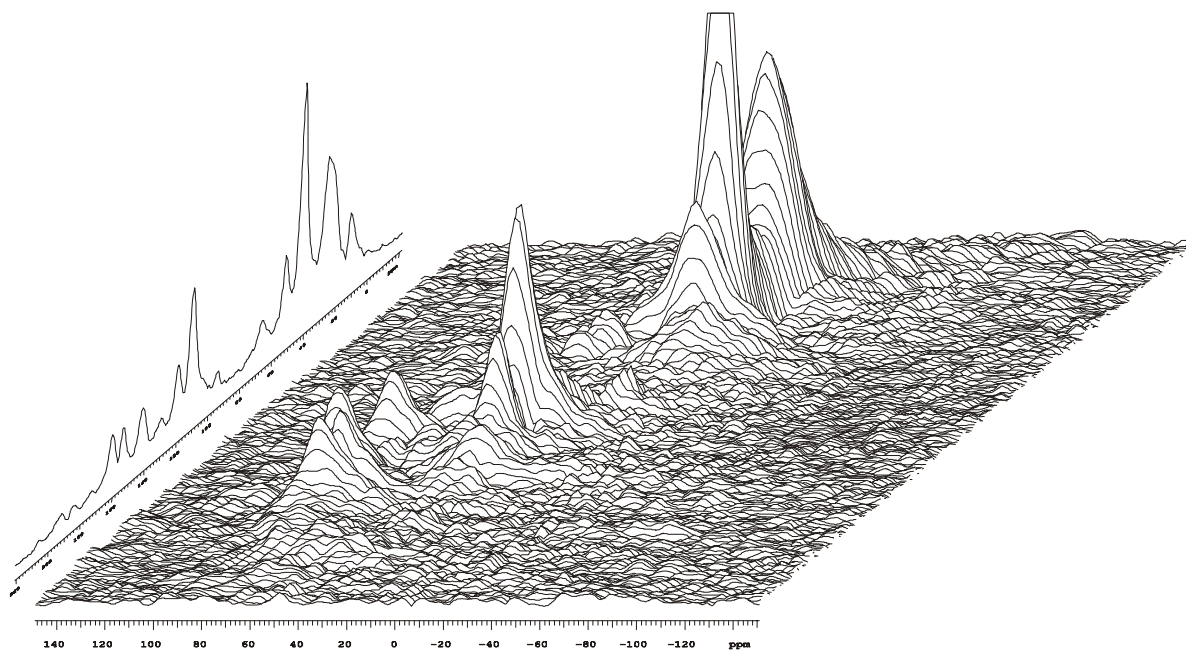


Figure 7-18b: CPMAS ^{13}C (100 MHz) NMR spectrum of polyacrylates (LCSPs), sample spinning speed used is 10.0 kHz with VARIAN 7mm MAS probe

The assignment result of the resonant lines in the ^{13}C CPMAS spectrum of figure 7-18b is given in the following:

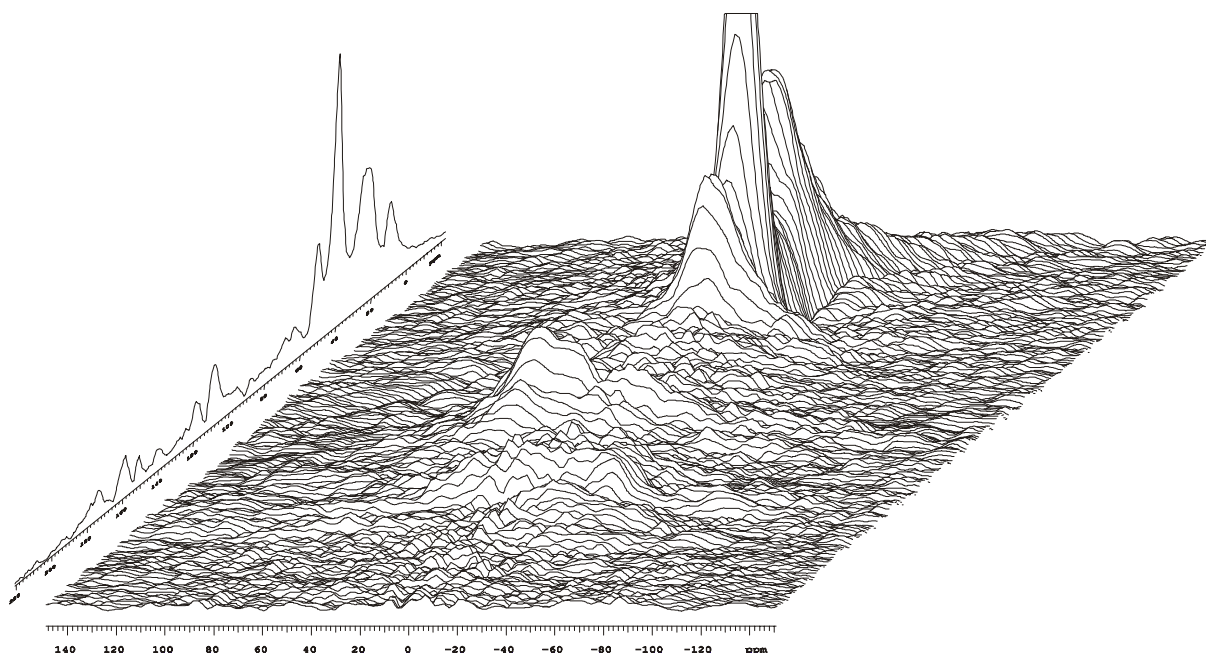
a(1):	17.1ppm	g (17):	122.2 ppm
b(6-9):	27.3ppm	h (13):	132.5 ppm
c(2):	45.2ppm	i (19):	145.5 ppm
d(20):	55.6ppm	j (16):	157.5 ppm
e(5):	65.9ppm	k (11):	164.2 ppm
f(12/18):	114.3ppm	l (4):	177.7ppm

In the 1D CPMAS spectrum, which is acquired under a spinning speed of 10.0 kHz with VARIAN 5 mm MAS probe, there are five spectral lines in the aliphatic area mainly from the main chain and seven lines in the aromatic area from side chain (mesogens). In principle, from one VACSYS experiment the orientation distribution of each molecular segment in both main chain and side chain can be analysed simultaneously. However, due to the problem of not sufficient signal to noise ratio of natural abundance polymer liquid crystal substances, not all anisotropic chemical shift patterns are well resolved in a VACSYS spectrum.



VACSX spectrum of polyacrylate (LCSPs) in oriented state

Figure 7-19a: 3D plot of VACSX ^{13}C (100 MHz) NMR spectrum of polyacrylates (LCSPs) in oriented state with the orientation procedure described in the text. Data is acquired for angle β sampling range of 35° - 90° in 30 steps, sample spinning speed used is 5.0 kHz



VACSX spectrum of polyacrylate (LCSPs) in isotropic state

Figure 7-19b: 3D plot of VACSX ^{13}C (100 MHz) NMR spectrum of polyacrylates (LCSPs) in isotropic powder state. Data is acquired for angle β sampling range of 35° - 90° in 30 steps, sample spinning speed used is 5.0 kHz

In fig7-19 the 3D VACSY spectra of LCSP polyacrylates in isotropic state and oriented state are shown. The VACSY experiments are conducted with 4.0 kHz spinning speed, in a angle range of 35°-90° with 30 steps. Final VACSY spectra are obtained by firstly interpolating the experimental data to 256 points in the anisotropic dimension using Frydman's normal interpolation procedure and then normal 2D FT. The procedure to create certain orientation distribution in LCSP polyacrylates is similar to the procedure applied to p-n-hexa-hexyloxyphenylene sample, that is (i) insert the rotor with sample into the main magnet of our VARIAN INOVA 400 MHz spectrometer(9.4T), the rotor axis direction is set parallel to the magnetic field direction. (ii) heat the sample up to 125°C and wait for about 20 minutes for equilibrium. (iii) at a temperature rate of 1K/min, slowly cool down the sample till below the phase transition temperature of liquid crystalline mesophase to solid phase. NMR measurements for the oriented samples are conducted at room temperature.

With the same arguments stated in section 7.4 for p-n-hexa-hexyloxyphenylene sample, we expect the mesogens of polyacrylates in liquid crystalline phase prefer an orientation in which the molecular rigid planes lie parallel to the rotor axis direction (external magnetic field direction), and the director perpendicular to it. Since all perpendicular orientations are equally probable, the directors are expected to distribute randomly in the radial plane.

The main characteristics of the orientation distribution created by the above described procedure is clearly seen from the changes of ¹³C anisotropy chemical shift patterns of ¹³C from aromatic area in the VACSY spectra: (i) the VACSY spectrum of the sample in isotropic state shows broad CSA patterns, this corresponds to a randomly distributed mesogens, although there are strong deviation from theoretical CSA powder patterns due to line broadening and poor S/N ratio. On another hand, the VACSY spectrum of the sample in oriented state shows strongly enhanced features and all the enhanced features are confined in a smaller spectral range relative to their CSA powder patterns, this indicates a narrower segmental/tensor orientation distribution range. (ii) comparing the VACSY spectrum of polyacrylates in oriented state with the VACSY spectrum of p-n-hexa-hexyloxytriphenylene in oriented state, it is not difficult to find that both of them are enhanced in the region between line-shape singularities σ_{xx} and σ_{yy} and strongly reduced in the region between σ_{yy} and σ_{zz} . This indicates that the orientation procedure has successfully changed the rigid planes of mesogens from an random orientation distribution to a preferred parallel orientation with respect to the rotor axis direction (external magnetic field direction). This conclusion is in good agreement with our theoretical analysis as well as the results from ¹H NMR experiments.

The projections from the slices parallel to the anisotropic dimension at each well resolved isotropic site are given in fig7-20, fig7-21 and fig7-22. The above stated CSA pattern changes between isotropic state and oriented state from ¹³C in aromatic region at positions (f), (g), (i), (j), (k) can be seen more clearly.

In principle, the CSA patterns at each well resolved isotropic site can be taken for orientation distribution analysis. In this way, the full orientation distribution function for each individual molecular segment, either in main chain or in mesogenic groups, can be obtained separately. However, as can be seen from fig7-20: firstly, the CSA patterns of aliphatic ^{13}C at position (b), (c), (d) do not show a significant change; secondly, due to their relative smaller CSA values and strong intensities, strong phase artefacts show up nearby as described in *chapter 4*. These two bad factors make the ^{13}C in aliphatic region (mainly from main chain) not suitable for orientation distribution study by the method of VACSY. Even in aromatic ^{13}C region, at some positions when the spectral intensity is very small like position (L), it is difficult to get any meaningful orientation information.

Lines at positions (f), (g), (i), (j), (k) show the same general orientation features, this is because that all these ^{13}C are from the mesogenic group and the mesogenic group which contains several phenyl rings from a quite rigid molecular segment, therefore they maintain a general orientation.

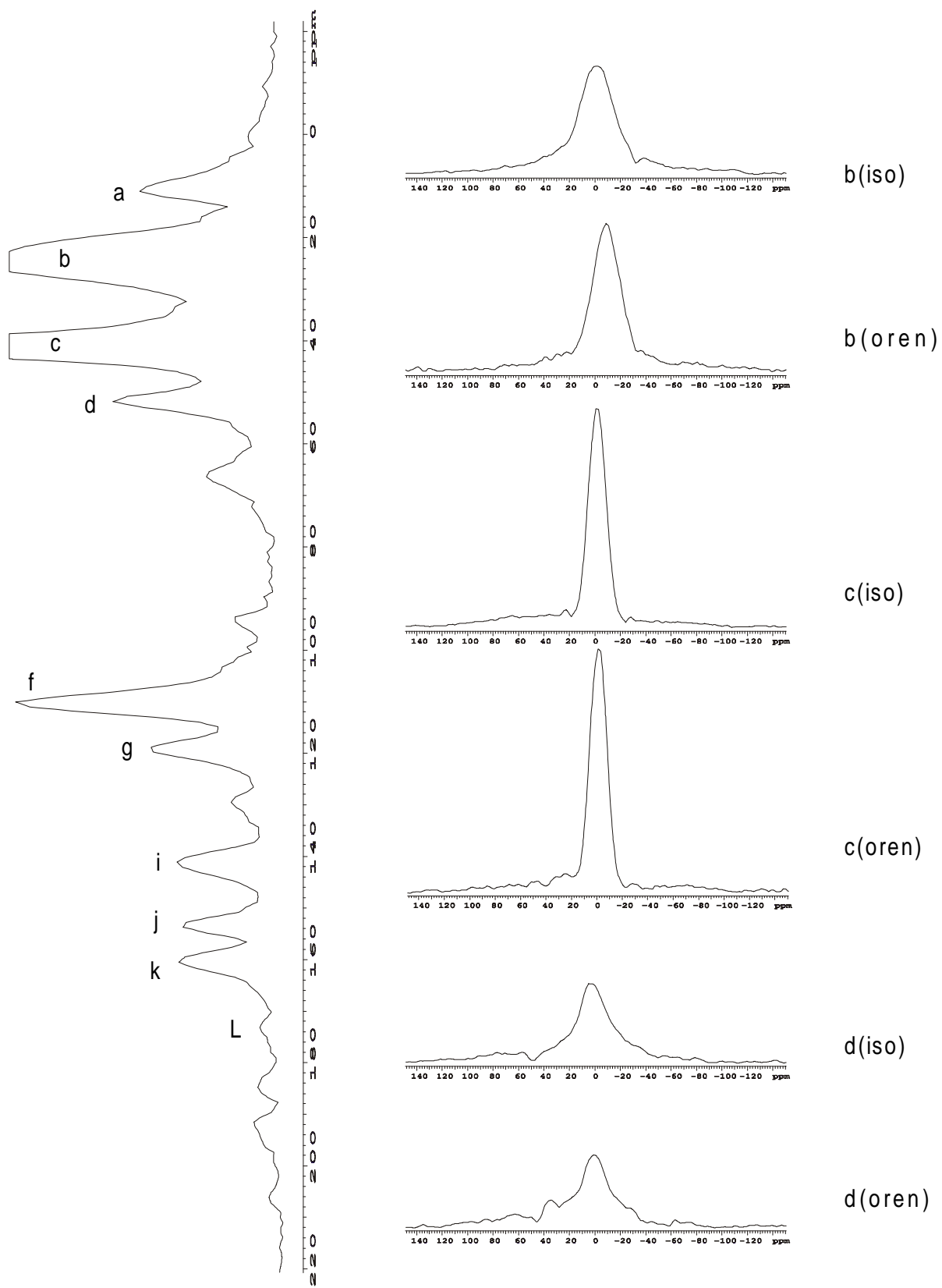


Figure 7-20: (Sky-line) Projections from slices of VACSZY spectra in both isotropic state and oriented state onto the anisotropic axis at isotropic line positions of (b), (c), (d) in aliphatic region.

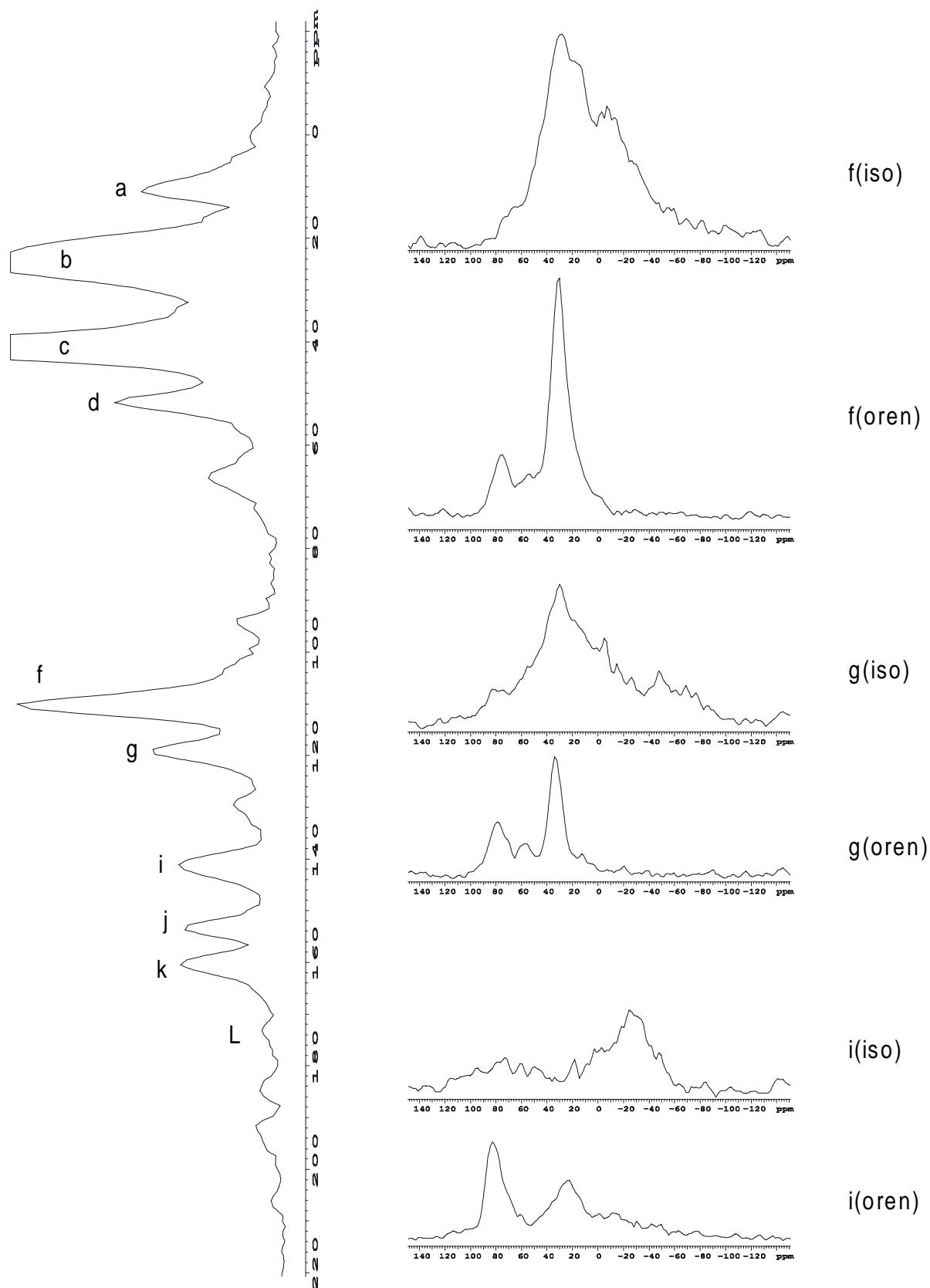


Figure 7-21: (Sky-line) Projections from slices of VACSX spectra in both isotropic state and oriented state onto the anisotropic axis at isotropic line positions of (f), (g), (i) in aromatic region.

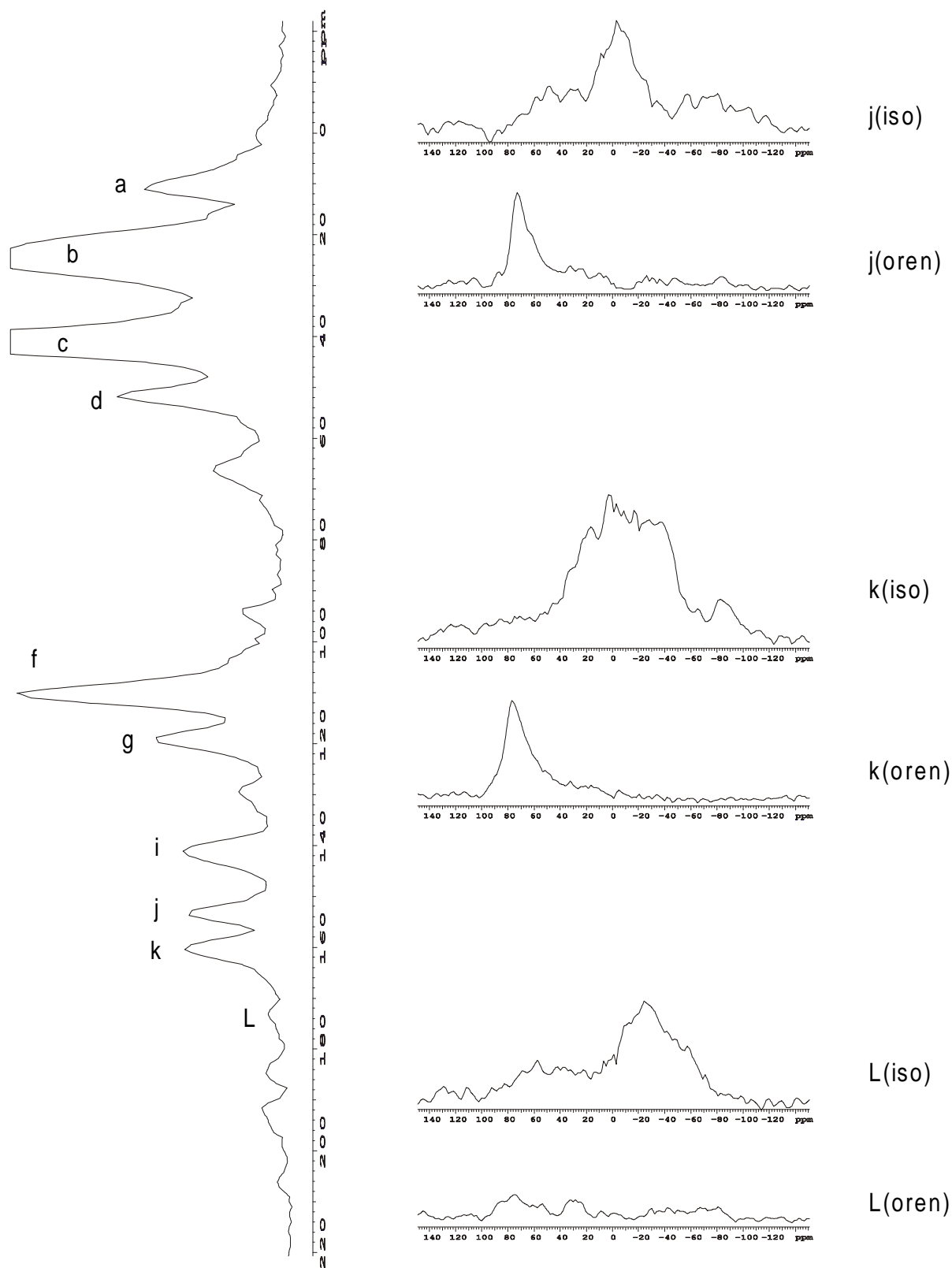


Figure 7-22: (Sky-line) Projections from slices of VACSYS spectra in both isotropic state and oriented state onto the anisotropic axis at isotropic line positions of (j), (k), (l) in aromatic region.

To make a quantitative analysis of the orientation distribution of the mesogenic groups of this LCSP polyacrylate sample, we chose the ^{13}C line at position (f) and apply the line-shape

fitting procedure. Again, the simple Gaussian distribution function as defined in equation (7-3) is selected. Because the spinning speed used to acquire the VACSY spectrum is only 3.5 kHz, the line-shape distortion due to a non-sufficient spinning speed has to be taken into account as described in *chapter 5*. Here, complete VACSY simulations with exactly the same experimental sample spinning speed are carried out, the result is shown in fig7-23.

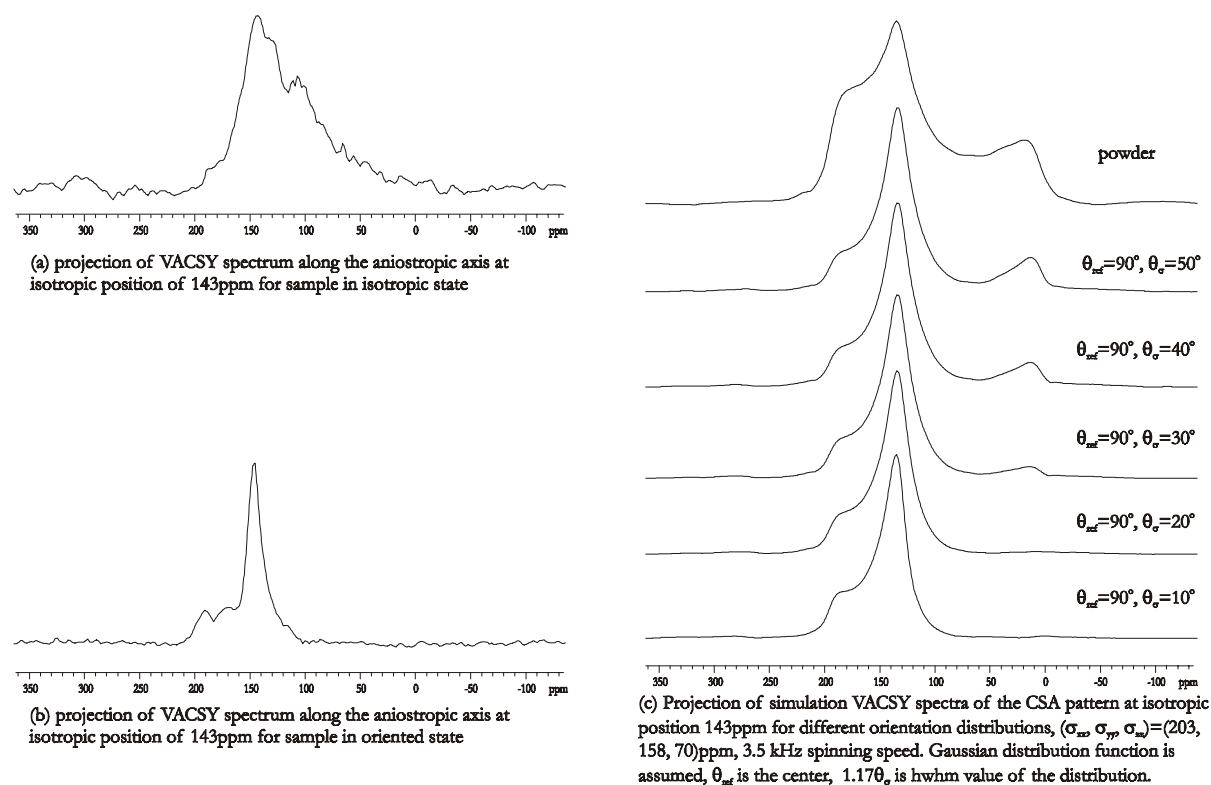


Figure 7-23: Analysis of orientation distribution in LCSPs - polyacrylates by the method of line-shape fitting from VACSY spectra of sample in isotropic state and oriented state, chemical shift tensor used for simulation is $(\sigma_{xx}, \sigma_{yy}, \sigma_{zz})=(207, 148, 18)$ (ppm). (a) projection of experimental VACSY spectrum of sample in isotropic powder state. (b) projection of experimental VACSY spectrum of sample in oriented state. (c) simulated CSA spectra of sample in oriented state for different orientation distributions. Comparing the spectra in (b) and in (c), the orientation distribution for the best fitting is $\theta_{ref} = 90^\circ$ and $\theta_{\sigma} \cong 18^\circ$, corresponding to an order parameter of $S=0.65\pm 0.1$.

The simulation result shows an orientation distribution of the mesogens in the investigated polyacrylate LCSP as: the σ_{zz} element of the chemical shift tensor for aromatic ^{13}C at position (f) from the mesogenic groups has a Gaussian orientation distribution function with the centre at 90° relative to the rotor axis direction, the hwhm is about 20° . With the same arguments as the discussion for p-n-hexa-hexyloxytriphenylene in section 7-4, it is equal to state that: the rigid mesogenic planes are highly oriented parallel to the rotor axis direction, the distribution function is described as an Gaussian function with an hwhm angle of about 20° which corresponds to an order parameter $S = 0.65 \pm 0.1$.

Comparing the experimental CSA patterns with the simulated CSA patterns in both isotropic powder state and oriented state, there are some degree of deviations. Especially for the experimental CSA pattern of the LCSP polyacrylate sample in powder state, where a theory-like powder line-shape as well as the three singularities could not be clearly identified. These deformation of CSA patterns are quite often met in macromolecular samples. In our opinion, these are due to (i) complicated structural conformations existed in polymer samples. (ii) possible anisotropic thermal motions although experiments are conducted under a temperature well below sample's Glass transition temperature T_g . (iii) not sufficient dipolar decoupling.

7.6 Summary

The following conclusions might be drawn from this work:

- (1) VACSY is practically one of most promising methods to obtain the correlation between chemical shift isotropy and chemical shift anisotropy. Firstly, it is not very sensitive to errors in experimental parameters like various methods of multi-pulses with MAS rotor synchronisation. Secondly, it does not require a very swift mechanical change of the rotor status like in the methods of stop-and-go, MAS-OMAS, Magic Angle Hopping.
- (2) VACSY can be used reliably to measure the values of chemical shift tensor elements. In the case of simple substance with few non-overlapping lines, CSA tensor elements can be easily measured by 1D VAS experiment with a better accuracy comparing with the popularly applied Hertzfeld-Berger approach. In the case of multiple lines with overlapped CSA tensors, VACSY can successfully separate them according to their isotropic chemical shift values and then measure their CSA tensor elements respectively.
- (3) VACSY is a promising alternative for the study of orientation distribution in polymer samples. Due to its ability to correlate each CSA patterns with their corresponding chemical shift isotropic values, when S/N ratio is high enough, VACSY is possible to obtain the complete orientation distribution of each individual molecular segments with one experiment, for example main-chain and side-chain orientation distribution or orientation distribution at different positions inside the side-chain of LCSPs.
- (4) An accurate orientation distribution analysis by the method of VACSY requires the sample spinning reaches a certain minimum speed with regard to the chemical shift anisotropy of the investigated sample. Otherwise, the distortion of CSA pattern due to a slow spinning speed may invalidate the results. Two solutions are suggested: (i) higher spinning speed. (ii) lower B_0 field. The (i) is the best solution, because it does not

sacrifice the sensitivity which is also a big trouble when macromolecular samples are studied.

- (5) In the case of nucleus with relative smaller anisotropic chemical shift values and bigger spectral intensities, like the aliphatic ^{13}C in our polyacrylate LCSPs, serious phase artefacts prevent an accurate orientation distribution analysis. In this case, Linear Prediction should be applied to relieve the phase artefacts.

REFERENCES

1. Abragam, A. (1961). *The Principles of nuclear Magnetism*. Oxford University Press, London
2. Alla, M. A., Kundla, E. I. and Lippmaa, E. T. (1978). *JETP Lett.*, 27, 194
3. Balta-Calleja, F. J. and Vonk, C. G. (1989). *X-ray Scattering of Synthetic Polymers*. Elsevier, Amsterdam
4. Barkhuijsen, R. de B., Bovee, W. M. M. J. and Van Ormondt, D.(1985). *Retrieval of frequencies, amplitudes, damping factors and phases for time-domain signals using linear least-squares procedure*, J. Magn. Reson. 61, 465
5. Bax, A., Szeverenyi, N. M. and Maciel, G. E. (1983a). *Isotropic Shifts and CSAs: 2D Magic-Angle Hopping NMR*. J. Magn. Reson., 52, 147
6. Bax, A., Szeverenyi, N. M. and Maciel, G. E. (1983b). *CS Anisotropy of Powders: 2D NMR with Flip of Spinning Axis*. J. Magn. Reson., 55, 494
7. Bax, A., Szeverenyi, N. M. and Maciel, G. E. (1983c). *CS Anisotropy in Powders Studied by 2D CP/MAS NMR*. J. Magn. Reson., 51, 400
8. Bennett, A. E. Rienstra, C. M., Auger, M., Lakshmi, K. V and Griffin, R. G. (1995). *J. Chem. Phys.*, 103, 6951
9. Bloembergen, N. and Rowland, J. A. (1953). *Acta Met.*,1, 731
10. Bovey, F. A. (1988). *Nuclear Magnetic Resonance Spectroscopy*. Academic Press, San Diego
11. Carlson, J. W. (1988). *J. Magn. Reson.* 78, 563
12. Champeney, D. C. (1973). *Fourier Transforms and Their Physical Applications*. Academic Press, New York
13. Chen, C.-N. and Hoult, D. I. (1989). *Biomedical Magnetic Resonance Technology*, Adam Hilgar, New York
14. Chmelka, B. F., Schmidt-Rohr, K. and Spiess, H. W. (1993). *Orientation Distributions in PET Films and Fibers from DECODER NMR*. *Macromolecules*, 26, 2282

15. Conroy, H. (1967). Molecular Schrödinger Equation. VII. *A New Method for the Evaluation of Multidimensional Integration*, J. Chem. Phys., 47(12)
16. Crozier, S., Luescher, K., Forbes, L. K. and Doddrell, D. M. (1995). *J. Magn. Reson.* 109, 1
17. De Beer, R., Van Ormondt, D., Pijnappel, W. W. F. and Van Der Veen, J. W. C. (1988) *Isr. J. Chem.* 28, 249
18. Doty, F. D. (1996a). *Probe Design and Construction*. Encyclopedia of NMR, 1996, Vol. 6, 3573
19. Doty, F. D. (1996b). *Solid State Probe Design*. Encyclopedia of NMR, 1996, Vol.7, 4475
20. Doty, F. D., Inners, R. R. and Ellis, P. D. (1981). *J. Magn. Reson.* 43, 399
21. Doty, F. D., Connick, T. J., Ni, X. Z. and Clingan, M. N. (1988). *J. Magn. Reson.* 77, 536
22. Eden, M. and Levitt, M. H. (1998). *Computation of Orientational Averages in Solid-State NMR by Gaussian Spherical Quadrature*. *J. Magn. Reson.* 132, 220
23. Ernst, R. R., Bodenhausen, G. and Wokaun, A. (1987). *Principles of Nuclear Magnetic Resonance in One and Two Dimensions*. Oxford University Press, Oxford
24. Elliott, D. F. and Rao, K. R. (1982). *Fast Transforms: Algorithms, Analyses, Applications*. Academic Press, New York
25. Flory, J. (1953). *Principles of Polymer Chemistry*, Cornell University Press, Ithaca
26. Frydman, L., Chingas, G. C., ..., Pines, A. (1992a). *Variable Angle Correlation Spectroscopy in Solid-State Nuclear Magnetic Resonance*, *J. Chem. Phys.* 97(7), 4800, Oct. 1992
27. Frydman, L., Chingas, G. C., ..., Pines, A. (1992b). *Correlation of Isotropic Chemical Shifts in Solids by Two-Dimensional Variable-Angle-Spinning NMR*. *Israel Journal of Chemistry*, 32, 161
28. Frydman, L., Lee, Y. K., Emsley, L., Chingas, G. C. and Pines, A. (1993). *Variable Angle Three-Dimensional Exchange NMR for the Study of Molecular Motion in Complex Solids*. *J. Am. Chem. Soc.*, 115(11) 4826
29. Frydman, L., Lee, Y. K., Emsley, L. (1994). *Solid-State Dynamic Processes in Complex Systems Analyzed by Two-Dimensional Isotropic-Anisotropic Correlation Nuclear Magnetic Resonance*. *J. Chem. Phys.*, 101(1), 111

30. Fukushima, E. and Roeder, S. B. W. (1996). *Experimental Pulse NMR - A Nuts and Bolts Approach*. Addison-Welsley Publishing Company
31. Fyfe, C. A. (1983). *Solid State NMR for Chemists*. C.F.C Press, Guelph
32. Gan, Z. (1992). *High-Resolution-Shift and CSA Correlation by Slow MAS*. J. Am. Chem. Soc., 114, 8307
33. Gordan, R. E. (1985). *Phys. Med. Biol.* 30(8), 741
34. Haeberlen, U. (1976). *High Resolution NMR in Solids - Selective Averaging*, Academic Press, San Diego
35. Harbison, G. S., Vogt, V.-D. and Spiess, H. W. (1987). *Partially Oriented Solids: Characterisation by 2D MAS NMR*. J. Chem. Phys., 86, 1206
36. Harper, J. K., McGeorge, G. and Grant, D. M. (1998). *Solid-State ¹³C Chemical Shift Tensors in Terpenes*. Magnetic Resonance in Chemistry, 36, 135
37. Hartmann, S. R. and Hahn, E. L. (1962) *Phys. Rev.* 128, 2042
38. Hayes, C., Edelstein, W., Schenck, J. Mueller, O. M. and Eash, M. (1985). *J. Magn. Reson.* 63, 622
39. Hediger, S., Singer, P., Tomaselli, M., Ernst, R. R. and Meier, B. H. (1997). *J. Magn. Reson.*, 125, 291
40. Hempel, G., Schneider, H. (1982). *Pure and Appl. Chem.* 54, 635-646
41. Hempel, G., Jacobi, A. et al. (1999). *Macromol. Chem. Phys.* 2000, 1608
42. Hentschel, R., et al. (1976). *Magn. Reson. Relat. Phenom.*, 19th Proc. Congr. Ampere, 1976, 381
43. Hentschel, R., Schlitter, J., Sillescu, H. and Spiess, H. W. (1978). *J. Chem. Phys.*, 68(1), 56, Jan 1978
44. Hentschel, R. and Spiess, H. W. (1979). *J. Magn. Reson.*, 1979, 35, 157
45. Hentschel, R., Sillescu, H. and Spiess, H. W. (1980). *Polymer*, 22, 1516, Nov. 1981

46. Henrichs, P. M. (1987). *Molecular Orientation and Structure with ^{13}C NMR: A Study of Biaxial Films of PET*. *Macromolecules*, 20, 2099
47. Herzfeld, J. and Berger, A. E. (1980) *Sideband intensities in NMR spectra of samples spinning at the magic angle*, *J. of Chem. Phys.* 73(121), 6021-6030, 15 Dec. 1980
48. Hoult, D. I. (1989). *Concepts Magn. Reson.* 1, 1
49. Hoult, D. I. and Richards, R. E. (1976). *J. Magn. Reson.* 24, 71
50. Hoult, D. I. (1978). *Prog. NMR Spectrosc.*, 12, 41
51. Hu, J. Z., Wang, W., ..., Grant, D. M. (1995). *Magic-Angle-Turning Experiments for Measuring Chemical-Shift-Tensor Principal Values in Powdered Solids*. *J. Magn. Reson.*, 113, 210
52. Ishii, Y. and Terao, T. (1998). *Manipulation of Nuclear Spin Hamiltonians by rf-Field modulations and Application to Observation of Powder Patterns under Magic-Angle Spinning*. *J. Chem. Phys.*, 109, 1
53. Jackson, J. D. (1975). *Classical Electrodynamics*. Wiley, New York
54. Kashiwagi, M., Folkes, M. J. and Ward, I. M (1971). *Polymer*, 12, 697
55. Kashiwagi, M. and Ward, I. M. (1972). *Polymer*, 13, 145
56. Kasiwagi, M., Cunningham, A., Manuel, A. J. and Ward, I. M. (1973). *Polymer* , 14, 111
57. Kay, S. M. (1988). *Modern Spectral Estimation theory and Application*, Prentice-Hall, Englewood Cliffs, New Jersey
58. Kolbert, A. C. and Griffin, R. G. (1990). *2D Resolution of Isotropic and Anisotropic Chemical Shifts in MAS NMR*. *Chem. Phys. Lett.*, 166, 87
59. Koskinen, M. F. and Metz, K. R. (1992). *J. Magn. Reson.* 98, 576
60. Kroschwitz, I. Ed. (1990). *Concise Encyclopedia of Polymer Science and Technology*, Wiley, New York
61. Kumaresan, R. and Tufts, D. W. (1982). *IEEE Trans. Acoust. Speech Signal Process.* ASSP-30, 833

62. Lee, Y. K., Emsley, L., ..., Pines, A. (1994). *Three-Dimensional Variable-Angle Nuclear Resonance Exchange Spectroscopy without Rotor Axis Hopping*. J. Chem. Phys., 101(3), 1852
63. Lee, Y. K., Vold, R. L., Hoatson, G. L., Lin, Y.-Y. and Pines, A. (1995). *Linear Prediction with Singular-Value Decomposition for Removing Phase Artifacts in 2D VACSYS Spectra*. J. Magn. Reson., 112, 117
64. Lin, Y.-Y., Ge, N.-H and Hwang, L.-P (1993). J. Magn. Reson. A 105, 65
65. Lpmaa, E. Alla, M. and Turherm, T. (1976). Proceedings of the 19th Congress Ampere, Heiderberg, 1976, 241
66. Maciel, G. E., Szeverenyi, N. M. and Sardashti, M. (1985). *CSA Powder Patterns: 2D Angle Flipping Effects of Crystallite Packing*. J. Magn. Reson., 64, 365
67. Mansfield, P. and Powles, J. G. (1963). J. Sci. Instrum. 40, 232
68. Maricq, M. M. and Waugh, J. S. (1979). *NMR in rotating solids*, J. Chem. Phys. 70(7)
69. McBrierty, V. J. and Ward, I. M. (1968). Journal of Physics, 1, 1529
70. McBrierty, V. J., McDonald, I. R. and Ward, I. M. (1971). Journal of Physics, 4, 88
71. McBrierty, V. J. and McDonald, I. R. (1973). Journal of Physics, 4, 88
72. McBrierty, V. J. (1974). Polymer, 15, 503
73. McBrierty, V. J. and Packer, K. J. (1993). *Nuclear Magnetic Resonance in Solid Polymers*, Cambridge Uni. Press, New York
74. McCall, D. W. and Hanmming, R. W. (1959). Acta Cryst., 12, 81
75. McCrum, N. G., Read, B. E. and Williams, G. (1967). *Anelastic and Dielectric Effects in Polymeric Solids*, Dover, New York
76. McGeorge, G., Alderman, D. W. and Grant, D. M. (1999). *Resolution Enhancement in ¹³C and ¹⁵N Magic-Angle Turning Experiments with TPPM Decoupling*. J. Magn. Reson., 137, 138
77. Mehring, M. (1983). *High Resolution NMR Spectroscopy in Solids*, Springer-Verlag, Berlin

78. Montigny, F., elbayed, K., Brondeau, J. and Canet, D. (1990) *Automatic Phase Correction of Fourier Transform Nuclear Magnetic Resonance Spectroscopy Data and Estimation of Peak Area by Fitting to a Lorentzian Shape*", Analytical Chemistry, 62 (8), 15 April 1990
79. Pines, A., Gibby, M. G. and Waugh, J. S. (1973). J. Chem. Phys., 59, 569
80. Rutledge, D. N. (Ed.) (1996) *Signal treatment and signal analysis in NMR*, Elsevier
81. Sachleben, J. R. and Frydman, L. (1997). *Orientational Alignment in Solids from Bidimensional Isotropic-Anisotropic Nuclear Resonance Spectroscopy: Applications to the Analysis of Aramide Fibers*. Solid State Nuclear Magnetic Resonance , 7, 301
82. Schaefer, J. and Stejskal, E. O. (1976). J. Am. Chem. Soc., 98, 1031
83. Schmidt-Rohr, K., Spiess, H. W. (1994). *Multidimensional Solid-state NMR and Polymers*, Academic Press, San Diego
84. Schmidt-Rohr, K., Wilhelm, M., Johansson, A. and Spiess, H. W. (1993). *Shift Tensors in Methlene Groups*. Magn. Reson. in Chem., 31, 352
85. Schneider, H. J. and Dullenkopf, P. (1977). Rev. Sci. Instrum. 48, 68
86. Slichter, C. P. (1980). *Principles of Magnetic Resonance*. Springer-Verlag, Berlin
87. Spiess, H. W. (1980). J. Chem. Phys., 1980, 72, 6755
88. Spiess, H. W. (1984). *NMR in Oriented Polymers*, In I. M. Ward (ed.), *Developments in Oriented Polymers*. Applied Science Publishers, London
89. Spiess, H. W. (1985). *²H NMR for Studying Mobility and Orientation in Polymers*. Adv. Polym. Sci., 66, 23
90. Stejskal, E. O., Schaefer, J. and Mckay, R. A. (1977). J. Magn. Reson., 25, 569
91. Stephenson, D. S. (1988) *Linear Prediction and Maximum Entropy Methods in NMR Spectroscopy*. Prog. NMR Spectrosc. 20, 515
92. Tekely, P.(1998). *To What Extent the Centralband and Each Spinning Sideband Contain Contributions from Different Parts of the Static Powder Pattern?*, Solid Sate NMR 14, 33-41, 1999

93. Terao, T., Fujii, T., Onodera, T. and Saika, A. (1984). *Switching-Angle Spinning NMR: Powder- Pattern-Resolved 2D Spectra*. Chem. Phys. Lett., 107, 145
94. Titman, J. J., Feaux de Lacronix, S. and Spiess, H. W. (1993). *Structure and Order in Solids by 3D MAS NMR*. J. Chem. Phys., 98, 3816
95. Traficante, D. D. (1989). Concepts Magn. Reson. 1, 73
96. Tycko, R., Dabbagh, G. and Mirau, P. A. (1989). *Determination of Chemical-Shift-Anisotropy Lineshapes in a Two-Dimensional Magic-Angle-Spinning NMR Experiment*. J. Magn. Reson., 85, 265
97. Wachter, E.A., Sidky, E.Y. and Farrar, T.C. (1989). *Calculation of Phase-Correction Constants Using the DISPA Phase Angle Estimation Technique*, J. Magn. Reson., 82, 239
98. Van Vaals, J.J. and Van Gerwen, P. H. J. (1990). *Novel Methods for Automatic Phase Correlation of NMR Spectra*, J. Magn. Reson. 86, 127-147
99. Van Vleck, J. H. (1948). Phys. Rev., 74, 1168
100. Vaughan, R. W. (1978). Annu. Rev. Phys. Chem. 29, 397
101. Ward, I. M., Ed. (1982). *Developments in Oriented Polymers*, Applied Science Publishers, London
102. Ward, I. M. (1985). *In Characterisation of Polymers in the Solid State I: Part A: NMR and other Spectroscopic Methods*, Kausch, H. H. and Zachmann, H. G. (eds.), Springer-Verlag, Berlin
103. William H. P., Brian P. F., Teukolsky, S. A., Vetterling, W. T. (1989). *Numerical Recipes*, Cambridge University Press, London
104. Yarim-Agaev, Y., Tutunjian, P. N. and Waugh, J. S. (1982). J. Magn. Reson., 47, 51
105. Zeigler, R. C., Wind, R. A. and Maciel, G. E. (1988). *Stop-and-Go Spinning in MAS*, J. Magn. Reson., 79, 299

Erklärung

Ich erkläre hiermit, dass die Dissertation selbständig verfasst wurde und nur die angegebenen Hilfsmittel benutzt wurden. Die Dissertation wurde noch an keiner anderen Universität oder Hochschule eingereicht.

Halle, den 20. 09. 1999

(Zhanjun Fang)

ACKNOWLEDGMENTS

I would like to thank all the people who have helped me in any respect for the realisation of this thesis. In particular, I want to thank:

Prof. Dr. H. Schneider for accepting me as a Ph. D. student and advising me through three years of Ph. D. study.

Dr. D. Reichert for introducing me all the secrets/tricks of experimental NMR and for having a lot of patience with me when I had various problems about probe, spectrometer, with mechanic workshop, even with immigration office.

Dr. G. Hempel for excellently explaining all the basic NMR theories to me, answering my questions in physics, chemistry, mathematics and for his talented suggestions to solve problems occurred in this project.

Dr. M. Braun for his kind help in the construction of the RF circuit of my VACSY probe.

all other members of Prof. Dr. Schneider's group for the pleasant atmosphere during work as well as in coffee breaks.

Curriculum Vitae

20. 03. 1965 Born in Beijing, P. R. China
- 1982 - 1987 Department of Electronic Engineering, Tsinghua University
Beijing, 100084, P. R. China
B. S. in Electronic Engineering
Title of Diploma work: 'Fabrication of Single Transverse Mode InGaAsP/InP Semiconductor Laser by Liquid Epitaxy'
- 1987 - 1990 Department of Electronic Engineering, Tsinghua University
Beijing, 100084, P. R. China
M. S. in Electron Physics and Devices
Title of Master degree work: 'Characteristics of the All Optic Switching Network in Time Domain Optic Fibre Communication System'
- 1990 - 1995 Division of Length Metrology, National Institute of Metrology
Beijing, 100013, P. R. China
Research Scientist
Research area: 'Small Scale Length Metrology'
- 1995 - 1996 Danish Institute of Fundamental Metrology
Lyngby, DK-2800, Denmark
Fellowship Research Scientist
Research area: 'Application of Scanning Tunnelling Microscope in Surface Roughness Metrology'
- 1996 - 1999 FB Physik, Martin-Luther-Universität, Halle-Wittenberg
D-06108, Halle/Saale, Germany
Ph.D. study in Physics
PhD thesis title: 'Accomplishment of VACSYS Experimental Set-up and its Application to Investigate Molecular Orientation Distribution of Solid-State Polymer'

Halle, den 20. 09. 1999,

Zhanjun Fang